UNIVERSITÀ DI PARMA

UNIVERSITÀ DEGLI STUDI DI PARMA

DOTTORATO DI RICERCA IN

NEUROSCIENZE

CICLO XXXVI

in CO-TUTELA con

KU LEUVEN

The visuotopic organization of the macaque superior colliculus

Coordinatore: Chiar.mo Prof. Luca BONINI

Tutore: Chiar.mo Prof. Luca BONINI

Co-tutore: Chiar.mo Prof. Wim VANDUFFEL

Dottoranda: Alessia SEPE

Anni Accademici 2020/2021 – 2022/2023

Index

Summary

The superior colliculus (SC) is an ancient midbrain structure containing topographic maps in different sensory and motor modalities to guide (c)overt orienting behavior. While the orderly progression space represented along the collicular surface in primates is well documented, the details regarding the representation of central versus eccentric visual space are controversial. Moreover, anatomical, behavioral and functional data collectively support the hypothesis of a pragmatic rather than a metric representation of the visual field in the primate SC, tuned for the detection of contralateral peripheral stimuli in the upper visual field and for hand-object interactions under foveal control in the lower visual filed.

Here, we used sub-mm and conventional resolution fMRI to perform retinotopic mapping in the macaque SC. In six monkeys, we performed phase-encoded retinotopic mapping fMRI experiments at 3T, with stimuli covering either 80° (n = 2) or 25° (n = 4) of the visual field. In two separate passive-viewing fMRI experiments (n = 2), we presented spatially restricted stimuli (80°, 25°, 18° diameter) at different locations (center, and at ~17° eccentricity in the lower left/right quadrants).

We obtained clear wide-field retinotopic maps of the macaque SC showing a topology largely consistent with previously reported fMRI maps in humans and most recent electrophysiological findings in macaques. These maps showed an overrepresentation of peripheral and upper visual fields. The same functional bias for the upper visual field was observed in areas FEF and LIP. Surprisingly, however, the representation of peri-foveal fields differed between the left and right SC of all monkeys in all experiments, being largely confined to the left colliculus. None of the other main regions of the oculomotor/attentional system nor early visual cortices showed a similar interhemispheric asymmetry. Overall, the left SC was more sensitive to variations in eccentricities, and the right SC to variations in polar angles. Smaller interhemispheric differences were also found in the intraparietal sulcus and inferior parietal lobule and, limited to eccentricity varying stimuli, in the MT/MST/FST complex.

Our fMRI study presents a detailed picture of macaque SC retinotopic maps aligned with most recent electrophysiological models. These findings support the hypothesis that the primate SC overrepresents relevant sectors of the visual space, and that this *pragmatic* organization may be a property of the whole oculomotor/attentional system. Finally, the unexpected interhemispheric asymmetries found within the macaque SC and, to a lesser extent, the posterior parietal cortex may suggest larger lateralized functional specializations in the macaque brain than know until now.

1. Introduction

Adaptive behavior and evolutionary success in the animal kingdom depend on the ability to efficiently interact with the environment by quickly and efficiently exploiting the available sensory information. This fundamental capacity is deeply ingrained in the nervous system of animals, and often implies the creation of *neural* maps of the surrounding space relative to the subject for detecting and localizing salient stimuli and planning appropriate motor responses. The superior colliculus (SC), known as tectum in non-mammalian vertebrates, retains a crucial role in this function throughout phylogeny.

In the SC, visual information is integrated with other sources of sensory information and allows the emergence of rapid and appropriate behavioral responses to environmental stimuli, such as approaching, avoiding, or just ignoring based on the specific context (Isa et al., 2021). Early in evolution, the SC/tectum likely emerged as a crucial component for rapidly detecting and responding to potential threats or opportunities in the environment (Foster et al., 2020; Helmbrecht et al., 2018; DesJardin et al., 2013).

In almost all nonmammalian vertebrates, the tectum consists of relatively expanded lobes of the mesencephalon, with the ventricular space extending mediolaterally and forming the tectal ventricle, connected to the main ventricular system of the brain (**Figure 1A**; Butler and Hodos, 2005). This midbrain structure serves as a central hub within the visual system of almost every animal (Bulter and Hodos, 2005), hence its name "*optic tectum*". In non-mammals, the visual cortex is less dominant, and it is even entirely absent in lower vertebrates, like fish. Therefore, in most simple animals, the tectum represents a primary center for visual processing, guiding simple behaviors based on elementary visual input. In the lamprey, for example, the tectal circuity is relatively simple, directly connected to the retina and brainstem's reticulospinal neurons, and the sight of a slowly moving stimulus on one side of the animal's body triggers an approaching movement by activating ipsilateral muscles, whereas a faster moving stimulus activates tectal neurons projecting to the contralateral brainstem, thereby evoking an escaping reaction (Butler and Hodos, 2005).

During phylogeny, the emergence of the neocortex enabled increasingly complex cognitive processes, which supported more and more flexible behaviors. Despite the similarity of the visual information reaching occipital-temporal regions and the colliculus, for example, the cortex allows to achieve a level of detailed processing and abstraction which surpasses considerably that of the colliculus (Isa et al., 2021; Daniel and Whitteridge, 1961; Rolls, 1994). The interplay between parietal and frontal cortices lead to the emergence of a repertoire of complex bodily actions deployed as multiple, potential sets of responses for dealing with environmental stimuli (Orban et al., 2021; Cisek, 2007), in a continuous perception-action cycle. Likewise, at a simpler scale, similar sensory-motor loops seem to occur at the level of SC (Isa et al., 2021; Basso et al., 2021).

The evolutionarily emergence of cortical sensorimotor networks paralleling similar, subcortical networks involving the SC/tectum for controlling eye and arm movements (Nummela and Krauzlis, 2010; Gandhi and Katnani, 2011) suggests a possible transition from relatively rigid and reactive mechanisms to a more flexible and context-dependent action selection system (Cisek, 2022).

It is interesting to note that the SC appears to function largely independently from the conscious processing of the stimuli. Indeed, damages to early regions of the visual cortex sparing subcortical visual structures - like the SC and the pulvinar - in both human (Stoerig and Cowey, 1997; Ajina and Bridge, 2016) and non-human (Cowey and Stoerig, 1995; Isa and Yoshida, 2021) primates, cause the lack of visual awareness of the stimuli. It is as if the subjects are cortically blind, yet with a spared ability to approach objects and avoid obstacles. This phenomenon is known as blindsight (Weiskrantz et al., 1974). Although debated, the SC is one of the main candidate structures thought to play a role in supporting unconscious vision in blindsight patients (Kinoshita et al., 2019; Ajina and Bridge, 2018; Takakuwa et al., 2021).

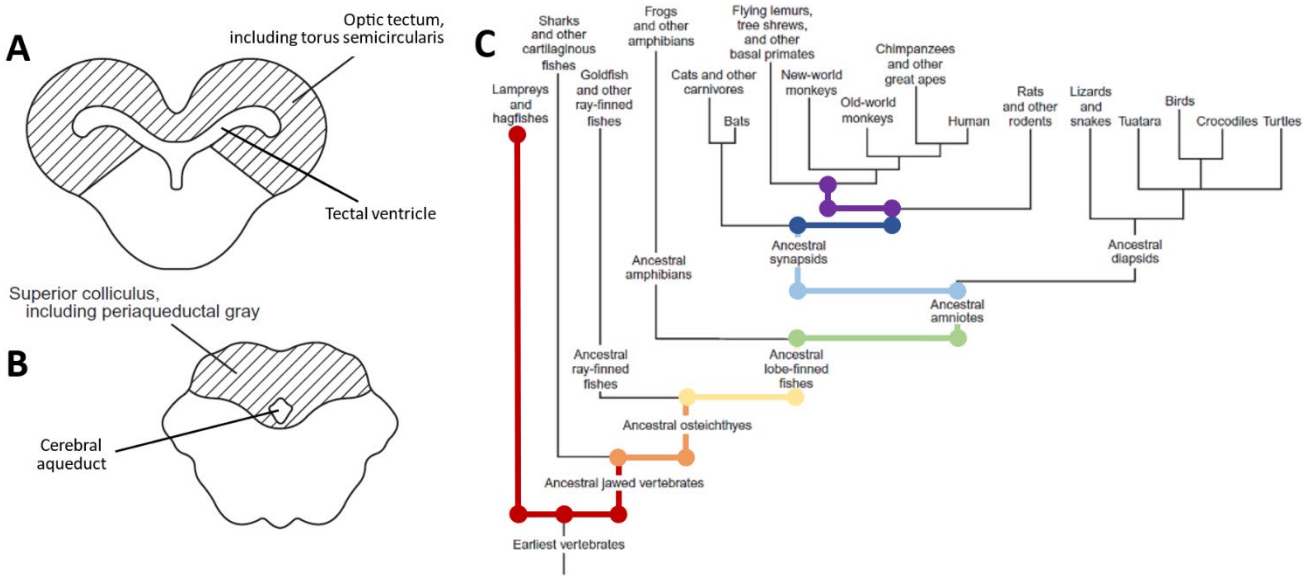

Figure 1. Schematic drawings of transverse sections through the midbrain in a generalized nonmammalian vertebrate **(A)** and mammal **(B)**. **C.** A schematic phylogenetic tree of selected groups of vertebrates. Colors indicate different branching from the most ancestral animal (at the bottom) to lampreys (red) and primates (from red to purple). Modified from Butler and Hodos (2005).

In conclusion, the SC constitutes an evolutionarily ancient and largely conserved structure involved in a form of automatic processing of sensory stimuli to drive attention and potential motor action to approach or avoid them, in parallel with neocortical networks subserving similar functions with higher flexibility and contextual specificity. The following chapters will review the anatomical, connectional, and functional evidence about SC organization in a comparative perspective, to trace its evolutionary history and possible roles in the primate brain.

1.1. Anatomo-functional organization of the superior colliculus

The SC consists of multiple layers of alternated gray and white matter, with afferent fibers traversing it parallel to the surface and dendrites oriented radially. The specific nomenclature used for these layers depends on the author and the specific taxa. Generally, the cell and fiber layers are classified as superficial, intermediate, and deep layers.

1.1.1. Retinal projections to the SC

In most vertebrates, the outermost layers are dominated by retinorecipient cells, hence the name '*optic tectum*'. Monosynaptic retinal projections are consistently organized in a retinotopic fashion across all vertebrates, from fish, amphibians, and birds to mammals (Dräger and Hubel, 1976; Frost et al., 1990; Cynder and Berman, 1972; Finlay et al., 1978; Jacobson and Gaze, 1964; Diao et al., 1983). The surface of this structure exhibit a retinotopic map of the visual field (**Figure 2**), in which the rostral part of SC maps the anterior visual field (or the central, binocular portion in animal endowed with frontal vision), and the caudal part maps the posterior visual field (or the periphery, up to the temporal crescent in animals like primates); furthermore, upper and lower quadrants are represented along the medio-lateral axis (Butler and Hodos, 2005).

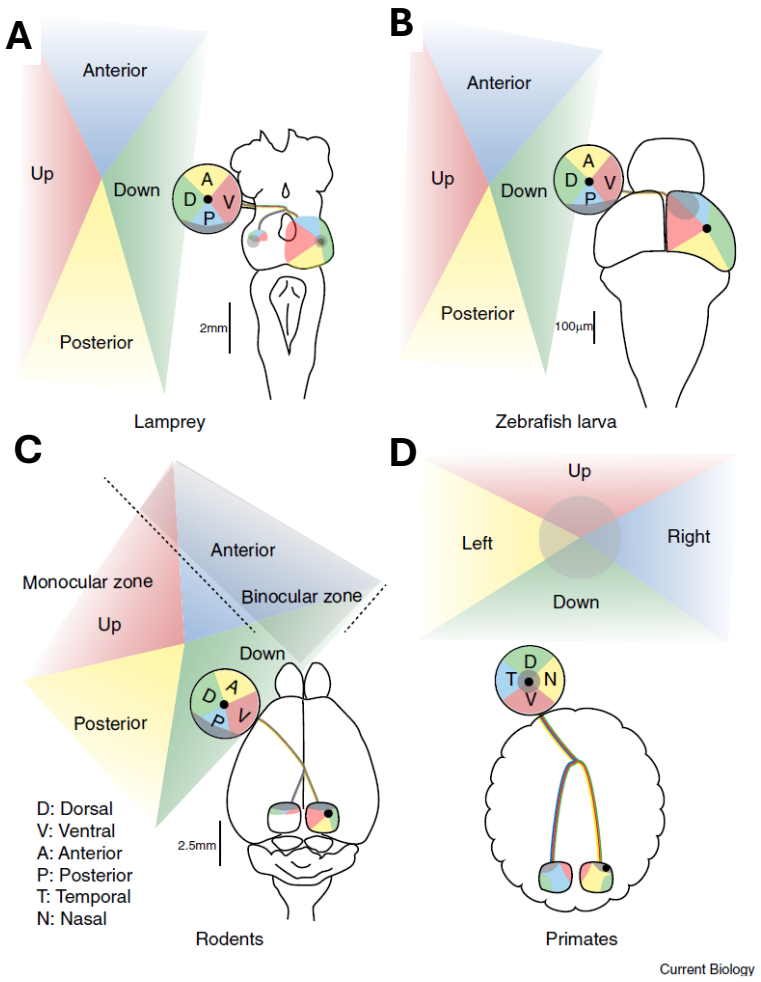

Figure 2. Visual topography of the retinotectal projections in the lamprey (**A**), zebrafish larva (**B**), rodents (**C**) and primates (**D**). Projections from various aspects of the visual field (Up, Down, Anterior and Posterior in (**A–C**), and Right and Left in (**D**)) to the retina and tectum/SC are shown in corresponding colors. The center of the retina is represented with black dots. The binocular zone for rodents (**C**) and the foveal region for primates (**D**) are shaded in gray. From *Isa et al, 2019*.

In macaques, the proportion of retinal ganglion cells projecting to the SC is about 10% of the whole optic nerve (Perry and Cowey, 1984). In other mammals, instead, it varies from about 80% in rodents (Linden and Perry, 1983; Hofbauer and Dräger 1985; Ellis et al. 2016) and rabbits (Vaney et al. 1981) to 50% in cats (Berson, 2008).

In primates, each eye projects to the superficial layers of both colliculi (stratum griseum superficiale and stratum opticum), with a bias for the contralateral eye (Dilbeck et al. 2022). Contralateral and ipsilateral fibers project with a ratio of 60/40 percent, respectively, similarly to the one in the primary visual cortex for eccentricities larger than 8° (Horton and Hocking, 1996). The wide dendritic field of SC superficial neurons integrates the information from the two eyes. Indeed, SC receptive fields are binocular, a property that in primates, in contrast to the cat or mouse with mainly contralateral retinal projections (Wässle et al., 1980; Hofbauer and Dräger, 1985), is not entirely dependent on the cortical input (Schiller et al., 1974; Grünert et al., 2021). In addition to this, retinal afferents from the two eyes show a pronounced laminar segregation (Dilbeck et al. 2022; Hubel et al., 1975; Pollack and Hickey, 1979). The contralateral eye projects more superficially to the caudal-most region and to deeper parts of the SC more anteriorly, and vice versa the ipsilateral eye. The corticotectal fibers, instead, course slightly deeper within the superficial layers, through the stratum opticum and stratum zonale (Lund, 1972).

1.1.2. Colliculo-thalamic and cortico-tectal projections: anatomo-functional circuitries

The SC does not project directly to any cortical area, but it influences cortical neurons via colliculo-thalamic-cortical pathways. Moreover, all cortical areas involved in this pathway directly project back to the SC (Fries, 1984; Cusick 1988). Thus, the SC receives projections from almost the entire neocortical mantle, with the exception of orbitofrontal (see also Leichnetz et al., 1981), primary somatosensory (Brodmann areas 3, 1, and 2), and cingulate cortex (Fries, 1984).

The thalamus is an important tectal-recipient structure in the brain of all vertebrates. The primate thalamus has been extensively studied, and specific thalamic nuclei have been identified as relays of tectal fibers to specific cortical aeras (Benevento and Fallon, 1975; Froesel et al., 2021). Superficial layers of the SC project to the lateral geniculate nucleus (LGN) and the pulvinar. Through a specific subpopulation of cells in the inferior pulvinar, superficial SC neurons reach extrastriate areas specialized for processing visual motion, i.e., area MT and area V3, but not areas V2 or V4 (Lyon et al. 2010; Berman & Wurtz 2010). Visual proprieties of many temporal areas beside MT (Rodman and Albright, 1990) are also modulated by SC activity, such as the polysensory area (STP; Bruce et al., 1986) or the fundus of the superior temporal sulcus (FST; Bogadhi et al., 2022). Deeper collicular neurons, instead, reach frontal (Brodmann area 8a or frontal eye field, FEF) and inferior parietal (area 7; i.e. lateral intraparietal sulcus, LIP) areas through the latero-medial pulvinar (Benevento and Fallon, 1975; Harting et al., 1980; Romanski et al. 1997). Crucially, these frontal and parietal projections are both ipsilateral and contralateral (Sommer and Wurtz, 2002; Huerta and Harting, 1984; Crapse and Sommer; 2009; Clower et al., 2001).

The ascending colliculo-thalamic pathways are not entirely directed to the cortex. Some tectal fibers originating from deeper layers pass through the thalamic component of the ascending reticular activating system (intralaminar nuclei, with a role in general arousal) and reach the striatum in the basal ganglia complex through the direct, indirect, and hyper-direct pathways (Redgrave et al., 2010; Alexander et al., 1986). From here, through the substantia nigra pars reticulata (SNr) and internal globus pallidus, information is sent back to the tectum/SC. This subcortical tecto/colliculo-thalamic-basal ganglia-tecto/colliculo loop (Redgrave et al., 2010) is implicated in the processing of saliency and detection of salient events (Sadikot & Rymar 2009, Smith et al. 2004, Van der Werf et al. 2002). Moreover, a direct colliculo-nigral pathway has been described in mammals (Comoli et al., 2003; McHaffie et al., 2006). Excitatory and inhibitory projections from the intermediate and deep layers of the SC reach the dopaminergic substantia nigra pars compacta (SNc), quite diffusely and in non-topographically manner in primates (May et al., 2009). The role of this colliculo-nigral pathway has still to be clarified, but it suggests a possible link of this system with the regulation of saliency of sensory stimuli (regardless of their modality or spatial location) by means of reinforcement learning mechanisms.

Concerning cortico-tectal projections, striate and extrastriate cortices (Brodman areas 17, 18, and 19) project to the superficial layers of the SC. The striate cortex is one of the main sources of tectal afferents in all mammals (Wurtz and Albano, 1980), and exhibits a precise retinotopic organization (Daniel and Whitteridge, 1961; Graham, 1979). All extrastriate visual areas project to the SC with nearly equal strength, and with a topography of projections related to their retinotopic organization (Fries, 1984; Cerkevich et al 2014; Gattass et al, 2013). High-level visual (IT; areas 20 and 21), somatosensory (SII; anterior bank of sylvian fissure, area 2), auditory (area 22), and vestibular (upper insular cortex, area 14; Grüsser et al., 1982) information reach the intermediated and deep layers of the colliculus. Ventral motor (area 4), premotor (area 6) and prefrontal (area 9, rostral 46vc and intermediate 12r; Borra et al., 2014) areas project to the intermediate and deeper layers. These projections seem to be topographically organized, with the finger-hand-arm-shoulder represented in the anterolateral part of the SC and the arm-trunk represented more caudally (Fries 1985). Similarly, also area SII sends projections from the limited area of the finger-hand-head representation (see also Juliano et al., 1983). More specifically, the somato-motor representation of the hand tends to be confined in the rostro-lateral part of the colliculus. The rostral SC hosts foveal neurons, which show a significant increase in their activity during reaching, particularly high when the reaching movement is coupled with target fixation (Reyes-Puerta et al., 2010). The lateral SC hosts neurons modulated by the contact of the hand with the target (Nagy et al., 2006). The convergence of hand-related and foveal information in the rostral SC, and the presence of neurons involved in gaze anchoring during reaching movements, places the rostral SC at the core of a brain network dedicated to the eye-hand coordination (Borra et al., 2014).

The SC is also involved in another important network: the parieto-frontal circuits devoted to the control of eye movements. Lower layers in the SC also receive projection from the posterior parietal cortex (PPC; Lynch et al, 1985), which is involved in oculomotor and attentional mechanisms and the construction of maps of the extrapersonal, far space (Mountcastle et al., 1975; Hyvarinnen, 1982). These regions receive several different extra-retinal inputs (Zeki, 1971; Mesulam et al., 1977; Hedreen and Yin, 1981; Selzer and Pandya, 1980; Maunsell and Van Essen, 1983b) and are visually-responsive (Robinson et al., 1978; Sakata et al., 1980, 1983). In particular, area LIP plays a clear role in target selection and contains a salience map to guide visual attention and saccadic eye movements (Bisley and Goldberg, 2010) by signaling distance and direction of a spatial location from current or anticipated center of gaze (Colby et al., 1993). The medial parietal lobe (area 7m) contains a medial parietal eye field (MEF) and, together with area LIP, belongs to the neural network of oculomotor-related structures that plays a role in the control of eye movement (Leichnetz 2001). Posterior parietal areas are tightly linked with another source of corticotectal projections: the frontal eye field (FEF) (Künzle et al., 1976; Leichnetz et al., 1981) and supplementary eye field (SEF) (Huerta and Kaas, 1990; Fries, 1984). The FEF may relay signals relevant for eye and attentional shifts (Bisley and Goldberg, 2010; Matsumoto et al, 2018), but the latency of visual responses are longer in the FEF (50-120 ms; Mohler et al., 1973) than in the SC (35-60 ms; Wurtz and Mohler 1976), suggesting the priority of a colliculo-pulvinar-FEF pathway in conveying visual and oculomotor signals (Sommer and Wurtz, 2008; Sommer and Wurtz, 2004) that, ultimately, the FEF can exploit to regulate attentional mechanisms and eye shift (Moore and Armstron 2003; Moore and Fellah 2001). Indeed, electrical stimulation at low current intensity in each node of the oculomotor network (LIP, FEF, MEF), including SC, causes saccadic eye movements (Shiller and Tehovnik, 2005).

1.1.3. Local circuits mediated by the inter-collicular commissure

A further important network is mediated locally by inter-collicular connections. The inter-collicular commissure is an axon bundle connecting the two colliculi (Butler and Hodos, 2005). In cats and monkeys, tectotectal cells are distributed in all layers, but apparently more concentrated in the intermediate ones, along the entire rostro-caudal extent of the colliculus (in the monkey) or more exclusively located in the rostral half of the SC (in the cat). All SC cell types (except the largest neurons) contribute to inter-collicular pathway of both species, suggesting that a sample of each layer is sent as an efference copy to the contralateral colliculus (Olivier et al., 1998). Tracing study of commissural projections of the human SC found a similar topographical organization (Tardif and Clarke, 2002).

About half of the inter-collicular fibers is GABAergic, and the other half is glutamatergic (Appell and Behan 1990; Olivier et al. 2000). More specifically in cats, a mirror-symmetric distribution of excitatory commissural projections link the medial to medial (upper field) and lateral to lateral (lower field) parts of the two SCs, with excitatory effects mainly restricted in their rostral pole (center of the visual field). The inhibitory commissural connections, instead, connect the medial part of one SC with the lateral part of the other SC, across the entire rostro-caudal extent of the SC (Munoz and Istvan 1998; Takahashi et al. 2005; Takahashi et al. 2007; Takahashi et al., 2010). Therefore, excitatory and inhibitory effects are deeply intertwined. Intracellular recording from rostro-lateral tectotectal cells during stimulation of the contralateral SC in cats revealed that rostro-lateral stimulation evokes excitation. Rostro-medial stimulation causes excitation followed by inhibition (Takahashi et al., 2010). In other words, different peripheral regions of the visual field are highly competitive in the caudal SC (regulated by inhibitory mechanisms), whereas for the central visual field the information is first integrated between rostral colliculi by the simultaneous contra- and ipsi- activation. Afterwards, this central information is refined by subsequent inhibition - to maintain precise information about the location of the stimulus. Moreover, excitatory and inhibitory modulations also affect the rostro-caudal extent within and between colliculi. Caudal neurons are inhibited by electrical stimulation of any part (caudal and rostral) of both the ipsi- and contralateral SC. Rostral neurons, instead, are inhibited by stimulation of the ipsilateral but not contralateral caudal region (Munoz and Istvan, 1998). The presence of fixation cells in the rostral pole led many authors to refer to the caudal and rostral regions as ‘saccade’ and ‘fixation’ zones, respectively. In other words, the fixation zone is silenced by the ipsilateral ‘saccade’ activity only. The saccade zone is silenced by ipsilateral as well as contralateral ‘fixation’ activity, which is probably used for maintaining stable visual fixation and suppressing unwanted saccades.

1.1.4. Multimodal integration in the superior colliculus

The evolutionary relevance of the SC/tectum is emphasized by its conservation across species, from simpler vertebrates to the more complex mammals, such as primates. One of its key evolutionary functions is the integration of multimodal sensory information for transforming the spatial location of the stimuli into goal-directed behavior aimed at making or avoiding contact with them (Kardamakis et al., 2016; Kardamakis et al., 2015; Suzuki et al., 2019; Sparks, 1986; Dean et al., 1989; Sahibzada et al., 1986). This transformation is enabled by the convergence, up to the single neuron level, of multiple types of sensory and motor information. Hence it, forms co-registered, multisensory and motor maps (Meredith and Stein, 1986; de Malmazet and Tripodi, 2023). For example, the visual information of a flying object approaching a subject from the upper-right side will activate neurons receiving, in addition to the visual information, somatosensory inputs from skin receptors located on the

upper right body surface, thereby triggering a defensive reaction to protect the threatened side of the body. This convergence of multimodal information sharing the same origin - or link with a sector of space surrounding the subject - will be referred to as “spatial co-registration” (see, e.g., Isa et al., 2021).

The superficial layer of the SC hosts neurons with primarily visual properties. Visual receptive fields are binocular and mainly contralateral, as in early visual cortex (Harvey and Dumoulin, 2011). Receptive field size correlates positively with eccentricity. Nevertheless, some SC neurons exhibit small visual receptive fields, of about 4° at 40° eccentricity (Cynader and Berman, 1972), which highlights the importance of relatively high spatial resolution in these SC maps. Visual SC cells can also signal the (dis)appearance of a stimulus within their receptive field and are modulated by relatively low-level visual features, such as stimulus size (see **Figure 3B**), contrast, and spatial/temporal frequencies (Malevich et al., 2022; Chen et al., 2018; Chen and Hafed, 2018).

The lower/intermediated layers of the SC receive a variety of multisensory and motor signals via topographically organized fibers from different brain areas/nuclei. Although the sensory modalities that undergo spatial co-registration depend on species-specific ethological adaptations, vision seems to serve as the primary modality, often supplemented by somatosensory and auditory inputs. Indeed, the eye is the only sensory organ sending direct connections to the tectum/colliculus, even though in some species additional information may add, such as those from the lateral line or electro-sensory information in some fishes (Gnathonemus petersii; Zeymer et al., 2018), magnetic information in birds or mole rats (Crytomys anselli; Nemec et al., 2001; Wiltschko and Wiltschko, 2019), and infrared signals in snakes (Crotalis viridis; Hartline et al., 1978). These multimodal inputs are co-registered with the retinal map used as a template, to generate a multilayer, multisensory and unified map of the surrounding environment (Isa et al., 2021).

The deeper layers of the SC host output neurons, organized in motor maps that match the overlaying sensory maps (Butler and Hodos, 2005). Electrical stimulation applied to the motor layer causes eye movements (McHaffie and Stein, 1982). Generally, stimulation applied to the rostral pole elicits small amplitude movements, while stimulation applied more caudally causes large amplitude eye movements. Small animal models, such as the lamprey, which can be tested in unconstrained experimental settings, allowed researchers to show that higher stimulation intensities applied to the caudal motor region of the SC can trigger locomotor movements (Saitoh et al., 2007). The basic parameters encoded by neurons forming these deep tectal maps are motion direction and amplitude, calculated on the basis of co-registered sensory target position and motion direction (Lee et al., 1988; Munoz and Wurts, 1995). Nevertheless, in primates or cats, the vast majority of superficial SC neurons is activated by flashing/moving stimuli with poor or no selectivity for motion direction (Marocco and Li, 1977), shape, orientation (Schiller and Koerner, 1971) or color (Wurtz and Albano, 1980). In general, the lack of stimulus

specificity exhibited by SC neurons led many authors to refer to these visual cells as 'event detectors' (Cynader and Berman, 1972; Schiller and Koerner, 1971), and as 'newness cells' (Dräger and Hubel, 1975), because of their strong tendency to habituate to repeated stimuli. In addition to receptive fields size, neuronal response latencies vary as a function of depth: superficial neurons exhibit shorter latencies and, possibly, signal high-velocity stimulus movement. Conversely, deeper cells display longer latencies, possibly conveying signals about low-velocity motion only (Marocco and Li, 1977).

The vertical, multimodal co-registration and integration of information takes place already at single cell level (Meredith and Stein, 1986). The layers of the tectum/SC contain neurons characterized by radially oriented

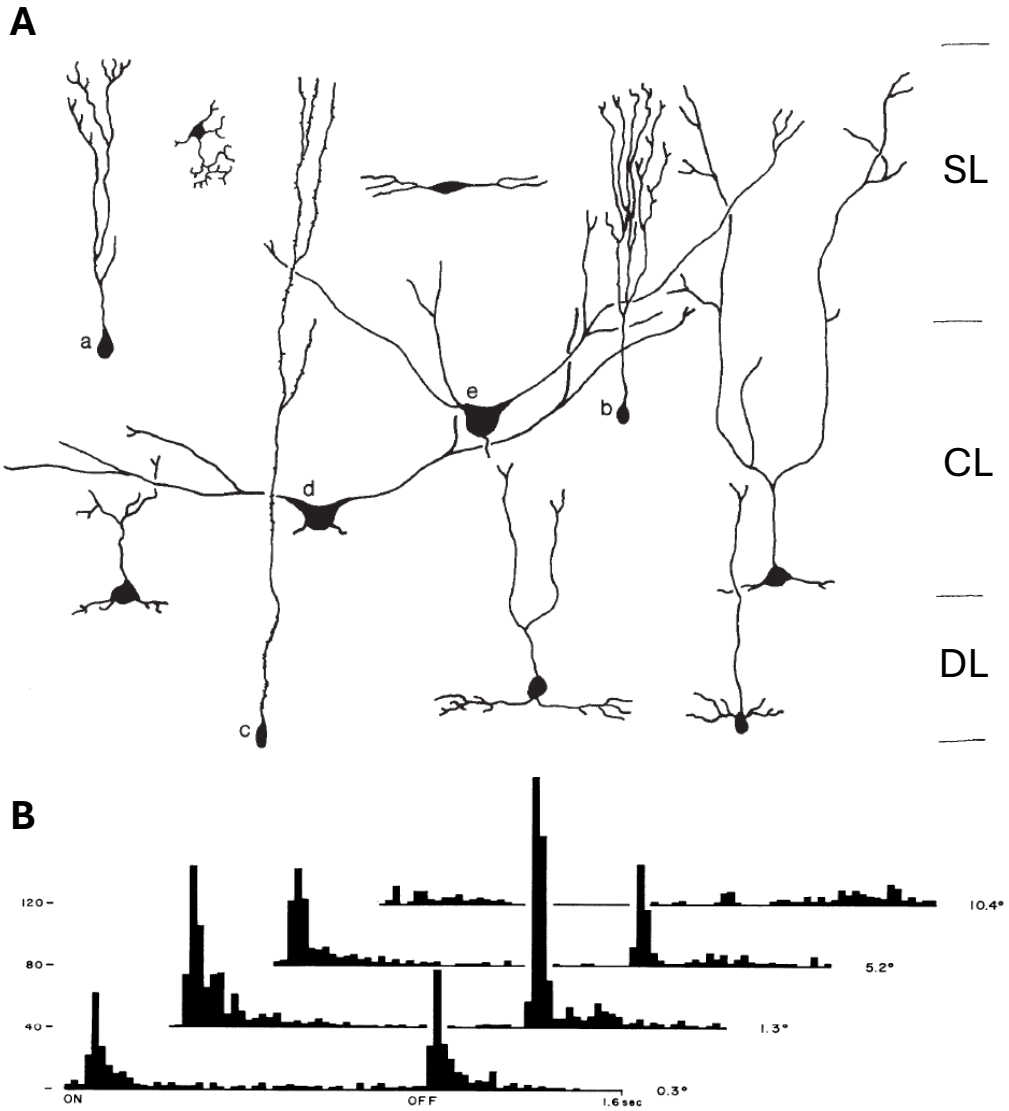

Figure 3. A. Neurons in the optic tectum of a frog (Golgi method). A piriform neuron (*c*) and GABAergic horizontal cells (d-e). SL, superficial layers. CL, central layers; DL, deeper layers. Modified from Székely (1971). **B.** Response profile of a superficial SC neuron in primate as stimulus size increased (0.3°, 1.3°, 5.2°,10.4°). Center-surround organization and temporal response characteristics to onset and offset of a stimulus (stationary flesh of light). Ordinate: total number of discharges per bin. From Schiller et al. (1974).

dendrites (piriform cells; **Figure 3Ac**), running through the vertical extent of the structure. Afferent fibers from different systems form synapses with confined and segregated bands along the vertical dendritic shafts of individual neurons. The input from a given region of space is projected onto a precise neuronal population of the tectum/SC along its horizontal extent. Information from the same spatial location in different sensory formats facilitates the response, while information from different spatial locations with same or different modalities, inhibit it (Meredith and Stein, 1986; Rizzolatti et al., 1974). This inhibition is enabled by the abundant presence of γ-aminobutyric acid (GABA)ergic interneurons, likely responsible for pronounced lateral inhibition observed within the SC. In mammals, the inhibitory system affects the superficial and deep layers of the SC in distinct ways. In the deep motor part of the SC, neurons generate broad excitations along the horizontal plane, forming an 'excitatory hill' possibly contributing to the generation of movement response vectors (Saito and Isa, 2004). In the superficial SC, however, such behavior would affect the precision of spatial mapping, visual acuity, and the detection of small objects (Hoy et al., 2019). The superficial SC, indeed, hosts neurons with narrow dendritic trees and ON/OFF center-surround receptive fields (**Figure 3**). These cells share many aspects of the receptive field organization with visually-responsive neurons of visual cortical areas: they respond to both ON- and OFF-set of the stimulus, and the response is enhanced for the central portion of the visual field and inhibited for the surrounding locations (Phongphanphanee et al., 2014). In these superficial SC cells, however, inhibition acts more like an attenuator of the response (**Figure 3B**) and there is no net separation into discrete ON and OFF areas (Cynader and Berman, 1972). This ON/OFF modulation is likely due to long range inhibition probably produced by GABAergic horizontal cells (**Figure 3Ad-e**; Kasai and Isa, 2016).

The GABAergic contribution is particularly relevant in mammals, in which the vertical sensory-motor stream is constantly under suppression of GABAergic inhibition (Isa et al., 1998). Visual bursts in the superficial layers alone are insufficient to induce saccade related activity in the deeper SC (Edwards, 1980). This vertical GABAergic inhibition forms the foundation for the dissociation between overt and covert orienting behavior. In order to produce attentional shifts to salient stimuli, saccades or orienting head/body movements, deep SC neurons have to be released from the inhibition of local interneurons as well as the inhibitory control from the basal ganglia (Hikosaka and Wurtz, 1983; Ghitani et al., 2014), and the modulation from other nuclei, such as basolateral amygdala (Waguespack et al., 2020), pedunculopontine tegmental nuclei (Harting & Van Lieshout 1991) or the isthmus nuclei (Basso et al., 2021). In addition to the GABAergic and cholinergic modulation, the tectum/SC receives also direct dopaminergic and serotoninergic inputs (Perez-Fernandez et al., 2017, Campbell and Takada, 1989; Li et al., 2018; Huang et al., 2017) refining the SC output based on the animal's motivation and stress status, and making it subject to modulation by reinforcement-based learning processes.

Thus, the layered tectum/SC is the sole structure in the brain that, even in the absence of a highly developed neocortex, can integrate a visual map of the space with ethologically relevant, multimodal information allowing to detect and react to sensory events in the outside world.

1.2. Pragmatic representation of functionally-relevant sectors of space within the SC

Classical models (Robinson, 1972; Ottes et al., 1986) depict the retinotopic organization of the SC in primates as a geometric representation of visual space, similar to low-level areas such as striate cortex. However, considering its functional roles – 1) detecting stimuli beyond the attentional focus (often aligning with the center of gaze) by using the eye to explore the extra-personal space, and 2) facilitating interactive and manipulative behavior in peri-personal space under the guidance of foveal vision – the rationale for a purely metric representation is weak. More recently, a new model of the topographic visual organization of the primate SC has been proposed (Hafed and Chen, 2016; Chen et al., 2019), offering a revised topography which magnifies behavioral relevant sectors of space (de Malmazet and Tripodi, 2023).

The new model was built upon asymmetries found in the representation of upper and lower visual fields (Hafed and Chen, 2016; **Figure 4**). While the lower visual field conveys information about the near peri-personal space, the upper visual field typically conveys information from the distant, extra-personal space. Superficial visual and deeper motor neurons show reversed biases for the upper and lower visual fields, respectively. Deeper neurons show stronger saccade-related motor burst for downward saccades than for upward saccades (Zhang et al., 2022), in line with the nature of peri-personal space allowing for manipulative and interactive behaviors.

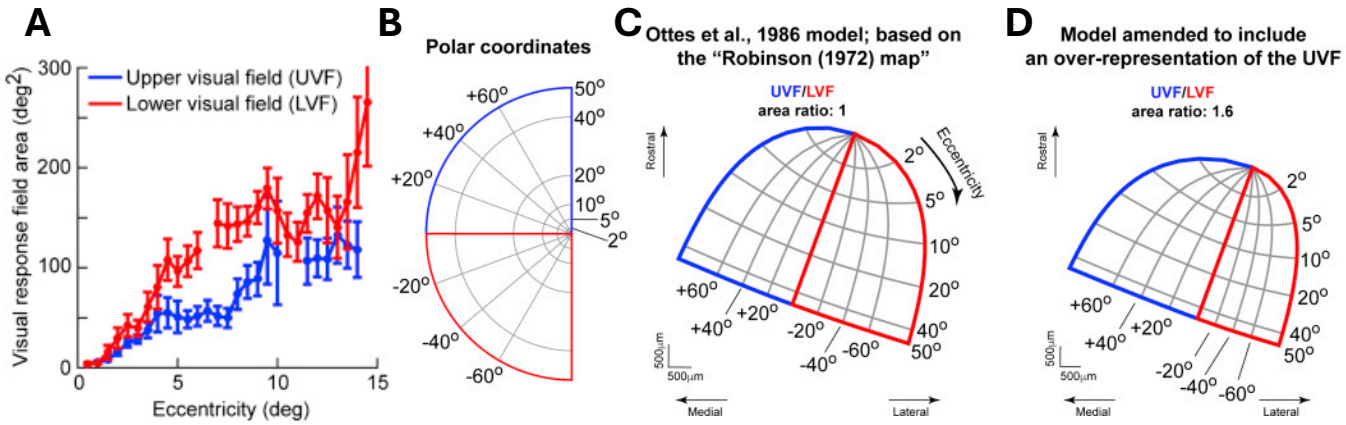

Figure 4. Representation of the upper (blue) and lower (red) visual field in the primate SC. A. Visual receptive field area at increasing eccentricities. From Hafed and Chen (2016); **B.** Visual field in polar coordinates; **C.** Traditional model of SC visual topography, from Ottes et al. (1986) based on Robinson (1972), showing identical upper and lower visual field representations. **D.** New proposed revised model, from Hafed and Chen (2016).

Superficial neurons show stronger, faster responses and smaller receptive fields for the upper visual field (**Figure 4A**), associated to extra-personal space in which objects are far and often smaller. This is consistent with an overall anatomical overrepresentation in the primate SC of the upper visual field (**Figure 4D**) and more accurate and lower-latency saccades towards upward targets (Hafed and Chen, 2016). Indeed, the enhanced visual responses for targets located in the upper visual field is not only present during fixation, but also during peri-saccade vision (Fracasso et al., 2023). During saccades, vision is largely suppressed but some residual visual processing still takes place (peri-saccade vision) specifically for the upper visual field, suggesting a prioritization for detecting extra-personal stimuli for rapid orienting responses also at the time at which perception may be most compromised by saccades. Indeed, even in humans, perceptual performance which is usually higher for stimuli presented in the lower visual field during fixation (Talgar and Carrasco, 2002; Barbot et al., 2021), is enhanced for stimuli within the upper visual field during peri-saccade vision (Fracasso et al., 2023). In this framework, space encoding in the SC shifts from a metric (**Figure 4C**) to a pragmatic format (**Figure 4D**), emphasizing the attentionally most relevant sectors of space (de Malmazet and Tripodi, 2023).

Moreover, the traditional model of its visual topographic organization was derived from a refined visuomotor map based on electrical stimulation (Robinson, 1972; Ottes et al., 1986). Only recently the scientific community has redirected attention to the visual organization of the colliculus (Willett, 2019), offering a revised model (Chen et al., 2019) which challenged the traditional view of the magnification of the macula. This is not surprising, given the difference in receptive field sizes between the visual superficial and deeper motor layers. Nowadays, the rostral representation of the central 10° is estimated to cover between ~35% to ~55% of the SC surface (Chen et al., 2019; Dilbeck et al., 2022; Cynader and Berman, 1972).

Although the magnification factor of the SC is still under debate, the ethological relevance of peripheral stimuli in a “stimulus detection system” can be inferred from the temporal–nasal asymmetry found in humans: target detection, saccadic movements and attentional orienting are facilitated for the temporal (peripheral) hemifield (Lewis and Maurer, 1992; Rothbart et al., 1990; Kristjansson et al., 2004; Rafal et al., 1991; Posner and Cohen, 1980; Dodds et al., 2002). The same temporal-nasal asymmetry has been found in the human SC showing stronger fMRI responses for temporal stimuli compared to nasal stimuli (Sylvester et al., 2007).

1.3 Foveal representation within the rostral SC

Electrophysiological studies of the rostral pole of the SC primarily focused on its role in motor behavior. Here, cells with (para)foveal receptive fields are located superficially, small-amplitude (<2°) saccade-related cells more deeply, followed by cells implicated in the control of visual fixation (“fixation cells”) (Munoz and Wurtz, 1993).

These deeper, 'motor' fixation cells present a prototypical response which is tonically maintained when the monkey actively fixated a visual target. The tonic response remains even if the visual stimulus is momentarily removed, or during smooth pursuit eye movements. Yet, it is interrupted by the onset of a saccade and during its entire duration. At every new fixation, these fixation cells increase their discharge rate for several hundred milliseconds until the next saccade. In light of the presence of microsaccade and fixation cells, the functions traditionally assigned to the rostral SC include gaze-shifting and gaze-holding (referred to as the 'microsaccade' vs 'fixation' hypotheses, respectively; Godlove and Schall, 2016).

Moreover, in primates, which are characterized by foveal vision, an interesting specialization has been documented. Several studies found that only ~4% of retino-tectal projections in monkeys arise from the *pars centralis* of the retina (up to 10° eccentricity; Wilson and Toyne, 1970; Hendrickson et al., 1970; Lund, 1972; Pollack & Hickey 1979, Dilbeck et al. 2022), whereas projections from visual cortex are distributed across the entire SC surface with dense targeting of its anterior region (**Figure 5A**; Wilson and Toyne, 1970; Lund, 1972). The lack of direct retinal afferents to the rostral colliculus suggests that perifoveal information in the primate SC must arise from the brain. It is possible that the rostral SC is innervated not directly by the retina but from other structures of the visual system. Likely more than one structure may contribute to the representation of foveal and parafoveal fields in the SC. A first candidate is the primary visual cortex (V1, Brodmann area 17), which shows the highest level of magnification factor for the central visual field (eccentricities of ~4°-5° of visual angle; Harvey and Dumoulin, 2011; Daniel and Whitteridge, 1961) and sends direct projection to the superficial layers of the

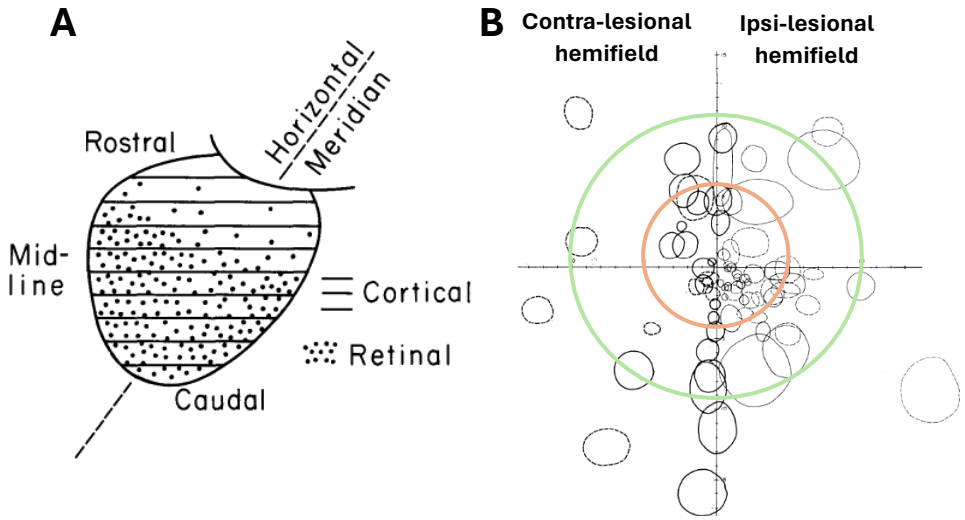

Figure 5. A. Location of labelled cells after retinal degeneration (dots) or cortical lesion (lines) along the rostro-caudal extent of the SC. From Wilson and Toyne (1970). **B.** Receptive filed locations of 31 contra-lesional (heavy lines) and 44 ipsi-lesional (thin lines) SC neurons after ablation of the right area 17. The affected hemifield is on the left. Data are recorded from two monkeys. The orange circle represents 5° eccentricity, green circle 10° eccentricity. Discontinuous and continuous lines represent data the two monkeys. Modified from Schiller et al. (1973).

SC. If V1 was the sole source of foveal responses in the SC, the rostral SC should be largely unresponsive to visual stimulation following ablation of visual cortex. Shiller and colleagues tested this hypothesis in 1974 (Shiller et al., 1974). After lesion of V1, visual responses were generally weaker, showed decreased binocularity and almost one third of the recorded cells showed "patchier" receptive fields, with unbalanced on-/off-responses (in favor of the off-stimulus responses) and no center-surround organization. Beside these alterations in visual responses, they could still record from superficial SC cells with receptive fields located in the foveal region up to 5° eccentricity (**Figure 5B**), but not from neurons located more deeply, where the visual responses appeared to be completely abolished. They concluded that ablation of V1 does not abolish visual responses in foveal superficial SC cells but suggested instead a prominent role of the visual cortex in controlling the information flow to the deeper motor layers. Unfortunately, these considerations cannot completely address the representation of the visual field up to 10° in absence of perifoveal retinotectal projections. Data reported in **Figure 5B** indeed show just very few receptive fields in the perifoveal region between 5° and 10° in the visual hemifield contralateral to the lesion.

Another possibility is that the foveal area in the colliculus is innervated from other structures than V1 that directly reach the superficial SC, such as extrastriate areas (e.g. area MT), the FEF, pulvinar or dLGN. In the FEF, distinct subpopulations of neurons subserve visual fixation and saccades, namely fixation and movement cells. Two subdivisions of FEF are responsible of short (ventrolateral FEF) and long (dorsomedial FEF) saccades. The former receives information about the fovea via retinotopically organized areas (such as V4, TEO, and MT), and from areas where the central field is overrepresented (e.g., caudal TE). The dorsomedial FEF, on the other hand, is innervated by i) parts of retinotopically organized areas where the peripheral visual field is represented, or ii) from areas that emphasize peripheral vision (e.g., V6/V6A and MSTd), or iii) from multimodal and auditory areas (Shall et al., 1995). However, even if lesions in FEF interfere with target selection (Shiller and Tehovnik, 2005), it sounds quite unlikely that a region with no retinal afferents and strongly implicated in saccade generation such as the FEF is the only source of visual foveal representations in the SC.

On the other hand, the dLGN and pulvinar can di-synaptically relay retinal information to the rostral SC (in rats, Taylor et al., 1986; in cats, Altman and Carpenter, 1961). The dLGN is one of the main targets of retinal projections and has a major representation of the central visual field. It is plausible that, in primates, a subpopulation of retinal cells project only to the dLGN, and another only to the SC (Lund, 1972; Michael, 1970; Crook et al., 2008). In the pulvinar, two large visually-driven nuclei, the dorso-lateral (PL) and the inferior (PI) pulvinar, hosts two separated retinotopic maps of the contralateral field with the vertical meridian in common and reversed representations of the rest of the visual field (Bender, 1981). The two representations of the visual fields are quite balanced across eccentricities, covering up to almost 100° eccentricity. PL and PI receive afferents from the deeper and superficial SC, respectively. Both PL and PI project to areas of the cortical ventral stream,

but only PI projects to dorsal stream areas (Kaas and Baldwin, 2019). Both nuclei receive retinotopically-organized visual information through segregated neuronal subpopulation of the same cortical areas (V1-V4, MT, IT; Ungerleider et al., 1983; Pessoa and Adolphs, 2010; Moore et al., 2019). However, the striate projections to PL seem to be limited to only the central 7°, whereas V1 projections to PI seem to cover the entire visual field (Ungerleider et al., 1983). PI and to a lesser extent PL receive direct projections from the retina. In PI, retinal projections seem to be confined to 10° eccentricity in marmosets (Grünert et al., 2021). This overrepresentation of central vision in this retino-pulvinar pathway has been suggested to be critical in establishing the normal connections of cortico-thalamic circuits driving visually-guided behaviors such as precision grasping and object manipulation (Mundinano et al. 2018).

1.4. Retinotopic mapping of the primate SC

Most studies on the topography of macaque SC primarily focused on its motor properties and the control of saccades. The description of its retinotopic organization mainly relied on motor field mapping with electrical stimulation, covering a relatively wide portion of the visual field (~40° eccentricity) (Robinson, 1972; Ottes et al., 1986). Recent electrophysiological investigations of the visual topography of the SC mainly focused on its foveal representation (Chen et al., 2019; Willett, 2019). These authors, proposed a new model which almost doubled the extent of surface representing foveal stimuli (up to 2° of eccentricity) in respect to the traditional model derived from motor field mapping.

On the other hand, the deep location of the SC and its small size hampered neuroimaging studies, such as functional Magnetic Resonance Imaging (fMRI). fMRI methods, however, are ideal to map the visuotopic organization of structures noninvasively, and to perform comparative functional mapping studies across primate species. A first attempt to map the 'spatiotopic' organization of the human SC with fMRI demonstrated the preferential response of each colliculus for the contralateral visual hemifield (DuBois and Cohen, 2000). Subsequent studies implemented more complex stimulation paradigms to extract eccentricity and/or polar angles maps of the human SC (Schneider and Kastner, 2005; DeSimone et al., 2015; Benson et al., 2018; Katyal et al., 2010). Whereas an orderly representation of polar angles is now well-documented, these studies failed to obtain complete and systematic anterior-to-posterior eccentricity maps across-subjects. Constrained by the experimental environment, fMRI mapping procedures of the human SC have been limited to the central portion of the visual field, covering up to 8° - 15° of eccentricity. As a consequence, peripheral visual field representations

have never been investigated in humans. Moreover, even with the largest stimuli used so far (15° eccentricity; Schneider and Kastner, 2005), most of the activity evoked was related to smaller, (para)foveal eccentricities.

1.5. Phase-encoded retinotopic fMRI mapping in humans and macaques

More than one third of the primate brain (~30% in humans, ~50% in macaques; Van Essen, 2004) is responsive to visual stimuli. fMRI is the ideal experimental tool to noninvasively visualize and map brain activity in response to visual stimulation. After its first introduction at the end of the last century (Ogawa et al., 1990), it became the major technique used for exploring sensory and cognitive processes in humans. The extensive spatial coverage afforded by fMRI enables the investigation of functional properties within broad neural networks throughout the entire brain. Notably, fMRI offers a fairly good spatial resolution allowing to measure the topographic organization of brain regions, yet its temporal resolution is comparatively modest. Lastly, its noninvasive nature allows comparative analysis of brain functions between humans and monkeys (see e.g. Vanduffel et al., 2002), thereby bridging knowledge derived from diverse technologies with different spatio-temporal sensitivity used in different animal species.

Applying fMRI in monkeys, e.g. to map the retinotopic organization of the primate SC, is highly useful to relate invasive electrophysiological findings in macaques with noninvasive neuroimaging observations in humans. This is enabled by comparing both methodologies on the same animal model (Klink et al., 2021), or by using the identical experimental procedure in both species (Vanduffel et al., 2002; Armendariz et al., 2019; Ferri et al., 2015). In macaques, achieving fMRI with good spatial resolution poses greater challenges than in humans. The smaller size of the macaque brain, constituting only 1/12th of the volume of a human brain, results in equivalent structures being smaller and more closely located to neighboring structures. Consequently, a comparable level of detail in macaque imaging requires higher spatial resolution, which is typically achieved using stronger magnetic fields. Moreover, investigating cognitive processes necessitates the involvement of awake behaving monkeys engaged in active tasks, which they are thought using operant conditioning techniques. In such cases, the monkey's body movements induce spatiotemporal fluctuations in the magnetic field, leading to susceptibility artifacts in the fMRI images when compared to those acquired in human subjects. A useful and effective strategy to compensate for the need of strong magnetic fields with behaving monkeys is the use of the MRI contrast-agent monocrystalline iron oxide nanoparticles (MION; Vanduffel et al., 2001), which allows to measure cerebral blood

volume changes. The MION signal is spatially more selective and more sensitive than BOLD signals measured in typical fMRI experiments.

The relationship between the fMRI signal and single unit activity is not direct, and predictions should be made with caution when comparing data obtained using different tools. fMRI measures a series of metabolic changes in blood flow, volume and oxygenation which is, most often, correlated with neural activity. This hemodynamic response has been correlated to synaptic activity (local field potentials or LFPs), rather than electrical activity (single- and multi-unit spiking activity; Logothetis et al., 2001). Thus, the fMRI signal is significantly driven by input and local processing relative to the spiking output recorded with electrophysiology. Given the high number of input signals that converge on few spiking cells, the metabolic response could spread (Grinvald et al., 1994) leading to spatially larger 'signals' than those reported by single unit recordings (Tootell at al., 2003). Moreover, fMRI signals cannot disambiguate excitatory and inhibitory responses and mechanisms which, instead, are usually at the base of very difference processes.

To date, the organization of the visual cortex has been extensively studied with fMRI in humans and macaques (Vanduffel et al., 2014), revealing that a substantial fraction in both species exhibits a topographically organized representation of the visual field, commonly referred to as 'retinotopy'. Phase-encoding mapping procedures (Engel et al., 1997; Sereno et al., 1995) have been the preferential tools to map retinotopy. The rationale is to present stimuli that slowly move across the visual field in a cyclical manner in order to induce a traveling wave of activity with a similar cyclical pattern within topographically organized visual areas. The hemodynamic (fMRI) signal acquired is then analyzed using a Fourier analysis to determine, for each voxel, when and where in the visual field the response is the highest, that is, when the stimulus passes through the receptive field of the specific voxel. Two types of slowly moving stimuli have been classically implemented in this method: a wedge that rotates clockwise or counterclockwise around the fixation point, which is used to map polar angle representations, and secondly, a single contracting or expanding annulus, which is used to extract eccentricity maps. The double direction of movement (expanding-contracting and clockwise-counterclockwise) is used to cancel phase errors caused by hemodynamic response lags. Wedges and annuli navigate the visual field as apertures superimposed on different types of high-contrast, dynamic textures used to stimulate optimally the visual system (Zhu et al., 2012; Janssens et al., 2014; Benson et al., 2018). Wedges and rings increase in size as a function of eccentricity to compensate for the cortical magnification (Daniel et al. 1961). By combining the eccentricity and polar angle maps, it is possible to identify borders between retinotopically-organized visual areas (Sereno et al., 1995; Zhu and Vanduffel, 2019). Adjacent areas are separated by the representation of either the vertical or horizontal meridians, and they represent the visual field with a mirror (from the horizontal to the

vertical meridian) or non-mirror (from the vertical to the horizontal meridian) image. The identification of the direction of polar angle mapping orthogonal to the progression of eccentricities allows to extract field sing maps (Sereno et al., 1995) (mirror versus non-mirror visual field representations). Reversals in field sign delineate borders of retinotopically organized areas, with particular precision for areas V1-V2 (Yu et al., 2020) Moreover, for voxels responding to both polar angle and eccentricity stimuli, it's possible to estimate size and location of the population receptive field (pRF) of the specific voxel by combining the phase-locked response during the two types of retinotopic mapping (Dumoulin and Wandell, 2008).

2. Objectives

In this study, we will map the visuotopic organization of the macaque SC with a set of fMRI experiments involving six macaque monkeys and we will pursue three main objectives:

1) We will employ phase-encoded retinotopic mapping to compare fMRI-based monkey retinotopic maps of the SC with the small-field retinotopic fMRI maps obtained in humans (25° diameter).

2) We aim at surpassing the typical limitations of neuroimaging techniques by extending our mapping to include eccentricity and polar angles across a wide visual field of 80° in diameter., as traditionally done with electrophysiological mapping procedures.

By exploiting the wild-field coverage of fMRI and the use of mapping stimuli with different visual field coverage, we will also investigate the *pragmatic* nature of space representations within the SC, and also in comparison to that in a network of cortical (parieto-fontal) and subcortical (pulvinar) regions of the oculomotor/attentional system.

3) We will use stimuli that are fixed to specific locations in the visual field as a complementary procedure to validate some aspects of the retinotopic organization of the SC obtained with phase-encoded mapping procedures.

3. Materials and methods

3.1 Subjects

Six male rhesus monkeys (Macaca Mulatta; 6 – 10 kg) were subjects in this study. All monkeys were implanted with a magnetic resonance (MR) compatible plastic headpost to minimize head movements during training and scanning. The headpost was attached to the skull by ceramic screws and covered by dental cement. Two of the six monkeys were additionally implanted with customized 8-channel (M4, M6) phased-array receive coils to allow sub-mm resolution (f)MRI at a 3T MRI scanner (Janssens at al. 2012, Li et al. 2019, Li et al. 2022). All operations were performed under propofol (3 mL/hour) or ketamine anesthesia (10 mg/kg, Ketalar®, i.m., Parke-Davis, Zaventem, Belgium) supplemented with xylazine (0.5 mg/kg, Rompun®, Bayer, Leverkusen, Germany). Antibiotics (50 mg/kg i.m., Kefzol®, Lilly, Brussels) and analgesics (4 mg/kg, i.m., Dolzam®, Zambon, Brussels) were given daily for 3–7 days following each surgery. The surgical procedures conformed to national, European, and National Institutes of Health (NIH) guidelines for the care and use of laboratory animals. Animal housing and handling were in accordance with the recommendations of the Weatherall report, allowing extensive locomotor and specie-specific behaviors, as social interactions, climbing and foraging. The monkeys were group-housed (cage size of 16-32 m^3 minimum) with cage-enrichments at the primate facility of the KU Leuven Medical School. Animal care and experimental procedures were in conformity with national and European laws (Directive 2010/63/EU) and approved by the Ethical Committee of KU Leuven.

3.2 Behavioral training

All monkeys were trained using operant conditioning paradigms to maintain fixation while they were constrained by their headpost in a natural 'sphinx' position inside a plastic, custom-made primate chair (**Figure 6**; see Vanduffel et al., 2001). The task required to fixate a red dot located in the center of the screen within a ~2°x2.5° virtual window, while visual stimuli were presented in the periphery. Subjects were cued to fixate when the central red dot appeared. To minimize body-motion induced susceptibility artifacts, the animals were trained, using operant conditioning techniques with positive rewards, to keep both hands still inside a small response box in front of the restraint chair. Hand positions were continuously monitored with two pairs of optical fibers that provided a signal when a hand was retracted (**Figure 6**). To be rewarded, the monkeys had to fixate the fixation spot and keep their hands in the correct position. Reward delivery was based on a reward schedule whereby the

interval between consecutive juice rewards decreased systematically (from 1700ms to 900ms inter-reward-intervals) while the monkey maintained its fixation and the hands in correct position. The monkeys were habituated to the sound of MRI acquisitions and the scanner environment, using a "mock" scanner bore to simulate the scanning experience in the training setup.

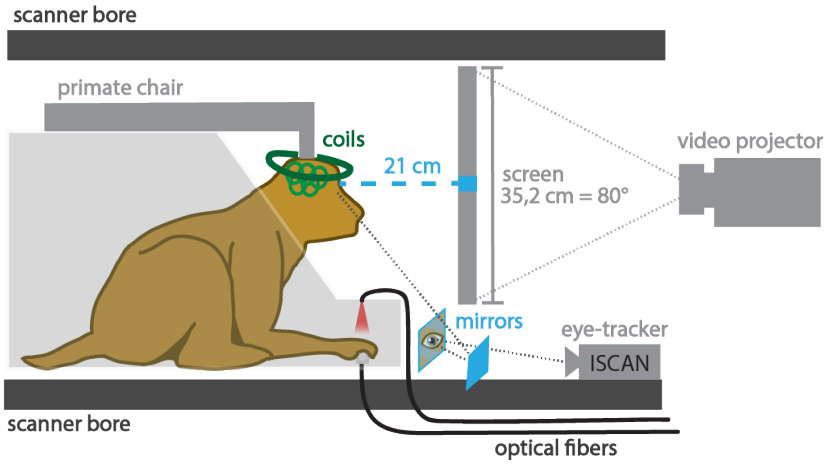

Figure 6. fMRI compatible monkey chair and experimental setup for M1-M2. Schematic representation of the monkey in its plastic restraint box during scanning. The monkey was seated in a natural 'sphinx' position while fixation and its hands were positioned within a response box and continuously checked through optical fibers. The monkey's head was partially constrained by a headpost and covered by the transmit/receiver coils (in green). The eye-tracker monitored the eye from a system of image reflection through two mirrors (in blue). Two pairs of optical fibers monitored the hands position signaling the retraction of the hand.

3.3 Experimental setup

The experiments were performed in a in dark room with the screen monitor as only source of light. Computers with custom-built hard- and software controlled stimulus presentations, reward delivery, and physiological and behavioral data collection. In the scanner room, visual stimuli were projected from a Barco LCD projector at 60Hz refresh rate and 1400 × 1050 resolution onto a translucent screen placed at 21cm (M1-M2; **Figure 6**) and 57cm (M3-M6) from the monkey's eyes. Screen's size and distance were calibrated in order to present stimuli covering 80 (M1-M2) and 25 (M3-M6) visual degrees in diameter. The position of one eye was continuously monitored by an infrared corneal reflection system at 120Hz (Iscan, MA, USA). Due to the short eye-screen distance used for M1-M2, a double-mirror system located below the screen was used to measure eye positions (**Figure 6**): a first mirror, oriented towards the monkey, projected the image of the eye onto a second mirror, which was directed towards the eye-tracker camera. The timing of onset of the stimulus was signaled by a photocell, attached to the bottom-left corner of the LCD monitor and invisible for the monkeys.

3.4 Visual stimuli and experimental design

Retinotopic mapping experiments. We first performed two phase-encoded retinotopic mapping experiments, during which different extents of the visual field were mapped (using wide and small diameter stimuli, respectively). The stimuli consisted of slowly moving clockwise-counterclockwise rotating wedges and expanding-contracting rings covering 0.5°-40° (M1-M2, wide visual field experiment or wVF; **Figure 7A**) or 0.25°-12.5° (M3-M6, small visual field experiment or sVF) radius of visual angle. Wedges and annuli navigated the visual field as apertures superimposed on different types of high-contrast, dynamic textures consisting of either colorful checkerboards with expressive monkey faces (wVF & sVF; Zhu et al., 2012) or walking humans (sVF; Janssens et al., 2014), or a pink-noise background with embedded chromatic objects, which were refreshed at 4 frames per second (fps) (wVF; i.e., the same texture as used by Benson et al., 2018). Wedges and rings increased in size as a function of eccentricity to compensate for cortical magnification (Daniel and Whitteridge, 1961). The moving ring and wedge apertures were used to drive phase-locked activations and for calculating eccentricity and polar angle representations, respectively. Opposing directions of movement (expanding-contracting and clockwise-counterclockwise) were used to cancel phase errors caused by hemodynamic response lags. One full cycle of the wedge/ring consisted of 64s (wVF) or 96s (sVF). Each run contained 6 cycles (wVF) or 4 cycles (sVF) of either the ring or the wedge moving in one of the two possible directions, with a total of 8 stimulus-sequence types.

During the two retinotopic mapping experiments, we used two different annuli-progression timings, reflecting the time the stimulus covered a particular eccentricity: for the sVF we used a pure exponential progression, as commonly used in phase-encoded retinotopic mapping experiments, to compensate for the (exponential) magnification factor of visual cortex. This results in two thirds of a full cycle covering parafoveal

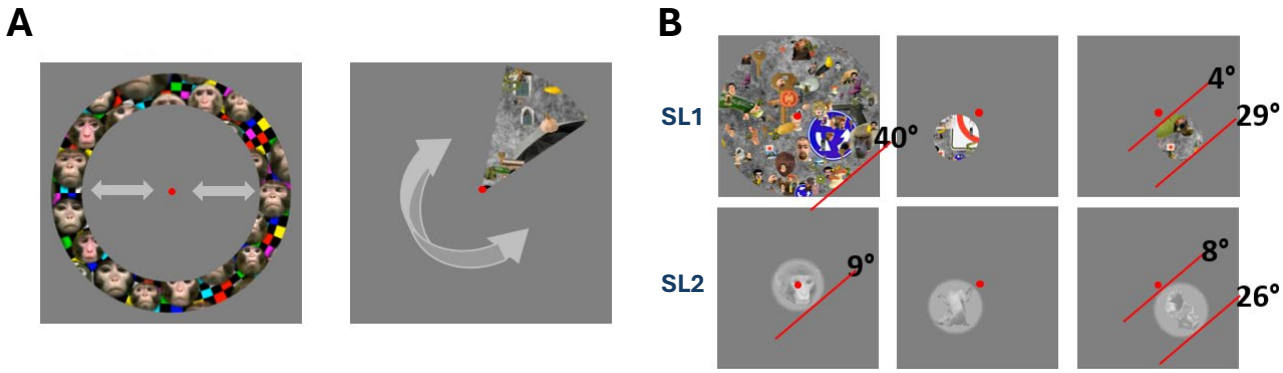

Figure 7. A. Schematic representation of the wVF retinotopic mapping stimuli. Contracting/expanding annuli (left) and a phase clockwise-counterclockwise rotating wedge (right) with a colorful checkerboard and monkey faces, or dynamic objects presented on a pink-noise background. **B**. Spatial localizer experiments. Schematic representation of the stimuli used in SL1 (up) and SL2 (down) and relative stimulus' extent in terms of eccentricity in visual degree (°). The red dot is the fixation point. The red lines were not visible to the monkeys and indicate the eccentricities of the boundary of the stimuli.

(~0-4 visual degrees) eccentricities. For the wVF, instead, we used a mixture between an exponential and linear stimulus progression, which is still suitable for capturing the cortical magnification factor, but also allows to map more peripheral eccentricities more optimally compared to a pure exponential progression.

Spatial localizer experiments. In M1-M2 we also performed separate block-design fMRI experiments (spatial localizer experiments 1-2, or SL1-SL2; **Figure 7B**). We presented spatially restricted stimuli of different sizes: 40° (SL1), 12.5° (SL1) and 9° (SL2) radius; and different eccentricities: center (SL1-SL2), 12.5° (SL1) and 17° (SL2) in the lower left and right quadrants. These stimuli consisted of either static circular apertures superimposed on one of the dynamic textures previously used (chromatic objects belonging to different categories embedded in a pink-noise background, updated at 6 fps; SL1) (Benson et al., 2018), or single categories of b/w monkey faces, bodies, objects, and their scrambled versions (SL2) (Popivanov et al., 2012). An example of each stimulus in each possible spatial location is reported in **Figure 7B** (SL1 in the top row, SL2 in the bottom row). It's important to mention that the specific content of the stimulus wasn't a focus of interest in this study, and no distinction was made between different category types in the SL2 (faces, bodies, objects, scramble) during further analysis (for category-driven activity in the visual cortex, see Panormita et al, 2023).

SL1 was made of three main stimulus conditions (1-3; see **Figure 7B**, upper row) and two control-stimulus conditions (4-5; not used in the following analysis): 1) wide-field (central stimulus with size of 40° radius); 2) peripheral left (peripheral stimulus, covering 4°-29° eccentricity along the central polar angle of the lower left quadrant of the visual field); 3) peripheral right (peripheral stimulus, covering 4°-29° eccentricity along the central polar angle of the lower right quadrant of the visual field); 4) reversed peripheral left (the wide-field central stimulus of 40° radius with a static circular gray patch superimposed, covering 4°-29° eccentricity along the central polar angle of the lower left quadrant of the visual field); 5) reversed peripheral right (the wide-field central stimulus of 40° radius with a static circular gray patch superimposed, covering 4°-29° eccentricity along the central polar angle of the lower right quadrant of the visual field); in (4) and (5) the color of the patch was matching the color of the background of all conditions.

SL2 was made of twelve stimulus conditions, containing 20 stimuli of the same category: 1) central face-category stimuli (central stimuli with size of 9° radius); 2) left peripheral face-category stimuli (peripheral stimuli, covering 8°-26° eccentricity along the central polar angle of the lower left quadrant of the visual field); 3) right peripheral face-category stimuli (peripheral stimuli, covering 8°-26° eccentricity along the central polar angle of the lower right quadrant of the visual field); 4) central body-category stimuli (stimulus' size and position as in (1)); 5) left peripheral body-category stimuli (stimulus' size and position as in (2)); 6) right peripheral body-category

stimuli (stimulus' size and position as in (3)); 7) central object-category stimuli (stimulus' size and position as in (1)); 8) left peripheral object-category stimuli (stimulus' size and position as in (2)); 9) right peripheral object-category stimuli (stimulus' size and position as in (3)); 10) central scramble-category stimuli (stimulus' size and position as in (1)); 11) left peripheral scramble-category stimuli (stimulus' size and position as in (2)); 12) right peripheral scramble-category stimuli (stimulus' size and position as in (3)). An example of face-, body, object-category stimulus for central, peripheral left and peripheral right positions, respectively, is reported in **Figure 7B** (bottom row).

Each block lasted for 30 seconds, consisting of either one stimulus condition or simple fixation. Each sequence contained of one block of fixation (red central fixation dot) followed by the five (SL1) or twelve (SL2) stimulus conditions. A second block started immediately without interruption with a fixation-only epoch which was followed by the same epochs presented in reverse order. Finally, a run finished with a block of simple fixation without stimuli. Across runs, a Latin square design was used to randomize the epochs, with a total of five (SL1) or twelve (SL2) stimulus-sequences.

3.5 fMRI acquisition

After visual fixation performance reached a stable criterion (i.e. above 95%), the monkeys were placed into a horizontal 3T Siemens PRISMA scanner bore. Custom made external (M1-M3, M5) or implanted (M4, M6) coils were used for scanning: a local single loop transmit coil positioned over the head, and 10-channel (M1-M2) and 8-channel phased-array receiver coils positioned tightly on each side of the head (M3, M5) (**Figure 6**). Immediately before scanning, monocrystalline iron oxide nanoparticle (MION, Feraheme, AMAG Pharmaceuticals; 8-11mg/kg) diluted in an isotonic saline buffer was injected into the femoral/saphenous vein to improve the contrast-to-noise ratio (CNR) and to avoid contribution of superficial draining veins (Vanduffel et al. 2001). To minimize the risk of iron accumulation, 1g/day deferoxamine mesylate (Desferal, Novartis; intramuscular injection) and 60mg/kg/day deferiprone (Ferriprox, ApoPharma; oral administration) were administered during and immediately after the scanning period, for 10-15 days, until serum iron and ferritin reached lower but stable levels.

Reference anatomical image. Before the experiments, in a separate session with anesthetized monkeys (ketamine-xylazine anesthesia), 12/15 T1-weighted 3D magnetization prepared rapid gradient echo (MPRAGE)

and 4 T2-weighted (VanEssen) high-resolution images were acquired for each monkey [0.4mm isotropic voxel size; repetition time (TR) = 2700ms; echo time (TE) = 3.5ms; flip angle (α) = 9°; inversion time (TI) = 882ms; in-plane field of view (FOV) = 104 x 128 mm; matrix size 250 × 320 × 208) to be used as a high-resolution reference anatomical image.

fMRI. Each functional scan consisted of T2* weighted echo echoplanar whole-brain images (EPI). Functional images have been acquired at different resolutions based on the type of coils used: 1.25mm isotropic voxel size with external coils for M1-M2, M4, M5 (TR = 1000ms; TE = 18/17ms (M1/M2) and 22/21ms (M4/M6); FOV = 84 x 84 mm; α = 90°; matrix size 140 × 140 × 48) and 0.6mm isotropic voxel size with implanted coils for M3,M6 (TR = 3000ms; TE = 22ms). For better registration between the EPI template image and the anatomical reference images (MPRAGE), at the beginning of each scanning day, a 3D gradient echo (GRE) image and a gradient recalled echo field map (GRE-FM) were acquired for each monkey at the same EPI voxel resolution. The field maps contained two images with different TE (TE1 = 6.48 ms, TE2 = 0 8.94 ms; α = 55°; matrix size 140 x 140 x 66) and were used to correct for EPI distortions caused by magnetic field inhomogeneity. Only scan sessions with excellent behavioral performance (above 94% for M1-M2 and 90% for M3-M6 of the total scan duration) were considered for statistical analysis. Data were acquired in 2-5 session for each monkey. **Table 1** shows the number of utilized runs for each monkey within each experiment.

Table 1. Number of runs used for each monkey for the analysis of the retinotopic mapping (w/sVF) and spatial localizer (SL1-2) experiments.

Monkey	w/sVF	SL1	SL2
M1	56	56	48
M2	72	50	50
M3	62	-	-
M4	63	-	-
M5	65	-	-
M6	56	-	-

3.6 Data analysis

Anatomical image segmentation and flattening procedures. Reference anatomical images were created by averaging all high-resolution T1-w images acquired in the single session with the anesthetized animal, to improve signal-to-noise (SNR) ratio. Cortical segmentation and surface creation was performed by applying automatic white matter segmentation and surface reconstruction in Freesurfer (Dale et al., 1999; Fischl et al., 1999) and, only for M1, adjusted by using an adapted pipeline from the non-human primate version of the Human Connectome Project (HCP) (Autio et al., 2020). T2-w images were used to eliminate the effect of cerebrospinal

fluid and pial veins during surface segmentation. Fine-tuned corrections were performed manually on the automatically reconstructed pial surface. The resulting gray-white matter boundary was used to create a 3D surface model of each subject's hemisphere, then inflated to obtain a smooth model of the brain where both sulci and gyri were visible on the surface. Virtual cuts were applied from the mid-brain (i.e. along the calcarine sulcus) to unfold each subject's surface hemisphere into a 2D flat map. Cortical and subcortical activations were analyzed in volumes and cortical activations were also visualized on flat maps with a statistical threshold of $p<0.0001$ (retinotopy experiments) or $p = 0.001$ (spatial localizer experiments).

fMRI image reconstruction and preprocessing. Pre-processing was performed using Freesurfer (http://surfer.nmr.mgh.harvard.edu). The "optimized generalized autocalibration partially parallel acquisitions" (GRAPPA) reconstruction method (Hoge and Polimeni, 2016) was used to reconstruct the EPI images to decrease artefacts caused by body movements. EPI images were masked to remove non-brain voxels, motion-corrected using the single, best EPI image as a template (6 degree of freedom rigid image-based motion correction) and slice-timing corrected with a slice-by-slice undistortion correction performed according to the same template using a B-spline grid-based nonlinear registration method to reduce frame-to-frame distortions.

General linear model (GLM) analysis. For the phase-encoded retinotopy experiments, retinotopic (polar angle and eccentricity) and field-sign maps were extracted following the procedure suggested by Sereno et al. (Sereno et al., 1995) using Freesurfer. For the spatial localizer experiments, *t*-score maps were calculated by fitting the GLM with Freesurfer. Temporal signal-to-noise ratio (tSNR) maps were also calculated for each monkey within each experiment by averaging the tSNR at each session using Freesurfer. Condition regressors were generated by convolving the predictors by a canonical gamma fit impulse response function (IRF) for the MION signal (Leite et al., 2002; Vanduffel et al., 2001). The four dummy scan images acquired at the start of each run were used to allow the scanner to reach equilibrium, but were not included in the GLM analysis. The mean fixation performance of the analyzed runs exceeded 94% of the run duration for every monkey, then no further regressors related to the fixation performance were used for the statistical analysis.

Registration between EPI and structural images, and cortical surface projections. The results of the GLM analysis in the 3D volume were registered to the reference anatomical image via an intermediate 3D GRE image acquired in the same session as the functional images using Freesurfer (http://surfer.nmr.mgh.harvard.edu) and JIP toolkit provided by Joseph Mandeville (http://www.nitrc.org/projects/jip). A fieldmap-based EPI distortion correction (Jezzard and Balaban, 1995) was performed using FSL (Jenkinson et al., 2012) for a better alignment between functional and structural data. The results were then projected on cortical surfaces. In order to minimize

contamination from cerebrospinal fluid, white matter and pial vein signals, and to reduce the cross-talk between superficial layers in the two banks of neighboring surfaces of the same sulcus (Glasser et al., 2013) activations located between 20% and 80% of the cortical depth (between the grey-white matter boundary and pial surface) were sampled in steps of 10% and averaged to create the surface maps. No spatial smoothing was applied on the volume data for the analysis, and only for visualization purpose heat kernel smoothing [Full Width at Half Maximum (FWHM) = 4 mm] (Chung et al., 2008) was applied on surface data.

3.7 Definition of Region Of Interest (ROI)

Field sign maps and striatal cortical ROIs. Functional ROIs in the striate cortex were defined in each monkey's native space, separately for each hemisphere. Field sign maps (Sereno et al., 1995) extracted from retinotopy maps were used to identify borders of the early visual cortices (V1, V2) in M1-M2. Field sign mapping allows to identify reversals in the direction of polar angle mapping orthogonal to the one of eccentricity. By calculating the local visual field sign (mirror image versus non-mirror image representation) it is possible to determine the borders of retinotopically organized visual areas such as V1 and V2.

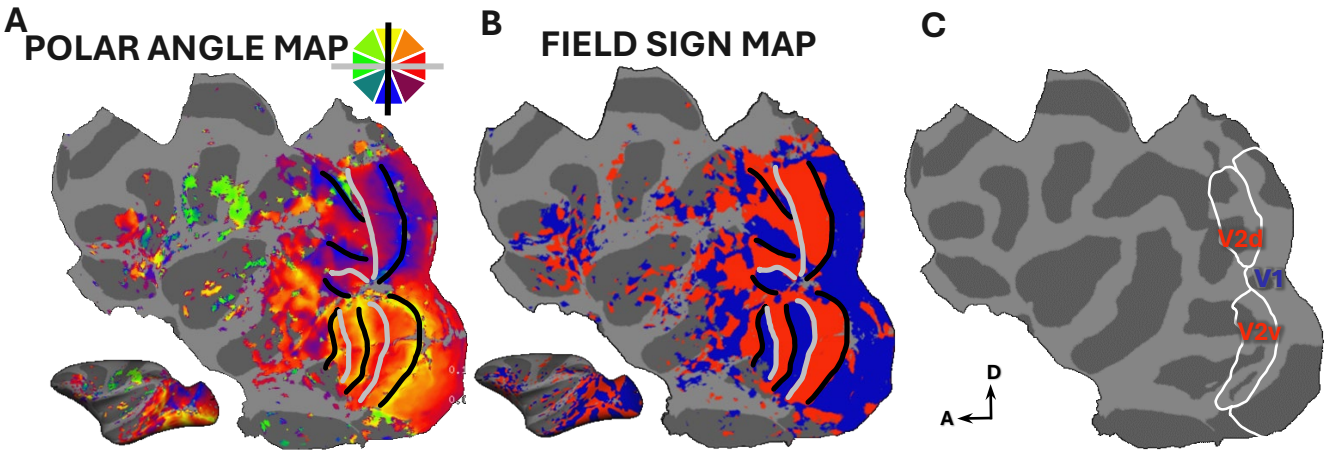

Figure 8. Retinotopy and functional ROIs on inflated surfaces and flat maps for the left hemisphere of a representative subject (M1). A-B. Polar angle ($p < .0001$; **A**) and field maps ($p < .0001$, FWHM = 8; **B**) of the left hemisphere of M1. Black and grey lines represent vertical and horizontal meridians, respectively. The small polygon at the top of the polar angle map is a schematic representation of the visual field showing the color code for the map and meridians. Red and blue colors in B represent the mirror image versus non-mirror image representation that is, the mirror-reversal of the retinotopic organization of polar angles across meridians (A). **C.** Borders (in white) of area V1, dorsal V2 (V2d) and ventral V2 (V2v).

Un-thresholded eccentricity and polar angle maps were used to generate field sign maps for each monkey, then a threshold mask ($p = 0.0001$) was applied. The resulting maps with different values of Full Width at Half

Maximum (FWHM = 4 and 8) was used to draw V1-V2 labels (**Figure 8**). The functionally identified V1-V2 borders were located along the posterior lip of the lunate sulcus, in accordance with their reported anatomical location. The resulting surface labels were converted in volumetric ROIs to be used in further statistical analysis.

Cortical parcellation and ROIs. To parcellate M1-M2 cortical regions, we selected the MEBRAINS Monkey Brain Atlas (Balan et al., 2023; https://www.ebrains.eu/tools/monkey-brain-atlas) and Cortical Hierarchy Atlas of the Rhesus Macaque (CHARM; Jung et al., 2021; Reveley et al., 2017; https://afni.nimh.nih.gov/pub/dist/doc/htmldoc/nonhuman/macaque_tempatl/atlas_charm.html) which offer a comprehensive parcellation of the macaque cerebral cortex, dividing it into discrete regions based on a combination of functional (MEBRAINS), and histological (CHARM) criteria. The MEBRAINS Monkey Brain Atlas is a comprehensive resource that provides in-depth insights into the anatomy, connectivity, and functions of the macaque monkey brain. It includes detailed information about the organization of the monkey brain at multiple levels, ranging from the microscopic level to the macroscopic level of the entire brain. It integrates complementary structure, function, and connectivity, including cyto-, myelo- and receptor architecture and function (e.g. probabilistic retinotopic maps). The multilevel macaque brain builds on the MEBRAINS Template, a nonlinear symmetric population-based monkey template which reflects the macroanatomical scale as a unifying principle of organization. The CHARM atlas is defined in the coordinates/space of the NMT v2 asymmetrical template, and parcellates the macaque cortex at different hierarchical, spatial scales. The finest level is based on the D99 atlas, while the broadest level forms four cortical lobes. Between these levels, regions are progressively grouped to form increasingly large composite structures. This allowed to choose a wider scale of investigation for this study, dividing each lobe in 3-9 macro-areas based on anatomo-functional similarities (e.g. superior parietal gyrus, inferior parietal gyrus, and intraparietal sulcus for the parietal lobe).

Anatomical cortical ROIs were defined in each monkey's native space, separately for each hemisphere. Coregistration of the monkey brain with the atlases template (affine and nonlinear transformations) and the subsequent application of the atlas onto the monkey's native space were performed using ANTs (https://github.com/ANTsX/ANTs). Based on atlas' cortical labels, the cortical regions were further processed to generate ROIs within the whole brain. This step was carried out using FreeSurfer (http://surfer.nmr.mgh.harvard.edu) and MATLAB (MATLAB and Statistics Toolbox Release 2012b, The MathWorks, Inc., Natick, Massachusetts, United States).

Subcortical segmentation and pulvino-tectal ROIs. For all monkeys (M1-M6), the superior colliculus (SC) and medio-lateral/inferior pulvinar (mlPul, iPul) have been manually segmented based on anatomical landmarks and

in accordance with different atlases to enhance the accuracy and consistency of ROI extraction. Specifically, we referred to the Paxinos Rhesus Monkey atlas (Paxinos et al., 2000), SARM atlas (Hertig et al., 2021), and the NeuroMaps macaque atlas (Dubach et al., 2009; Rohlfing et al., 2012; Bakker et al., 2015), which have been widely recognized and validated in the field of neuroanatomy. The extraction of subcortical ROIs was performed on the high-resolution anatomical (T1-w and T2-w) images (0.4mm isotropic voxel size) within each monkey's native space for each hemisphere, with reference to precise anatomical landmarks, namely 1) the habenula and brachium for the identification of the SC rostral and lateral borders, respectively (Borra et al., 2014; May, 2006), and 2) the caudal side of the lateral geniculate nucleus for the identification of the Pul rostral border.,

3.8 Statistical analysis

The ROIs which we defined above (see 3.7) were utilized in several statistical analyses, including SNR assessment, volumetric analyses, and region-specific comparisons, performed using custom-made scripts in MATLAB (MATLAB and Statistics Toolbox Release 2012b, The MathWorks, Inc., Natick, Massachusetts, United States) and R (R Core Team 2022,; R Foundation for Statistical Computing, Vienna, Austria https://www.R-project.org/).

Temporal SNR (tSNR) assessment. Since the subcortical structures are located deep in the brain (i.e., at a relatively large distance from the receive coils), we analyzed the temporal SNR (tSNR) to assess the quality of the signal. tSNR maps were extracted for each experiment using Freesurfer, with the following formula:

$$tSNR = \frac{offset}{SD_{residuals}} \quad (1)$$

where $offset$ is the regression coefficient of the regressor of all TRs (e.g., TR = 1 sec) and $SD_{residuals}$ is the standard deviation of residuals. After the full model is fit, the estimated time course is subtracted from the actual time course to extract the residuals. Then, the resulting tSNR is similar to the one extracted with the classical formula (temporal mean signal of a voxel divided by its standard deviation over time), but calculated after removing task signal and nuisance regressors. tSNR levels were compared between hemispheres (i.e. left/right SC), or across different parts of the same ROI (i.e. caudal vs rostral SC) using a two-sample t-test (for single comparisons, i.e., LH vs RH) and one-way ANOVA with Bonferroni correction (for multiple comparisons, i.e., LH rostral/caudal versus RH rostral/caudal).

Visual field mapping of the SC. Phase values extracted from the eccentricity maps were converted in visual degrees. The estimation of the eccentricity values in visual degree was performed through linear interpolation between the two known eccentricity values (in visual degree) associated to the first step (0.5° in wVF; 0.25° in sVF) and last step (40° in wVF; 12.5° in sVF) of the annulus progression, using as interpolation points the phase values associated to each step (N step = 64, in wVF; N step = 32, in sVF).

Functional differences between the left and right SC along the rostro-caudal axis. Number of voxels activated by the retinotopic stimuli, median and interquartile range (IQR) of polar angle or eccentricity phase values were extracted for each coronal slice along the rostro-caudal extent of the SC. The medians were used to indicate the (median) eccentricity/polar angle of the stimulus evoking the largest response in all voxels of that slice, whereas the IQR as the range of eccentricity/polar angle of the stimulus evoking the largest response in all voxels of that slice. To allow fair comparisons across monkeys with varying SC sizes, the total distance between the rostral and caudal pole of the SC was normalized by dividing it in percentiles.

To evaluate interhemispheric differences between the retinotopic maps along the rostro-caudal axis of the SC, a Lateralization Index (LI) was calculated for each coronal slice, separately for eccentricity (LI_{ecc}) and polar angle (LI_{pol}) representations (phase values; at a threshold, $p < 0.0001$). The following classic formula (Seghier, 2008) was used:

$$LI = f \cdot \frac{N_X - N_Y}{N_X + N_Y} \quad (2)$$

where X and Y are left (LH) and right (RH) hemispheres, respectively, and N is the number of voxels significantly activated by polar angle (LI_{pol}) or eccentricity (LI_{ecc}) varying stimuli at each slice in each hemisphere. The factor f is a scaling factor that defines the range of LI values. Here, it's held to 1 so that the LI can vary between -1 for a complete RH dominance to +1 for a complete LH dominance. LIs of |0.3| indicate that the contribution of one hemisphere is two times higher than the other; LIs of |0.5| indicate a threefold interhemispheric difference in spatial representations. Instead of using arbitrary thresholds, the LI threshold (LI_{TH}) was calculated empirically (Seghier, 2008) using the averaged LI ($mean_{LI}$) and its standard deviation (sd_{LI}) from the distribution of LI values of all coronal slices of both eccentricity and polar angle maps, with the following approach:

$$LI_{TH} = \begin{cases} mean_{LI} - sd_{LI} & mean_{LI} > 0 \\ mean_{LI} + sd_{LI} & mean_{LI} \leq 0 \end{cases} \quad (3)$$

The distribution of LIs made of LI of each slice related to eccentricity (LI_{ecc}) and polar angle (LI_{pol}) varying stimuli were grouped into a single distribution of LIs for the calculation of the LI_{TH}, in order to allow comparisons between indices related to the two different stimuli. The LI_{TH} was calculated on this distribution using two sd_{LI}, obtaining a quite conservative value of $|0.4|$. Besides the amplitude of LIs in single slices, statistical tests were performed on the rostro-caudal distributions of LIs to assess the hemispheric dominance at the level of the entire SC. Since the data were not normally distributed (Shapiro-Wilk test), nonparametric Wilcoxon Tests were used for the statistical analysis of potential interhemispheric biases.

Then, the rostro-caudal progression of eccentricity representations was analyzed, separately for the left and right hemisphere, based on the median eccentricity of the stimulus evoking the largest response in all voxels of single slices. Median, first and third quantiles of the distribution of eccentricity values of each coronal slice. were used to create the antero-posterior distribution of eccentricity representations. The relationship between eccentricity representations and their anatomical location along the rostro-caudal axis was tested within each hemisphere by fitting a linear model with MATLAB on median eccentricity values for 20 equal partitions along the caudo-rostral axis of the SC.

These analyses (LI index and progression of eccentricity representations along the caudo-rostral axis of the SC) were performed first at single-subject level, then on the group-averaged level (separately for the sVF and wVF experiment).

Further statistical analyses were performed at single-subject level to evaluate the degree of interhemispheric bias for polar angle representations along the rostro-caudal extent of the SC, in terms of interquantile range (IQR) of polar angle (phase values) stimuli evoking the largest response in all voxels of single slices, using the nonparametric Wilcoxon test.

On the group-averaged level, we calculated the number of voxels significantly activated ($p < 0.001$) by the presentation of spatially-restricted stimuli (SL1-SL2) at each slice along the rostro-caudal axis of the SC, to identify the sector of the SC which is optimally activated by spatially-restricted stimuli (SL1-SL2). T-scores maps (threshold $p < .001$) were calculated by contrasting stimulus versus rest. In the SL1, t-scores maps were calculated from either full-field or peripherally-restricted stimuli versus fixation. Given that we aimed to isolate only visually-driven activity in this test, in SL2 no distinction was made between different category types (faces, bodies, objects). Therefore, the stimulus categories were grouped together and contrasted against fixation for the stimuli covering different portions of the visual field (i.e. central or peripheral).

Upper/lower, center/periphery, eccentricity/polar angle biases and whole-brain analysis. Quantitative analyses were performed at the group level in subcortical (i.e. pulvinar) and cortical (i.e. LIP, FEF, V1, V2) ROIs to estimate asymmetries in the representations of specific sectors of visual space (e.g. between central and more peripheral portions of the visual field, or between upper and lower hemifields). We calculated the degree of representational bias, in the percent volume of the ROI (i.e., the fraction of voxels in that ROI) activated by stimuli presented centrally (0.5° - 10°), peripherally (10° - 40°) (for the wVF experiment), or in the upper and lower hemifield (for the wVF, sVF experiments). The cutoff of center-periphery asymmetry was arbitrary selected at 10°. The biases were first calculated within single monkeys, and then averaged at group level, separately for the wVF and sVF experiments. Different statistical thresholds ($p < .01$, $p < .0001$) were used for this analysis. An asymmetry index (AI) was calculated within each region, separately for polar angle (for the sVF and wVF experiments) and eccentricity representations (wVF experiment). The same approach as in formula (2) was used, where X and Y were upper/center visual and lower/peripheral visual subfields, respectively, and N was the number of voxels significantly activated for X and Y in each ROI in each hemisphere. The AI threshold (AI_{TH}) was calculated empirically, using the same formula as in (3), separately for the distribution of LIs related to upper/center visual field and the distribution of LIs related to lower/peripheral visual fields, since these two distributions were reflecting independent measurements not directly comparable. The AI_{TH} was calculated at one sd_{LI}, obtaining values of |0.2| (polar maps) and |0.3| (eccentricity maps).

Finally, a whole-brain analysis was used to test in a large number of ROIs for the sensitivity for either polar angle or eccentricity varying stimuli alone, or both. Based on the total number of voxels of each ROI, we first calculated the fraction of voxels activated (at a threshold, $p < 0.0001$) by both eccentricity and polar angle varying stimuli (referred to as 'conjoined map'). Then, we calculated the fraction of voxels activated ($p < 0.0001$) by only eccentricity varying stimuli (referred to as 'only ecc map') by removing from the number of voxels activated by eccentricity varying stimuli the number of voxels activated by polar angle varying stimuli. We used the same approach, but reversed, for the calculation of the fraction of voxels activated ($p < 0.0001$) by only polar angle varying stimuli (referred to as 'only pol map'). We either merged or kept the data from both hemispheres separated. Given the small sample size (a total of 6-12 hemispheres), a nonparametric bootstrap t-test with pooled resampling method (10000 permutations; Dwivedi et al, 2017) was used for the statistical analysis. Bonferroni correction was applied to correct for multiple comparisons. To complement the analysis, a lateralization index (LI) was calculated within each region, separately for the number of voxels of conjoined, only ecc and only pol maps. The LI_{TH} was calculated on the distribution of LIs of all maps of all ROIs, at one sd_{LI}, obtaining a value of |0.2|.

4 Results

4.1 Wide-field and small-field retinotopic maps in the SC

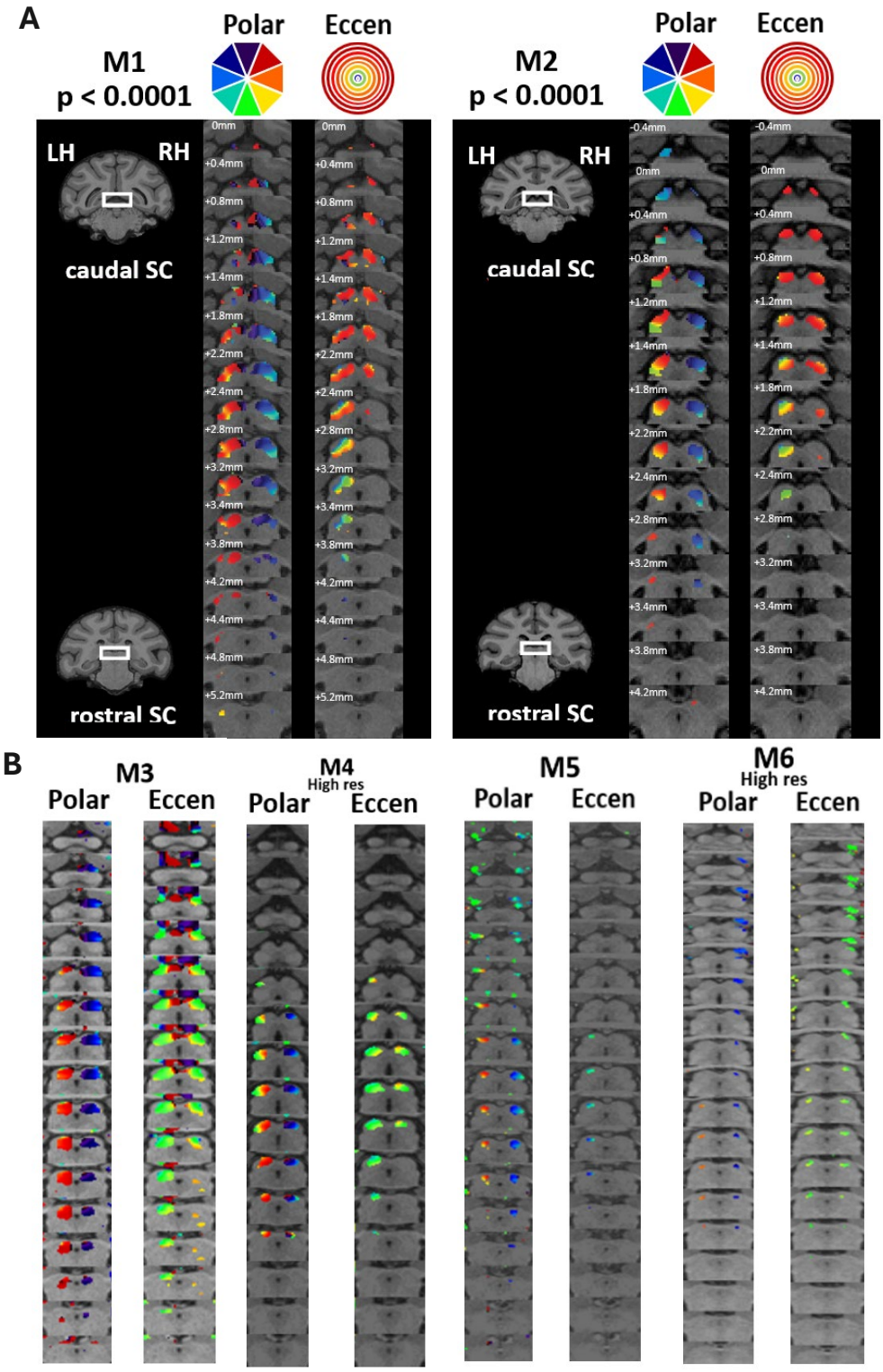

Figure 9. Retinotopic maps derived with wide-field (wVF; A) and small-field (sVF; B) stimuli (threshold p < .0001) for individual slices along the caudo-rostral extent of the SC. A. wVF polar-angle (first column) and eccentricity (second column) maps are shown overlying coronal T1-weighted slices of the SC (subjects M1-M2). On the left, the entire anatomical (T1-weighted) image of the first and last coronal slice covering the SC is shown. White boxes indicate the location of the most caudal and rostral slices of the SC. The small polygons at the top of the maps are a schematic representation of the visual field showing the color code of the polar angle and eccentricity maps, respectively. The position of each coronal slice in mm relative to the interaural line is shown at the upper-left corner; **B.** sVF polar-angle (first column) and eccentricity (second column) maps are shown overlying coronal T1-weighted slices of the SC (subjects M3-M6). Data from M4 and M6 were acquired at higher spatial resolution (0.6mm isotropic voxel size) in respect to M1-M3 and M5 (1.25mm isotropic voxel size). Color code as in (A).

We obtained polar angle and eccentricity maps of the primate superior colliculus (SC) using phase-encoded retinotopic stimuli covering up to 40° (wVF) and 12.5° (sVF) degrees eccentricity. Previous retinotopic mapping experiments in our lab did not find consistent differences between maps derived using phase encoding retinotopic mapping stimuli with different textures (e.g. checkerboards with dynamic faces or bodies; Janssens et al., 2014). Therefore, we pooled data from the different experiments, independent of textures, to increase our statistical power. The combi nation of a high fixation performance (> 94% accuracy), the control of hand positions, together with the use of contrast agents and biologically-relevant phase-encoding retinotopic mapping stimuli, allowed us to obtain high-quality subcortical retinotopic maps beyond what has been obtained thus far in the SC.

Figure 9A shows retinotopic maps obtained with large stimuli covering 40° eccentricity ($p < .0001$) in M1 and M2 (wVF) for individual slices along the entire caudo-rostral extent of the SC. We obtained detailed polar angle and eccentricity maps in all monkeys (see **Figure 9B**). Polar angle maps revealed a clear contralateral representation of the visual field in the SC. The fovea was represented rostro-laterally, the periphery more caudally, and the upper and lower quadrants in the medial and lateral sectors of the SC, respectively. Smooth progression of eccentricity and polar angles values can be observed orthogonally along the rostro-caudal and medio-lateral axis, respectively.

Retinotopic mapping experiments with smaller stimuli (12.5 deg eccentricity) in M3-M6 (sVF; $p < .0001$; **Figure 9B**) led to relatively smaller activation maps in the SC compared to the wVF experiment, a difference that was particularly evident in M5-M6 (see also **Table 2**).

Table 2. Volume (number of voxels, resampled at 1mm isotropic) of anatomically defined SC ROIs and percentage of voxels activated in the eccentricity (ecc) and polar angle (pol) mapping experiments ($p<0.0001$), per hemisphere.

		N voxels ROI volume		% activated voxels			
				ecc maps		pol maps	
		LH	RH	LH	RH	LH	RH
wVF	M1	1875	1978	29,07	11,78	35,25	45,30
	M2	1410	1355	16,52	12,77	27,02	25,54
sVF	M3	1408	1430	44,18	29,86	33,45	43,57
	M4	1186	1190	20,24	10,50	22,18	19,33
	M5	1092	1029	3,85	0,00	8,15	17,69
	M6	1520	1488	3,09	4,84	1,71	3,70

	Average % activated voxels and standard deviation			
	ecc maps		pol maps	
	LH	RH	LH	RH
wVF	22,79 ± 8,86	12,27 ± 0,7	31,13 ± 5,82	35,41 ± 13,97
sVF	17,83 ± 19,25	11,3 ± 13,1	16,37 ± 14,24	21,06 ± 16,56

Interestingly, the sVF mapping experiment confirmed the lateromedial distribution of polar angles, but failed to provide a reliable and complete eccentricity map along the anterior-to-posterior extent of the SC in most monkeys (M4-M6). The representations of small eccentricities were observed posteriorly (**Figure 10A**, sVF). More specifically, the group-averaged median eccentricity represented at 75% from the rostral pole was 3° (see **Figure 10A**, LH sVF). In other words, stimuli of 3° eccentricity evoked responses covering almost 3/4 of the rostro-caudal axis. Reversely, in the wVF experiment, the same area of the SC was activated by stimuli covering 7 times larger eccentricities (the group-averaged median eccentricity represented at 75% from the rostral pole was 20°, see **Figure 10A**, LH wVF), and almost half of the caudo-rostral extent of the SC was activated by stimuli covering up to 10° eccentricity (see **Figure 10A**, LH wVF).

4.2 Interhemispheric asymmetry within the rostral SC

4.2.1 Interhemispheric asymmetry for eccentricity but not polar angle in rostral SC

We obtained clear and bilateral polar angle maps in all six monkeys (in the wVF and sVF experiments; see **Figure 9**). The range (interquartile range; IQR) of polar angle (phase) values was calculated in each coronal slice along the rostro-caudal axis, separately for hemispheres in each monkey. We compared the distribution of IQRs in the left (LH) and right (RH) hemispheres, separately for each monkey, and we found no significant difference for all monkeys (Wilcoxon test, **Table 3**).

Table 3. Wilcoxon Rank Sum tests on interhemispheric difference in IQRs of polar angles (phase) values.

		Rank sum	p
wVF	**M1**	301	0,1689
	M2	198	0,8343
sVF	**M3**	291,5	0,3073
	M4	214	0,6111
	M5	206	0,9057
	M6	307	0,0824

Although the polar angle maps do not differ between hemispheres of all monkeys, an interesting interhemispheric asymmetry can be observed in the eccentricity maps of all monkeys, regardless the size of the stimuli used (i.e., in the wVF and sVF experiments). The asymmetrical effect was related to (1) the anatomical distribution of responses to eccentricity-varying stimuli and (2) the degree of the anterior-to-posterior progression of representations of gradually larger eccentricities.

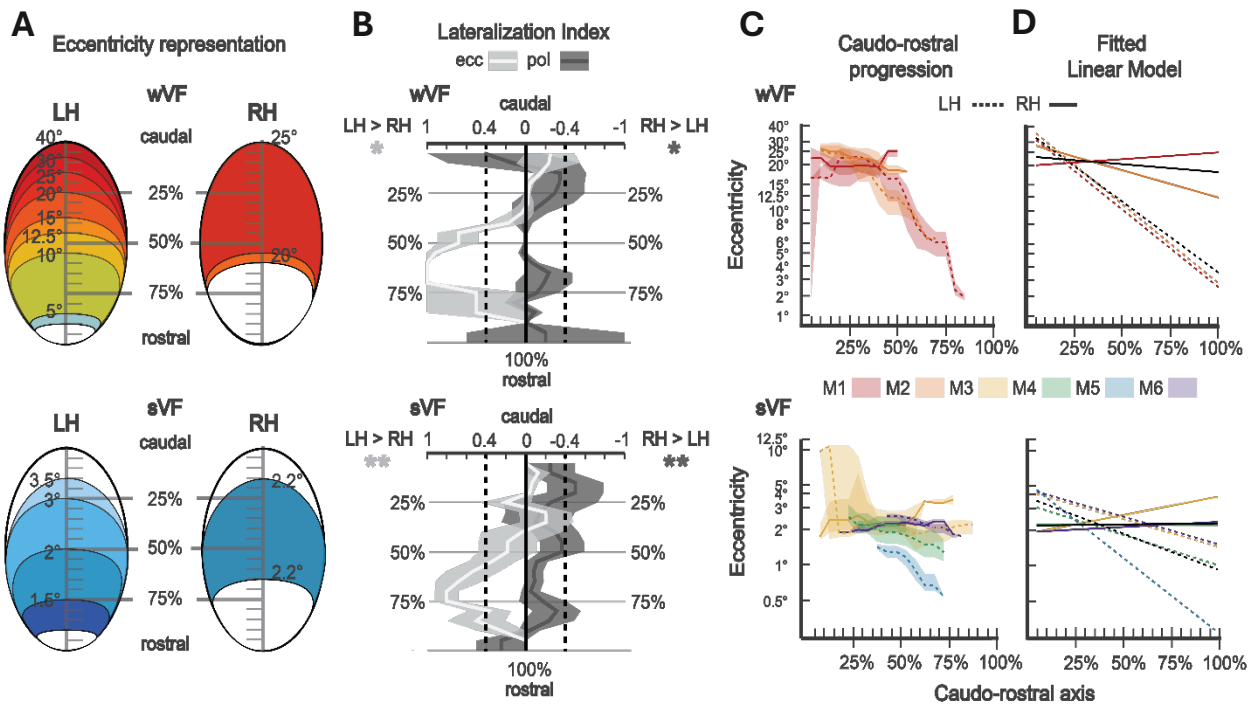

Figure 10. Left-right SC asymmetries observed during the wVF (upper row) and sVF (lower row) experiments along the caudo-rostral axis of the SC (expressed in percentiles of the SC across monkeys). A. Schematic reconstruction of the topographic representation of eccentricities in the left and right hemispheres. Radial lines from the rostral pole indicate group-averaged median eccentricities represented at that location. Representative eccentricities are shown for the LH. Given the limited range of eccentricities within the right SC, the rostral-most and caudal-most median eccentricity representations are only shown for the RH. White areas indicate non-responsive regions across all monkeys. Color code as in Figure R1; **B** Group-average lateralization index (LI) of eccentricity (light gray) and polar angles (dark gray) maps ($p < .0001$). Shadowed areas indicate standard error (SEM) across monkeys. Dashed lines indicate the calculated LI threshold at 2 standard deviations. Statistical tests were performed on the entire extent of the ROIs: Wilcoxon test; *** $p \leq .001$, ** $p \leq .01$, * $p \leq .05$; **C.** Median eccentricity representations and relative IQR (shadowed area) extracted from single coronal slices along the caudo-rostral axis and expressed in percentiles for the LH (dotted line) and RH (straight line), separately for each monkey (colors from red to purple); **D.** Fitted linear model on the median eccentricity representation for single monkeys (colors) or for the average data (black). Conventions as in C.

Firstly, only the left SC responded to eccentricity-varying stimuli along the entire anterior-to-posterior extent of the SC, whereas activity in the right SC, induced by the same stimuli, was limited to its caudal and middle sectors (**Figure 9**). This emerged at the population level in both the sVF and wVF experiments. For each coronal slice along the rostro-caudal axis, the number of voxels activated by eccentricity- and polar angle-varying stimuli in LH and RH and the relative lateralization index (LI) were calculated for each monkey and then merged between monkeys of the wVF (M1-M2) and sVF (M-M6) experiments. The distribution of number of voxels activated across slices by eccentricity-varying stimuli differed significantly between LH and RH ROIs in both the wVF and sVF experiments (Wilcoxon test, p(wVF) = 0.019, p(sVF) = 0.011) (**Figure 10B**). The lateralization index (LI) calculated along the rostro-caudal axis (**Figure 10B**) suggests that the eccentricity-varying stimuli activate distinct regions mainly in the left SC, resulting in a strongly leftward lateralization ($LI_{ecc} > 0.5$) for eccentricity varying stimuli,

which is most pronounced in the rostral sector of the SC (**Figure 10B**). The right SC, on the other hand, showed an higher number of voxels activated by polar-angle varying stimuli compared to the LH, especially when a small stimulus (sVF experiment) was used (Wilcoxon test, p(wVF) = 0.053, p(sVF) = 0.002) with small LIs (LI_{pol}< 0.4) for these stimuli along the entire rostro-caudal axis of the SC.

Secondly, eccentricity representations in the right SC were substantially different compared to the left SC. Both in the wVF and sVF experiments, a clear variation in eccentricity representation was virtually absent along the entire rostro-caudal axis of the right SC. **Figure 10A-C** shows how the eccentricity representations observed during the wVF and sVF experiments changed along the caudo-rostral axis (expressed in terms of percentile of the SC volume starting at the caudal pole). The relationship between eccentricity representations and their anatomical location along the rostro-caudal axis was tested within each hemisphere by fitting a linear model on median eccentricity values for 20 equal partitions along the caudo-rostral axis of the SC. By fitting a linear model, eccentricity values decrease as a function of the anatomical position of the slices along the caudo-rostral axis of the left SC (p < .001; slope (phase) = -0.045, R^2adj = .84 in wVF; slope (phase) = 0.023, R^2adj = .94 in sVF). This was not the case for the right SC, which instead shows a surprisingly similar eccentricity representation along its caudo-rostral axis (p = .05, slope(phase) = -0.005, R^2adj = .35 in wVF; p = .5, slope(phase) = 0.001, R^2adj = -0.16 in sVF).

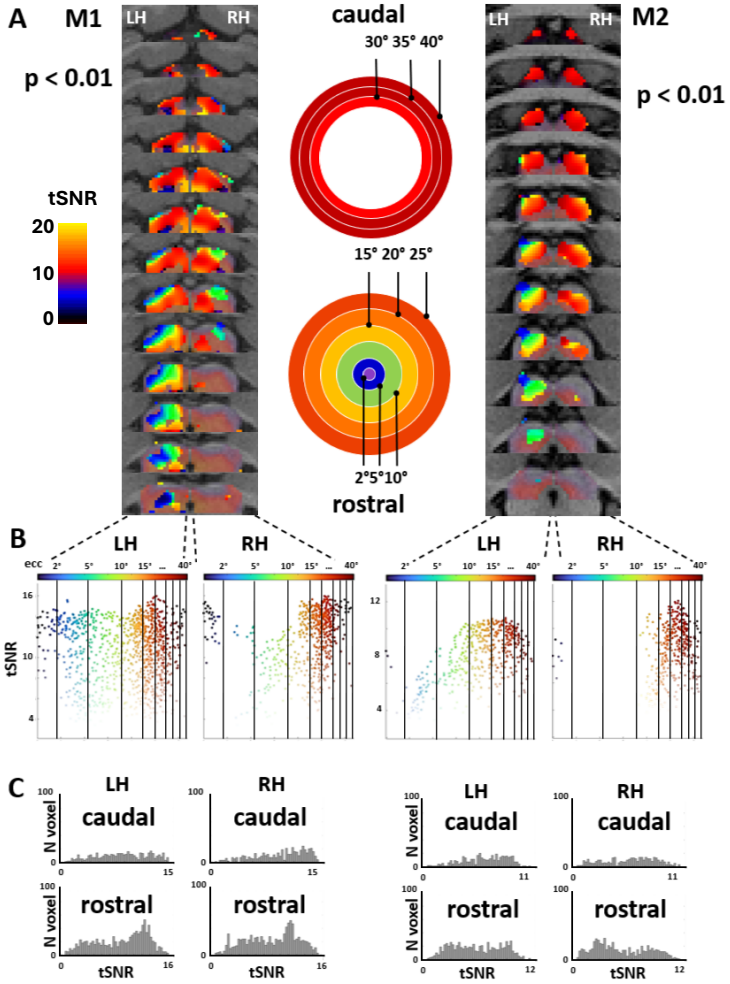

Figure 11. Rostro-caudal SC eccentricity maps with lower significance threshold and temporal signal-to-noise ratio (tSNR). A. Eccentricity maps extracted from phase maps with a threshold of p < .01, superimposed on tSNR maps. The color bar on the left of M1 is the color code for tSNR maps, which are semitransparent in the tSNR map to be distinguished by the color code of the superimposed eccentricity maps; black in the tSNR color bar is fully transparent in the tSNR map. **B.** Eccentricity values (x axis and color bar) against the quality of the signal (tSNR; y axis and transparency) for each voxel of LH (on the left) and RH (on the right) in both monkeys. **C.** tSNR within caudal/rostral and left/right SC. Across hemispheres, tSNR differs statistically in M1 (p<0.001 caudally, p=0.003 rostrally) but not in M2 (p=1 caudally, p=0.05 rostrally; ANOVA one-way unbalanced with Bonferroni correction).

The LH/RH bias in eccentricity representations remained visible, even after lowering the statistical thresholds to $p < .01$. In this case, the most rostral pole of the SC in the right hemisphere was still unresponsive for the eccentricity-varying stimuli of the wVF experiment (**Figure 11A**). The right SC mostly represented eccentricities larger than 10° in the wVF experiment (**Figure 11B**).

Moreover, the lack of responses to eccentricity-varying stimuli in the right rostral SC is likely not accounted for by differences in temporal signal-to-noise (tSNR). By restricting the SC ROIs to only coronal slices with active voxels in at least one hemisphere and then dissecting them into equal rostral and caudal volumes, we found heterogeneous tSNR levels that cannot explain the systematic lack of eccentricity representations found in the rostral right SC. tSNR differed statistically between hemispheres in M1, but both caudally ($p < 0.001$; ANOVA one-way unbalanced with Bonferroni correction) and rostrally ($p = 0.003$). Moreover, this was not the case in M2 ($p = 1$ caudally; $p = 0.05$ rostrally) (**Figure 11C**).

4.2.2 Interhemispheric asymmetry for central but not wide-field stimulation in rostral SC

Interestingly, we found a similar interhemispheric asymmetry in the rostral SC in an independent experiment during which we presented spatially-restricted stimuli (SL1-SL2; **Figure 12**). When a large visual stimulus covering 40° eccentricity of the visual field was presented to the monkeys, the evoked activity was strong along the entire caudo-rostral axis of both the left and right SC. Conversely, when the stimulus was limited to the central 9°of the visual field, the rostral-most (25%) sector of the right SC became unresponsive. Using median and IQR eccentricity values of each percentile of the rostro-caudal axis (in step of 5%) in the left SC as a putative reference for the right SC (**Figure 12B**), it appears that the response to central stimuli in the right SC was not excluding the region responsive for putative eccentricities up to 6°±1°. Mimicking our findings with the small visual field eccentricity stimuli, the central sector of the SC in both hemispheres, became more responsive using small stimuli of the second experiment. The small stimuli activated regions typically representing stimuli covering 20°±5° eccentricity, evoking responses for about three quarters of the entire extent of the SC (**Figure 12B**, middle panel). A similar effect was observed in the right SC when we presented stimuli more peripherally (e.g. SL2, stimulus covering 8°-26° eccentricity; **Figure 12**, right panel), with evoked responses engaging the entire SC, except for the rostral-most sector.

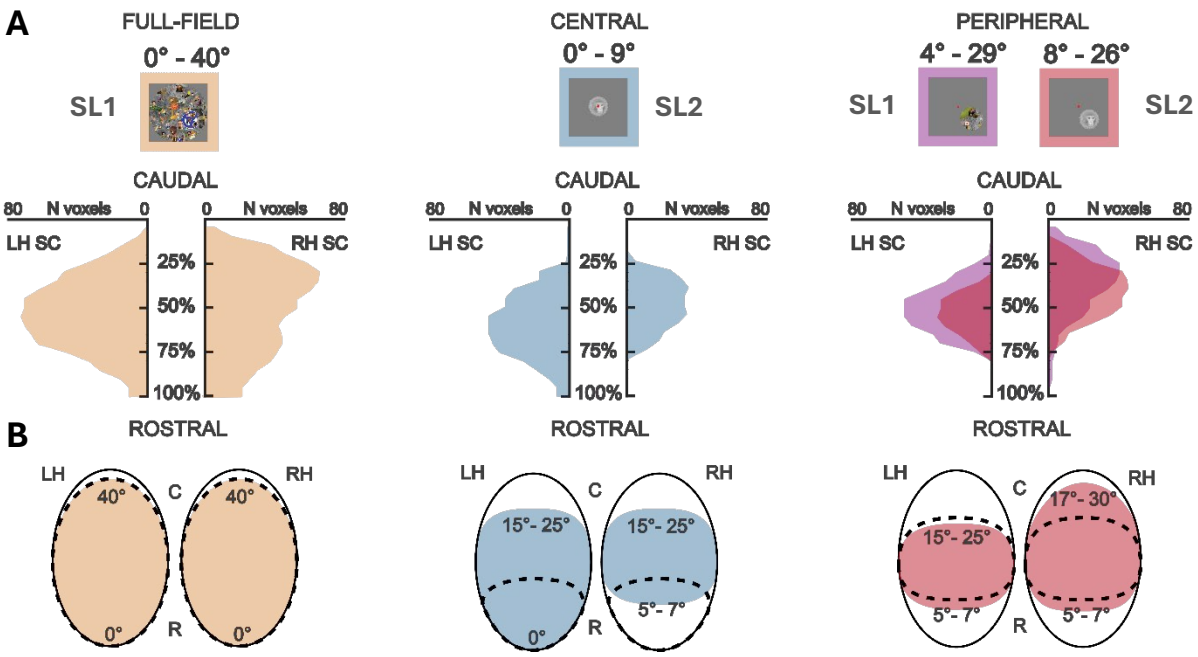

Figure 12. Left-right asymmetry for central but not wide-field stimulation in the rostral sectors of the SC. A. number of voxels activated (p<0.001) for wide field (SL1; yellow), central (SL2, blue) and peripheral (SL1, purple; SL2, red) visual stimuli along the caudo-rostral axis of the left and right SC (expressed in percentile of the extent of the SC across monkeys M1 and M2). **B.** Schematic representation of the left and right SC with the activated sectors by a wide-field, central and peripheral stimulus based on the putative retinotopic organization of the SC (dashed lines) and actual activated regions (solid colors). The estimation of the caudo-rostral position for the eccentricity values (median and IQR) is extracted from the eccentricity map of the left hemisphere as measured during the wVF experiment (averaged between M1 and M2). Central stimulus: 0° - 9°, LH = 0° - ~20°±5°, RH = ~6°±1°-~20°±5°; Peripheral stimulus SL2: 8° - 26°, LH = ~6°±1°-~20°±5°, RH = ~6°±1°-~24°±7°. C, caudal; R, rostral.

4.3 Visual field maps and representational biases within the oculomotor/attentional system

We calculated the average percentage of voxels activated by parafoveal and mid-eccentric (0.5° - 10°) or peripheral (10° - 40°) stimulation (obtained in the wVF experiment) and the average percentage of voxels activated by stimuli restricted to the upper/lower VF (from both the wVF and sVF experiments). The number of activated voxels were derived from the respective eccentricity and polar angle maps, thresholded at different levels ($p < 0.0001$ and $p < 0.01$). The aim was to compare the representations of different sectors of the visual field using differently sized visual stimuli (wVF, sVF) not only within the SC, but also in a number of cortical and subcortical regions of the oculomotor/attentional system.

Specifically, we included in our analysis the pulvinar, the primary visual cortex (V1) in the occipital lobe, frontal area FEF, and parietal area LIP. In **Figure 13** the representation of the visual field in each of these areas and the distribution of voxels responding to different polar angles and eccentricities are reported for the wVF

experiment at the highest threshold of $p < 0.0001$. None of these regions showed an interhemispheric asymmetry for eccentricity representations as observed in the SC. Then, we grouped data from LH and RH for further analysis.

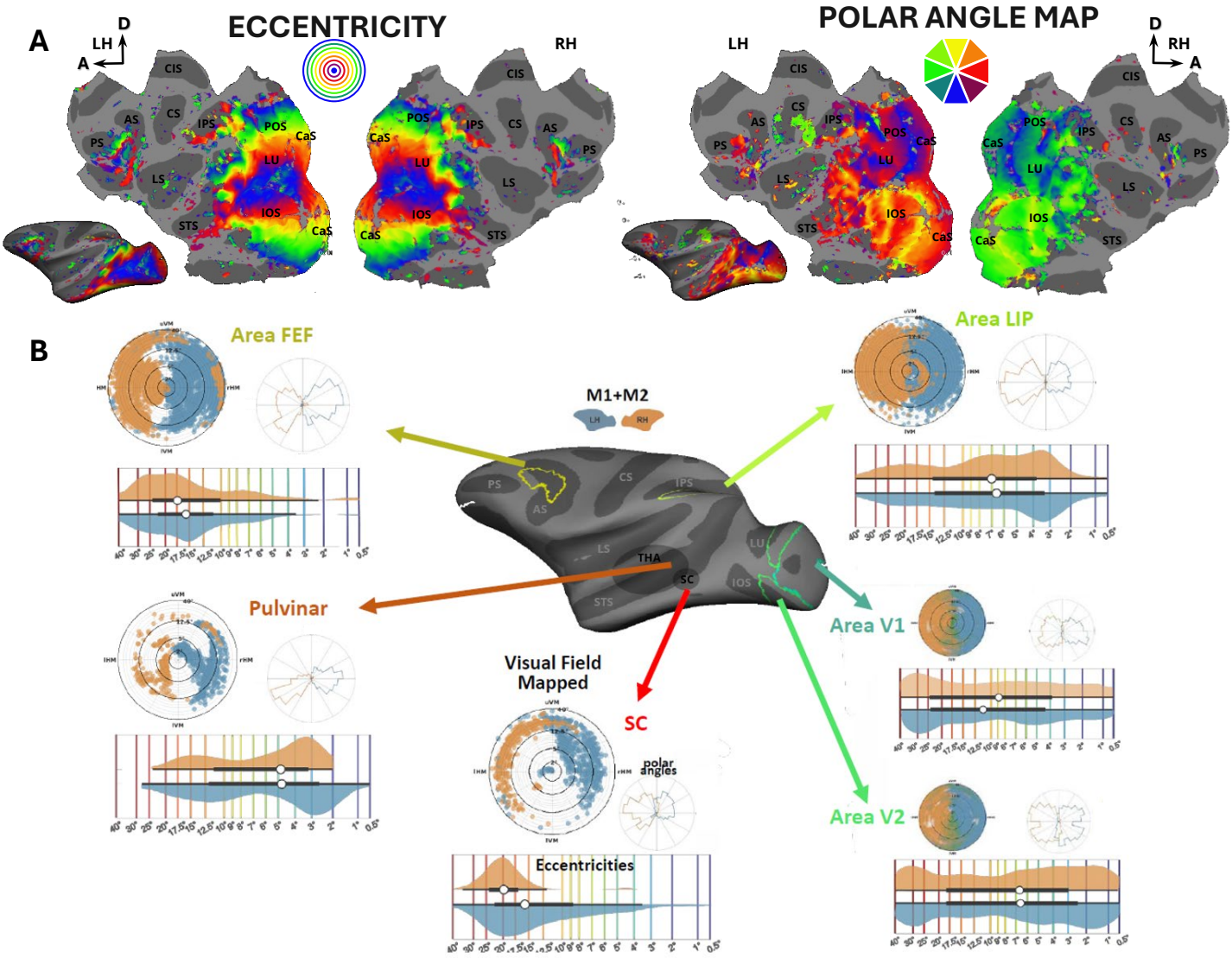

Figure 13. Eccentricity and polar angle maps within the attentional/oculomotor system and V1-V2. A. Eccentricity and polar angle maps ($p < .00001$) on inflated surfaces and flat maps for a representative subject (M1) within the left (LH) and right (RH) hemispheres. The small polygons at the top are schematic representations of the visual field showing the color code for the retinotopic maps. **B.** Visual field coverage ($p < .0001$) within SC, pulvinar, parieto-frontal (lateral intraparietal area, LIP; frontal eye fields, FEF) and areas V1-V2. Cortical ROIs are shown on inflated surface of a representative subject (M1). Data are shown for LH (cyan) and RH (orange), separately. In the 'visual field mapped' plot (on the left of each area), single dots represent single voxels; eccentricity and poral angle values of each voxel are used as *rho* and *theta* coordinates of the *polar scatter plot*. The 'polar angle' plot (on the right of each area) represents the probability density function of polar angle representations. The 'eccentricity' plot (at the bottom of each area) represents the distribution of eccentricity representations. uVM, upper vertical meridian; lHM, left horizontal meridian; lVM, lower vertical meridian; rHM, right horizontal meridian. *CaS, calcarine sulcus; LU, lunate sulcus; IOS, inferior occipital sulcus; POS, parieto-occipital sulcus; STS, superior temporal sulcus; IPS, intraparietal sulcus; LS, lateral sulcus; CS, central sulcus; CIS, cingulate sulcus; AS, arcuate sulcus; PS, principal sulcus; THA, thalamus; SC, superior colliculus; FEF, frontal eye field; LIP, lateral intraparietal area; V1, primary visual area; V2, secondary visual area.*

Table 4 shows the fraction of voxels in each of the ROIs activated by the stimuli restricted to either the central (C; 0.5° - 10° eccentricity) or peripheral (P; 10°-40° eccentricity), and the upper (U) and lower (L) parts of the visual field during the wVF and sVF experiments. The cutoff for a center-periphery asymmetry was arbitrarily selected at 10°. Thus, the center-periphery asymmetry is a relative measurement that only allows comparisons between areas. Data are shown for different statistical threshold ($p < .01$, $p < .0001$). Three Asymmetry Indices (AI) were calculated for each area (wVF C/P AI, wVF U/L AI and sVF U/L AI). AIs and calculated thresholds (|0.3| for C/P asymmetry, and |0.2| for U/L asymmetry; see 3.8 in Materials and Methods) are shown in **Figure 14**. AIs of V1 and V2 were all sub-threshold (i.e. C/P AIs < |0.3|, U/L AI < |0.2|). In area V1, which is known for its magnified representation of the center of the visual field, half of its eccentricity map represented the central and mid-eccentric stimuli (0.5° - 10°), and half the peripheral stimuli (10° - 40°). The overall representation of polar angles was perfectly divided between upper and lower VFs, independently from the threshold applied ($p < .01$, $p < .0001$) or the size of the stimulus used (in the wVF and sVF experiments).

Table 4. Averaged percent of voxels activated by eccentricity and polar angle varying stimuli restricted to parafoveal and mid-eccentricity (0.5° - 10°), peripheral (10° - 40°) (wVF) and upper/lower parts of the visual field (wVF and sVF). Data are derived from the respective retinotopic maps with high ($p < .0001$) or low ($p < .01$) threshold.

SC

	wVF		sVF	
	p < .0001	p < .01	**p < .0001**	p < .01
upper VF	63,02%	67,39%	51,03%	45,40%
lower VF	36,98%	32,61%	48,97%	54,60%
0°-10°	18,57%	27,61%		
10°-40°	81,43%	72,39%		

Area FEF

	wVF		sVF	
	p < .0001	p < .01	**p < .0001**	p < .01
upper VF	63,13%	62,21%	49,90%	47,41%
lower VF	36,87%	37,79%	50,10%	52,59%
0°-10°	22,83%	22,80%		
10°-40°	77,17%	77,20%		

Area V1

	wVF		sVF	
	p < .0001	p < .01	**p < .0001**	p < .01
upper VF	49,17%	49,70%	45,87%	47,76%
lower VF	50,83%	50,30%	54,13%	52,24%
0°-10°	49,83%	50,81%		
10°-40°	50,17%	49,19%		

Pulvinar

	wVF		sVF	
	p < .0001	p < .01	**p < .0001**	p < .01
upper VF	38,57%	41,60%	32,91%	39,64%
lower VF	61,43%	58,40%	67,09%	60,36%
0°-10°	54,67%	49,81%		
10°-40°	45,33%	50,19%		

Area LIP

	wVF		sVF	
	p < .0001	p < .01	**p < .0001**	p < .01
upper VF	53,26%	51,91%	62,03%	62,02%
lower VF	46,74%	48,09%	37,97%	37,98%
0°-10°	65,88%	65,56%		
10°-40°	34,12%	34,44%		

Area V2

	wVF		sVF	
	p < .0001	p < .01	**p < .0001**	p < .01
upper VF	49,82%	49,92%	56,35%	56,15%
lower VF	50,18%	50,08%	43,65%	43,85%
0°-10°	61,12%	61,26%		
10°-40°	38,88%	38,74%		

Each region besides area V1-V2 showed a bias for the upper or lower visual field (i.e., at least one of U/L AIs is greater than |02|). Interestingly, for regions showing larger or smaller magnification factors compared to V1, the upper/lower bias appeared to be dependent on the stimulus size used (covering only the parafoveal and mid-eccentricity regions of the visual field (in the sVF experiment), or peripheral stimuli (in the wVF experiment). Using retinotopic maps at different thresholds ($p < .01$, $p < .0001$) to extract the fraction of activated voxels did not affect the observed biases.

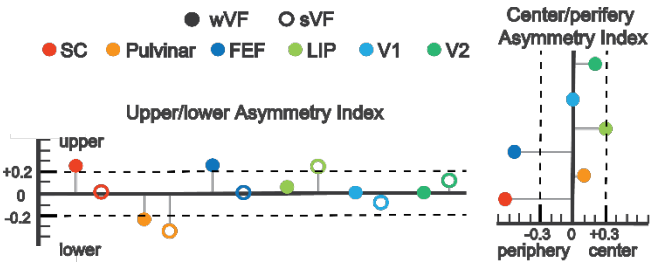

Figure 14. Asymmetry Index (AI) for upper/lower (on the left) and center/periphery (on the right). AIs for SC, Pulvinar, FEF, LIP, V1 and V2 are shown in different colors. Filled and open circles refer to data obtained in the wVF and sVF experiments, respectively. Dashed lines indicate the calculated AI threshold at one standard deviation.

Interestingly, the SC and pulvinar showed opposite upper versus lower and central versus peripheral asymmetries. In the SC, stimuli covering the peripheral VF occupied most of the voxels activated by eccentricity-varying stimuli (72 - 81%) compared to stimuli covering parafoveal and mid-eccentric portions of the visual field (19 - 28%). Moreover, during the wVF experiment, 63% of all voxels activated by the polar angle stimuli were activated by the contralateral upper VF stimuli, and only 37% by the contralateral lower VF wedges. These numbers are threshold dependent. However, when the threshold was lowered to $p < .01$, the upper VF bias was maintained (67% upper VF, 33% lower VF). Interestingly, the upper-lower VF bias was not obvious in the experiment with the small stimuli (sVF). The pulvinar, instead, had a bias for para-foveal and mid-eccentricity stimuli as 50-55% of all voxels activated by eccentricity-varying stimuli were activated by such stimuli. Moreover, it showed a bias for the lower visual field both for large (wVF) and small (sWF) stimuli (33 - 42% and 58 - 67% of all voxels activated by polar angle varying stimuli were activated by upper and lower VF stimuli, respectively).

Within the cortical areas of the attentional/oculomotor system, the FEF showed a peripheral field bias as 77% of its voxels was activated by large peripheral stimuli. Moreover, an upper visual field was observed with large stimuli (62 - 63% and 47 - 50% of its voxels represented the upper visual field with large stimuli in the wVF experiment and small stimuli in the sVF experiment, respectively). Area LIP, on the other hand, had a central field bias (66% of its voxels activated by eccentricity-varying was actually activated by the parafoveal and mid-eccentricity stimuli). Moreover, there was a mild upper field bias for small stimuli (52 - 53%, and 62% of all voxels activated by polar angle varying stimuli were activated by upper field stimuli in the wVF and sVF experiments, respectively).

4.4 Whole-brain interhemispheric asymmetries of eccentricity and polar angle representations

Interhemispheric asymmetries for eccentricity representations appear to be confined to the SC (see **Figure 13**). Moreover, our detailed functional analysis of eccentricity and polar angle representations along the rostro-caudal axis of the SC revealed well-organized eccentricity and polar angle maps, mainly restricted to the left and right colliculi, respectively (see **Figure 10**).

To test whether other areas show interhemispheric biases for eccentricity and polar angle representations, we extended the analyses of interhemispheric asymmetries for these stimuli to the entire brain. Within cortical (occipital, parietal, temporal and frontal areas) and subcortical (SC and pulvinar) regions, we first quantified the percentage of voxels responsive to both eccentricity and polar angle stimuli (**Figures 15A-16A**, conjoined maps). This reflects the fraction of voxels in each of these areas that are sensitive for both variations in eccentricity and polar angle varying stimuli. We also calculated the number of voxels–whose responses were sensitive *only* for either eccentricity or polar angle varying stimuli. We considered these quantitative measurements as a degree of sensitivity for eccentricity and polar angle varying stimuli, respectively. Finally, we performed the same analysis separately in each hemisphere to calculate putative interhemispheric biases for these measures.

Within the anatomically-defined SC and pulvinar ROIs, the overall volume (i.e. fraction of voxels) activated by retinotopic stimuli (only eccentricity, only polar angle and both conjoined) was less than 50% of the overall ROI. Within the SC, the volume activated by only eccentricity was significantly smaller than the volume activated by both stimuli (p(ecc-conj) = 0.014; p(pol-conj) = 1; nonparametric bootstrap t-test with pooled resampling method, 10000 permutations, with Bonferroni correction; **Figure 15A**). Similarly, the pulvinar showed a lower sensitivity for eccentricity compared to polar angle-varying stimuli (p(ecc-conj) = 0.04; p(ecc-conj) = 0.06; p(pol-conj) = 0.41). The results on the LIs confirmed our previous finding of asymmetric retinotopic organization of the SC (**Figure 15B**). The fraction of voxels activated by both stimuli (conjoined) was biased towards the LH (LI(conj) = 0.29, $p(conj_{LH\text{-}RH})$ = 0.04; nonparametric bootstrap t-test with pooled resampling method, 10000 permutations). The fraction of voxels activated by eccentricity-varying stimuli alone tended to be larger in the left hemisphere (LI(ecc) = 0.44), yet this did not reach statistical significance ($p(ecc_{LH\text{-}RH})$ = 0.06). The polar angle varying stimuli, on the other hand, activated a larger fraction of SC voxels in the right hemisphere (LI(pol) = -0.49, $p(pol_{LH\text{-}RH})$ = 0.045). A similar trend can be noticed in the pulvinar (**Figure 15B**), with positive LI indices (LI(ecc) = 0.46; LI(pol) = 0.26; LI(conj) = 0.41) but whereby the interhemispheric differences in the fraction of voxels activated by these different stimuli are not pronounced enough to reach statistical significance ($p(ecc_{LH\text{-}RH})$ = 0.1; $p(pol_{LH\text{-}RH})$ = 0.26; $p(conj_{LH\text{-}RH})$ = 0.21). Moreover, the overall volume activated by only eccentricity was significantly smaller than the volume

activated by both stimuli (p(ecc-conj) = 0.014; p(pol-conj) = 1). Similarly, the pulvinar showed a lower sensitivity for eccentricity compared to polar angle-varying stimuli (p(ecc-conj) = 0.04; p(ecc-conj) = 0.06; p(pol-conj) = 0.41).

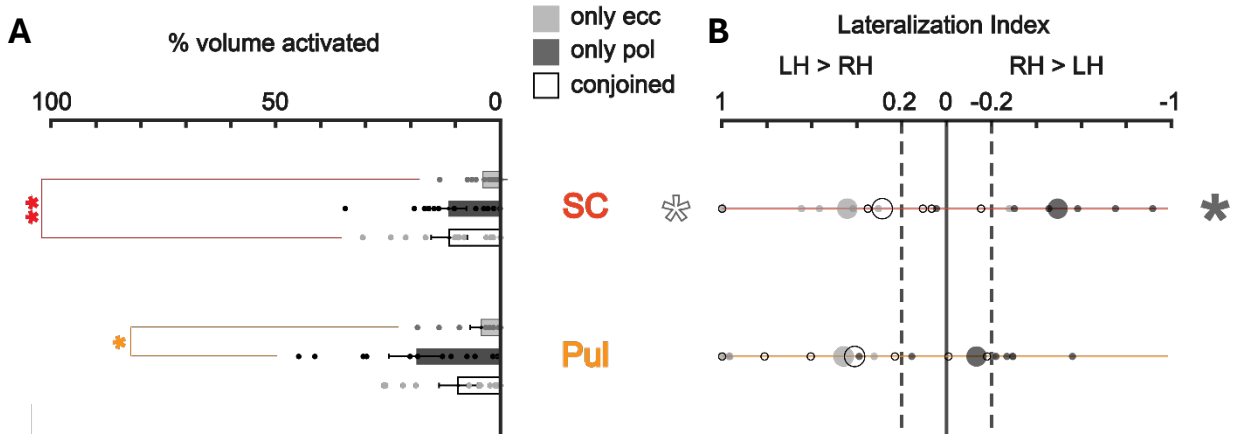

Figure 15. A. Mean fraction of voxels activated (%) in all monkeys (wVF and sVF experiments) by only eccentricity (light gray) or polar angle stimuli (dark gray) or both stimuli (white) in SC (red) and Pulvinar (Pul; orange). Error bars indicate SEM. The data of individual hemispheres are shown by the single dots. Nonparametric bootstrap t-test with pooled resampling method (10000 permutations) with Bonferroni correction; *** p ≤ .001, ** p ≤ .01, * p ≤ .05; **B.** Lateralization Index (LI; big dots) based on the fraction of voxels activated by only eccentricity, only polar or both types of stimuli within LH and RH. The LIs of individual monkeys are shown by the dots. Dashed lines indicate the calculated AI threshold at one standard deviation. Statistical tests as in (A) on the difference in voxels activated in the LH and RH. Asterisks on the left and on the right indicate statistical significance for LH > RH and RH> LH, respectively. Nonparametric bootstrap t-test with pooled resampling method (10000 permutations).

Cortically (**Figure 16A**), we found the highest fraction of voxels that are sensitive to the eccentricity and polar angle varying stimuli in occipital cortex (> 60%; striate cortex, V1; extrastriate cortex, V2-V4) and, as expected the lowest (< 5%) in auditory (core/belt), primary somato-motor (SI/SII, MI) and medial cortex (posterior medial cortex, pmC; medial temporal cortex, mTC; insula, anterior cingulate cortex, ACC, medial premotor cortex, PMm). Also as expected, we found a decreasing fraction of voxels sensitive to the eccentricity and polar angle varying stimuli along a posterior-to-anterior (TEO, TEp, TEa, TP) and ventral-to-dorsal (vmSTS, STG/dSTS) axis in temporal cortex. Similar trends were also evident in the parietal cortex (see **Figure 16A**), with the highest fraction of voxels sensitive to the eccentricity and polar angle varying stimuli in the intraparietal sulcus (IPS; and lower fractions in the inferior parietal lobule, IPL; superior parietal lobule, SPL; primary and secondary somatosensory areas, SI/SII). In prefrontal cortex the highest fraction of voxels sensitivity for the retinotopic stimuli were found in the arcuate region (arc; area 8A, 8B, 45), which decreased towards the lateral prefrontal (lPFC) and orbitofrontal cortex (OFC). Within the premotor cortex, the highest fraction of voxels sensitivity for the retinotopic stimuli were found ventrally (PMv), and this fraction decreased within dorsal (PMd) and medial cortex (PMm).

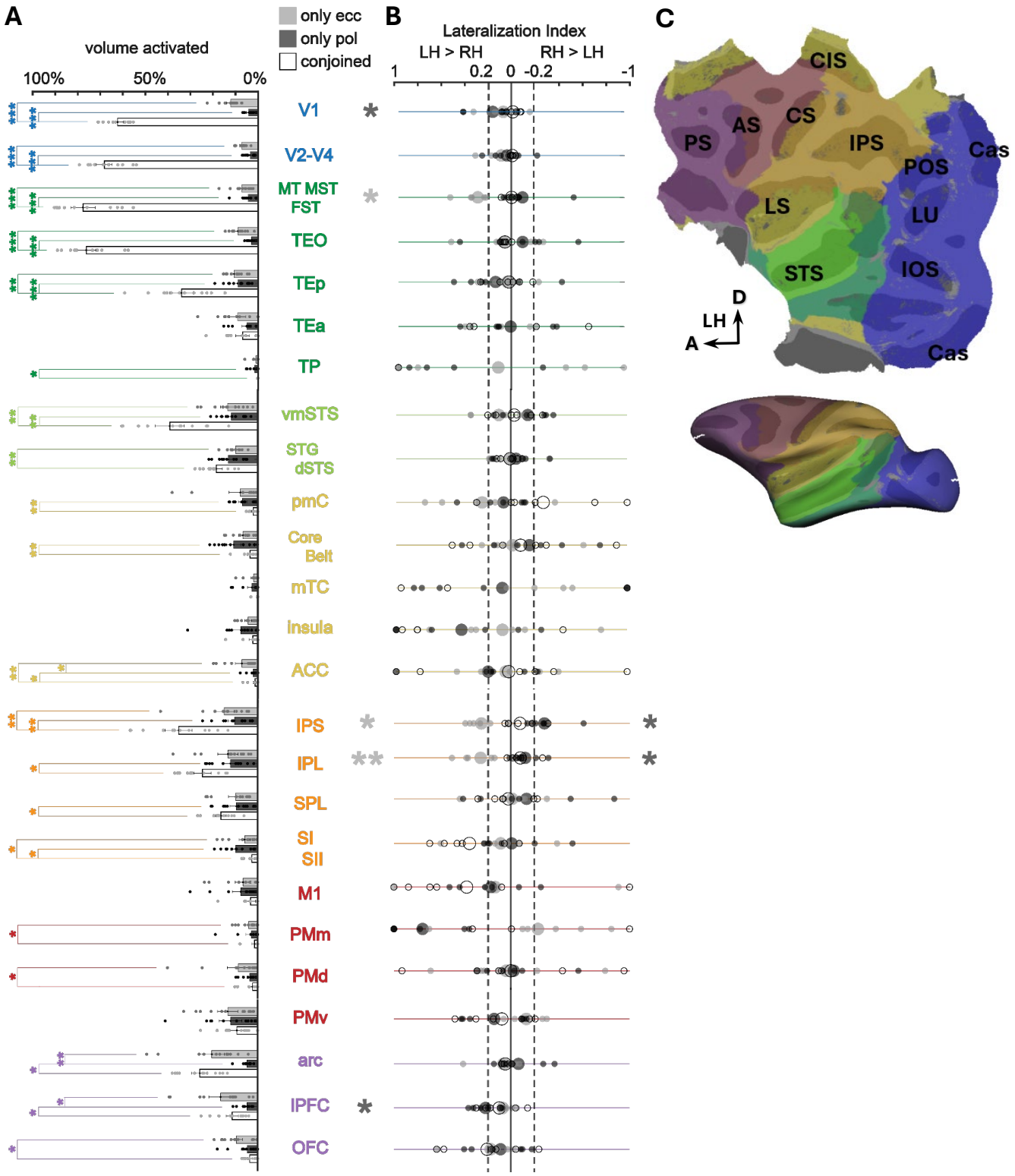

Figure 16. Mean volume activated (%; **A**) and LI (**B**) in all monkeys (wVF, sVF) for voxels activated only by eccentricity (light gray), only polar (dark gray) or both stimuli conjoined (white) in occipital cortex (blue), infero-posterior temporal (dark green) and medio-superior temporal cortex (light green), mesial cortices (yellow), parietal cortex (orange), motor cortex (red), prefrontal cortex (purple). Nomenclature and statistical analysis as in Figure R8. **C.** Grouped cortical ROIs (occipital, infero-posterior temporal, medio-superior temporal, mesial, parietal, motor, prefrontal cortex) represented on flat map and inflated surface for a representative subject (M2) within the left (LH) hemispheres. Color code as in A-B.

None of these cortical areas listed above showed a statistically significant interhemispheric difference in their sensiti vity for both eccentricity and polar angle varying stimuli (**Figure 16B**, conjoined; $p > 0.05$).

In most cortical areas that are sensitive for both polar angle and eccentricity-varying stimuli, there is no difference in the fraction of voxels activated by these stimulus types separately ($p(ecc\text{-}pol) > 0.05$; nonparametric bootstrap t-test with pooled resampling method, 10000 permutations, with Bonferroni correction; see **Figure 16A**). Moreover, the fractions of voxels activated either by the polar angle or the eccentricity stimuli only is smaller than the fraction of voxels that are sensitive for both stimulus types conjoined ($p(ecc/pol\text{-}conj) < 0.01$). This is the case for occipital cortex (blue), posterior occipito-temporal regions (MT/MST/FST, TEO, TEp, vmSTS; green) and parietal IPS (orange), but not for the prefrontal cortex (arcuate region and lPFC; purple) in which more voxels are activated by the eccentricity than polar angle stimuli ($p(arc)(ecc\text{-}pol) = 0.01$; $p(lPFC)(ecc\text{-}pol) = 0.03$). Here, the fraction of voxels sensitive for eccentricity varying stimuli only is equal to the number of voxels sensitive for both types of retinotopic stimuli conjoined ($p(arc)(ecc\text{-}conj) = 0.37$; $p(lPFC)(ecc\text{-}conj) = 0.36$).

Surprisingly, posterior temporal and parietal areas showed a similar interhemispheric bias as the SC (**Figure 16B**), that is, a leftward bias for voxels sensitive for eccentricity varying stimuli in the MT/MST/FST complex ($LI(ecc) = 0.3$, $p(ecc_{LH\text{-}RH}) = 0.03$), IPS ($LI(ecc) = 0.26$, $p(ecc_{LH\text{-}RH}) = 0.02$), IPL ($LI(ecc) = 0.26$, $p(ecc_{LH\text{-}RH}) = 0.01$) and a right hemisphere bias in the number of voxels activated by polar angle varying stimuli in the parietal IPS ($LI(pol) = -0.28$, $p(pol_{LH\text{-}RH}) = 0.02$) and IPL ($LI(pol) = -0.11$, $p(pol_{LH\text{-}RH}) = 0.03$). Small interhemispheric biases for polar angle varying stimuli were also found for left V1 ($LI(pol) = 0.16$, $p(pol_{LH\text{-}RH}) = 0.043$) and lPFC ($LI(pol) = 0.22$, $p(pol_{LH\text{-}RH}) = 0.03$).

5 Discussion

The superior colliculus (SC) is a deep and hence challenging brain structure to investigate with fMRI due to its relatively large distance from the receive coils and hence the usually poor SNR. Here, leveraging highly trained monkeys that achieved optimal fixation performance (exceeding 94% accuracy), hand position control, and the use of contrast agents, we achieved high-quality subcortical fMRI maps of the SC. The use of biologically-relevant stimuli, such as phase-encoding retinotopic mapping and single-category stimuli, further enhanced the quality of our results.

Three observations motivate this study. First, the retinotopic organization of the primate SC has been investigated with electrophysiology in macaques and fMRI in humans, leaving a knowledge gap due to the use of different animal models and different techniques. Second, the representation of the central visual field (smaller than 10° eccentricity) has been recently challenged with electrophysiology (Chen et al., 2019; Dilbeck et al., 2022) and the extraction of eccentricity maps with central, relatively small stimuli (up to 15° eccentricity; Schneider and Kastner, 2005) have been nontrivial with fMRI. Third, the classical model of the polar angle topography assumes a geometric representation of the visual field (Robinson, 1972; Ottes et al., 1986) and a symmetrical representation of the upper and lower visual fields. A recent model instead suggested a magnification of the area representing the upper visual field, which would align space encoding in the macaque SC with its functional role in visual exploration (Hafed et al., 2016; de Malmazet and Tripodi, 2023).

5.1 Retinotopic maps of the primate SC and widespread activations for small foveal stimuli

Wide-field retinotopic maps of the macaque SC and macular magnification. Here, we report the first wide-field retinotopic maps of the macaque SC using fMRI (40° eccentricity; wVF; **Figure 9**). The polar angle and eccentricity maps revealed several features that are consistent with previously reported fMRI maps in humans, and electrophysiological findings in monkeys.

First, contralateral upper and lower quadrants are represented on the medial and lateral parts of the SC, respectively. Second, the central region of the visual field is represented rostro-laterally and the periphery caudally. The central 10° of visual field is known to be overrepresented in the SC, varying between ~35% and ~55% of its surface (Cynader and Berman 1972; Chen et al., 2019; Dilbeck et al., 2022), although less pronounced compared to other structures, such as in the lateral geniculate nucleus (73% of the total volume; Schneider et al. 2004). In the wVF fMRI experiment, we confirmed this overrepresentation of the central 10° in the primate SC, covering **almost half** of its rostral-most volume (see LH wVF in **Figure 10A**) which is in line with recent electrophysiological investigations (Chen et al., 2019).

SC eccentricity maps depend on the extent of the visual field being stimulated. Here, we also report retinotopic maps based on smaller stimuli with size of maximum 12.5° eccentricity (sVF experiment; **Figure 9**), which are similar in size to those commonly used in human retinotopic mapping studies of the SC. As expected, smaller retinotopic stimuli activated less voxels in the SC, as also observed in visual cortex (Fize et al., 2003; Vanduffel et al., 2002; Janssens et al., 2014; Kolster et al., 2014; Zhu and Vanduffel 2019). In the sVF experiment, we

reproduced similar polar angle maps as extracted in the wVF experiment. Reversely, we complete anterior-to-posterior eccentricity maps only in the monkeys (M1-M2) which were tested with large retinotopic stimuli, covering by definition a wider portion of the peripheral visual field (wVF experiment), and in only one monkey (M3) in which we tested smaller stimuli (12.5° eccentricity) in the sVF experiment. Moreover, testing the eccentricity preference along the rostro-caudal extent of the SC using small stimuli (sVF experiment) led in all monkeys (M3-M6) to relatively widespread activations with respect to stimuli with the same eccentricity but presented in the wVF experiment. Stimuli of the sVF experiment of less than 4° activated voxels located across more than 2/3 of the rostro-caudal extent of the SC. This is in line with previous human retinotopic mapping studies of the SC in which a similar paradigm and stimuli were used (maximum stimulus size: 15° eccentricity, Schneider and Kastner, 2005; 13° eccentricity, DeSimone et al., 2015; 8° eccentricity, Benson et al., 2018). The former study revealed polar maps but failed to obtain complete and systematic anterior-to-posterior eccentricity maps in most subjects. In fact, most of the SC activity in all these human fMRI studies was evoked by stimuli restricted to foveal eccentricities.

The dependency on the extent of the stimulated visual field in fMRI-based mapping procedures has recently been shown at the level of the visual cortex (V1-V3; Prabhakaran et al, 2020). Specifically, reduced peripheral stimulation (by using stimuli of radius 14°, 7° or 4°) led to a proportional shift in foveal population receptive fields (pRFs) and an overall enlargement of pRFs size - likely due to reduced surround suppression in small versus large stimuli. Here we observed that more voxels are activated by small eccentricity stimuli (e.g. 3°) if the peripheral stimulation is reduced (in the sVF versus wVF experiment; see **Figure 10A**). Although we did not directly compare fMRI-based pRFs sizes between the sWF and wVF experiments, the strong activity for small (sWF) stimuli in posterior SC may reflect reduced surround inhibition, or changes in the underling pRFs size induced by the absence of peripheral stimulation.

Representation of the central visual field: surround and fixation-related modulations. The fMRI responses to spatially-restricted stimuli in two independent passive-viewing experiment (SL1-2; **Figure 12**) largely confirmed the antero-posterior topographic organization we obtained with the phase-encoding retinotopic mapping. These studies also reproduced the strong activation for small stimuli in posterior SC. Central and relatively small stimuli (covering 9° eccentricity; in the SL2 experiment) evoked widespread activations along the rostro-caudal extent, covering approximately 3/4 of the antero-posterior extent of the SC. The response to peripheral stimuli, instead, were more restricted to the expected posterior portion of the SC. Stimuli covering 8°-26° (SL2), for example, activated on average the region of the SC which should represent eccentricity ranges between ~5°-7° and ~15°-30° (see **Figure 12**, right panel).

The stronger fMRI response to central, relatively small stimuli (sVF, SL2), activating ~75% voxels along the anterior-to-posterior extent of the SC can be partially explained by the magnification of the macula (central 10°). The representation of the central 10° on the SC is still debated, yet previous electrophysiology data and fMRI retinotopic data reported in the present study (wVF experiment) suggest that such small stimuli activated roughly half of the surface of the SC (54%, Robinson, 1972; Ottes et al., 1986; Chen et al., 2019; 47%, Dilbeck et al., 2022; 36%, Cynader and Berman, 1972).

A more parsimonious explanation for the more extensive fMRI responses for small central stimuli than predicted based on the (expected) topographic organization of the SC may be related to contextual or fixation-related modulatory effects. Contextual suppression, also known as surround inhibition (inhibition exerted by the presence of peripheral stimulation) is a basic mechanism in visual processing and a fundamental feature of receptive field organization. Surround inhibition is present at single-cell level (Shapley and Victor 1979; Jones et al., 2001; Levitt and Lund, 1997) but also at single-voxel level as revealed by visual fMRI studies (Nurminen et al., 2009; Press et al., 2001; Williams et al., 2003). In particular, in retinotopically organized early visual cortex (V1-V3), the fMRI response to foveal and small stimuli is reduced in the presence of peripheral, surrounding stimuli. This is likely induced by local short- and/or long-range modulatory mechanism, or lateral interactions, that can regulate the stimulus representation based on the surrounding context through excitation and inhibition (Polat, 1999). In the SC, surround inhibition has been documented at single-neuron level (Schiller et al., 1974; Phongphanphanee et al., 2014) and, similarly to the cortex, lateral interaction mechanisms modulate the responses of the neurons. As already observed with retinotopic mapping stimuli (sVF versus wVF experiments), using relatively small central stimuli in the absence of peripheral stimulation would reduce surround inhibition leading to broad activations as a result of less attenuated excitatory activity for central stimuli.

Moreover, a local network of excitatory and inhibitory interneurons governs functional interactions between the rostral ‘foveal-fixation’ zone and the more caudal ‘peripheral-saccade’ zone, both within and across hemispheres (Munoz and Istvan, 1998). Firstly, the rostral SC neurons are mainly modulated by excitatory connections such that the stimulation of rostral foveal neurons in one hemisphere cause excitation of contralateral foveal neurons. This mechanism is not present within caudal parts of the SC. These excitatory mechanisms are supposed to be involved in interhemispheric integration of the binocular areas of the visual field. Conceivably, during central visual stimulation, this inter-collicular excitation mechanism may induce larger fMRI activity by small central but not large stimuli encompassing both the foveal and peripheral parts of the visual field. Secondly, during continuous fixation the caudal saccade zone is bilaterally inhibited by rostral SC neurons, which may be instrumental for maintaining stable visual fixation and suppressing unwanted saccades (Munoz and

Istvan, 1998). The caudal SC, instead, inhibits the rostral pole only ipsilaterally when stimulated (Munoz and Istvan, 1998). During sustained fixation, the bilateral inhibition mechanisms within the SC may be strong enough to reduce fMRI activity caudally when a peripheral stimulus is present, which may be stronger than the ipsilateral inhibition on the rostral SC.

5.2. Interhemispheric asymmetry of eccentricity and poral angle representation

Surprisingly, we observed an interhemispheric leftward asymmetry in the eccentricity maps of all monkeys, regardless the bilaterally almost equivalent polar angle maps acquired during the same experiment. The asymmetrical effect was twofold: (1) the lack of responses in the rostral pole of the right colliculus and (2) the virtual absence of an expected anterior-to-posterior progression of representations of gradually larger eccentricities in the right colliculus. The leftward asymmetry in the representation of central-eccentricity stimuli was not only evident in the two independent retinotopic experiments (wVF and sVF; see **Figure 10A-B**), and in eccentricity maps with low threshold ($p < 0.01$, see **Figure 7**), but also when stimuli were presented centrally in a third independent experiment (SL1 and SL2; see **Figure 12**). In other words, the right colliculus showed activations in its rostral-most region only when a wide stimulus encompassing both foveal and peripheral eccentricities was presented (polar angle varying stimuli in the wVF and sVF experiments, **Figure 9**; wide-field stimuli in the SL1, first panel in **Figure 12**). The absence of an anterior-to-posterior progression of representations of gradually larger eccentricities even for peripheral stimuli (**Figure 10C-D**) suggests that the eccentricity map in the right SC is poorly organized along its rostro-caudal axis and less sensitive and precise for perifoveal stimuli.

Overall, the SC seems less sensitive (in terms of fraction of voxels activated) to eccentricity than polar angle varying stimuli (**Figure 15A**). This corroborates the results of a human fMRI study (Schneider and Kastner, 2005), which showed that the mean volume of the SC which is activated by rotating wedge stimuli was almost the double of the mean volume activated by expanding ring stimuli (67.8 ± 7.2 mm^3 and 36.1 ± 9.1 mm^3, respectively). One possible explanation can be that a wedge (polar angle varying) stimulus is wider and covers more portions of the contralateral visual field than a ring (eccentricity varying) stimulus, activating more voxels in retinotopically organized areas as do large retinotopic stimuli relative to smaller stimuli (Fize et al., 2003; Vanduffel et al., 2002; Janssens et al., 2014; Kolster et al., 2014; Zhu and Vanduffel 2019). However, this cannot explain the interhemispheric asymmetry found in the retinotopic maps, since the right SC was less widely activated by eccentric than polar varying stimuli (**Figure 10B**), and the left SC was less widely activated by polar

angle than eccentricity varying stimuli (**Figures 10B** and **15B**). The larger rightward sensitivity for polar angle varying stimuli is slightly apparent in the polar maps of a human fMRI study on the SC (in Katyal et al., 2010). Three of their five subjects showed bilateral polar maps, whereas the other two had complete polar angle representations only in their right colliculi. Yet, the signal amplitude (measured as percent fMRI modulation) was similar for both colliculi in all subjects. Nevertheless, none of the previously reported studies on the human SC systematically analyzed putative asymmetries in polar angle or eccentricity maps.

This result was quite unexpected. fMRI-based eccentricity maps in the right SC differs from the topography observed in the left SC and also from expectations based on prior electrophysiological mapping studies. It needs to be noted, however, that models of the SC visual topography based on electrophysiology (Cynader and Berman 1972; Chen et al., 2019) are typically based on data merged from both hemispheres. Moreover, electrophysiology studies rarely speculate about putative interhemispheric differences, not only because recording sites are often located in just one hemisphere in each animal, but also because it is nontrivial to obtain data from exactly the same homotopic anatomical locations in both hemispheres.

Moreover, functional brain asymmetries have been largely considered prototypical features of the human cortex. Nevertheless, lateralized behavior and brain functions are present in many animal species, from non-vertebrates to mammals and nonhuman primates (see, for review, Güntürkün et al., 2020). For example, more than half of vertebrate species studied so far (Ströckens et al., 2013), including macaques (Itani et al., 1963; Lehman, 1978; Hörster and Ettlinger, 1985; Warren, 1953), show side preferences during unimanual activities. Birds like pigeons (*Columba livia*), chicken (*Gallus domesticus*) and quail (*Cotux japonica*) display asymmetries in visually-driven behaviors resulting in left hemispheric dominance for complex learning, discrimination and categorization tasks (Manns and Güntürkün, 2009; Rogers, 1990; Yamazaki et al., 2007), and right dominance for spatial navigation (Nagy et al., 2010; Prior et al., 2004; Tomassi et al., 2012; Tommasi and Vallortigara, 2001), social cognition and sexual behavior (Daisley et al., 2009; Vallortigara and Andrew, 1994; Gülbetekin et al., 2009; Rogers, 1990). The avian tectum is characterized by a complete anatomo-functional asymmetrical specialization, resulting in visual feature detection capacities primarily dominated by the left hemisphere and visuospatial processing by right hemisphere (Tommasi and Vallortigara, 2001; Yamazaki et al., 2007; Rogers, 1995). In humans, damage to the left posterior parietal cortex causes deficit in functions related to handedness and in the motor sequencing domain, like apraxia (e.g. Rounis et al., 2021). The same lesion in the right hemisphere, instead, leads to neglect for the left hemispace, that is, an impaired or lost ability to process or react to sensory stimuli presented in the contra-lesional hemispace (Karnath et al., 2002). Inactivation of the SC in nonhuman primates causes similar behavioral (neglect-like) deficits and enhancements (bias) for the contra- or ipsi-lesional hemifield,

respectively. Saccade velocity, detection accuracy and sensorimotor gating (the attentional shift to salient stimuli) are reduced for targets located in the contra-lesional visual field; on the other side, perceptual decision biases facilitate saccade selection toward the ipsi-lesional visual field (McPeek and Keller, 2004; Jun et al., 2021). The paradoxical facilitation for the ipsilesional visual field can be anatomically explained by the presence of reciprocal inter-collicular inhibition mediated by the collicular commissure (Hilgetag, 2000; Sprague, 1966; Weddell, 2004; Valero -Cabré et al., 2020). Interestingly, the visuospatial bias induced by unilateral cortical lesion is supposed to be mediated by similar inhibitory mechanisms regulating interhemispheric communications through the corpus callosum (Wang et al., 2023; Innocenti 2009; Bloom and Hynd, 2005).

Cortical asymmetries in the sensitivity to eccentricity and polar angle varying stimuli. Except for the SC, we found no evidence for interhemispheric asymmetries in the range of eccentricities represented (in pulvinar, areas FEF, LIP, V1, V2; **Figure 13B**), nor in the percent of volume activated by both eccentricity and polar angle varying stimuli (in pulvinar and whole cortex; **Figure 16B**, conjoined). However, the percentage of volume responsive to stimuli changing only in eccentricity or polar angle, reflecting the portion of volume sensitive to spatial variations only with respect to the gaze center or only with regard to vertical and horizontal meridians, exhibited lateralization in certain cortical regions (**Figure 16B**). Similar to the SC, the intraparietal sulcus (IPS) and the inferior parietal cortex (IPS) showed a slight leftward and rightward asymmetry for eccentricity and polar angle varying stimuli, respectively. Although weaker, but still significant, the MT/MST/FST complex and lateral prefrontal cortex (lPFC) also showed a leftward bias for eccentricity and polar angle varying stimuli, respectively.

Whereas the human parietal cortex and frontoparietal networks are clearly rightward lateralized in visuospatial processing (Chen et al., 2019b), in monkeys there is no clear evidence for a functional unbalance (Wilke et al., 2012; Balan et al., 2018) or for its absence (Wan et al., 2022). It needs to be noted, however, that it is never systematically investigated as one typically needs a large number of subjects to obtain conclusive evidence in this respect. Nevertheless, comparative studies have delineated a continuum in the emergence of anatomical hemispheric asymmetries along the primate taxa (Wan et al., 2022; Preuss 2011; Hopkins 2022). In chimpanzees, the inferior parietal lobule (IPL) and superior temporal sulcus (STS) are places of structural interhemispheric asymmetries (Vickery et al., 2022; Gilissen and Hopkins 2013; Hopkins and Avants 2013; Phillips et al. 2013; Hopkins et al. 2014). The IPL is also the region showing a rightward asymmetry in intra-species variability already in macaques (Croxon et al., 2018). Intra-species variation influences direction and outcome of natural selection and sets the basis for further evolution (Godhe and Rynearson, 2017). Different regionally specific loci of intra-species variability have been found in both macaques and humans. Interestingly, the regions showing largest left-right asymmetries in both macaque and humans were mainly those showing the largest

degree of hemispheric dominance in humans (Wang et al. 2014). Moreover, increasing brain size has been taken as the evolutionary motive for hemispheric specialization. Species with larger brains have smaller callosal commissures. Thus, as hemisphere size increases, hemispheres become increasingly more isolated from each other (Hopkins et al., 2015). Compared to primary sensory and motor cortex, the IPL underwent processes of disproportionate expansion during primate brain evolution (Mantini et al., 2013; Chaplin et al., 2013; Orban et al., 2006). A new anterior portion appeared in the human IPS (Orban et al., 2006). The IPL enlargement also resulted in a substantial displacement of some areas of the IPS from macaques to humans. Specifically, the macaque ventral intraparietal (VIP) area is sitting medial relative to LIP, whereas the human VIP+ is paradoxically located more lateral to human LIP+ (Sereno and Huang, 2014). Additionally, population-level rightward asymmetries in macaques were revealed in the length and depth of the frontal arcuate sulcus (where the FEF is located; Sewada, 2020) and the surface area and cortical thickness of STS (Bogart et al., 2012; Xia et al., 2020).

In summary, our observations emphasize the presence of lateralized features in the nonhuman primate brain at different levels: 1) subcortically, at the level of an ancient, evolutionary conserved structure as the SC which, in some animals (i.e. birds) shows a complete anatomo-functional asymmetrical specialization; 2) cortically, at the level of the posterior parietal cortex which shows the largest degree of hemispheric dominance in humans and forms of anatomical interhemispheric asymmetry in macaque and chimpanzee. This unexpected finding opens avenues for future research to elucidate the functional significance of this asymmetry and its potential implications for visual processing in the macaque monkey.

5.3 Pragmatic representation of functionally-relevant sectors of space within the oculomotor/attentional system

Upper visual field and peripheral biases in the primate superior colliculus. In the last years a new conceptualization of the SC visual topography has been proposed, based on a pragmatic rather than geometric representation of the visual field, whereby the most relevant sectors of space for exploratory behaviors are overrepresented (Hafed and Chen, 2016; de Malmazet and Tripodi, 2023). Here, we found in the macaque SC a functional overrepresentation of specific sectors of visual space, that is, the peripheral and upper visual field (**Figure 14**). This is in line with the role of the visual SC in detecting stimuli outside the current focus of attention (i.e., in the periphery) and in the far, extra-personal space (associated to the upper visual field). Notably, the observed biases remained consistent when the polar angle and eccentricity fMRI data, on which the asymmetries were based,

were thresholded at different levels of significance ($p < .01$, $p < .0001$). The upper visual field bias appeared only when tested with stimuli reaching the periphery (up to 40° eccentricity, wVF experiment) and was not detectable with smaller stimuli covering only parafoveal and mid-eccentricity regions (up to 12.5°) of the visual field (in the sVF experiment). The dependency of the upper visual field bias on the extent of the visual field being tested mirrors again our first finding related to the importance to use stimuli with appropriate sizes for testing spatial-related properties with fMRI - as recently also documented in a human fMRI study on V1-V3 (Prabhakaran et al, 2020).

The overrepresentation of the upper visual field, especially for peripheral locations, mimics the magnification of this sector of space already shown with electrophysiology (Hafed and Chen, 2016). Visual SC cells have smaller receptive fields in the upper visual field compared to the lower visual field (Hafed and Chen, 2016). Notably, this difference was better detectable for eccentricities exceeding 4° (see **Figure 4)**, which is in line with our finding reported here. Although never directly investigated, "particular paucity" of polar angle representations near the lower vertical meridian has been already noted in an fMRI study on the human SC (Katyal et al., 2010).

One limitation of our study is the inability to differentiate responses from superficial or deeper SC layers. Therefore, the increased volume dedicated to the periphery in the SC (**Figure 14**) may also result from responses in the deeper visuo-motor layers known to have larger receptive fields (Cynader and Berman, 1972; Marocco and Li, 1977) which are not sensitive to small eccentric stimuli. Nevertheless, a putative bias for the peripheral visual field in the primate SC can be already seen in the predominance of monosynaptic retinal projections in macaques for eccentricities above 10° (Wilson and Toyne, 1970; Hendrickson et al., 1970; Lund, 1972; Pollack & Hickey 1979; Dilbeck et al. 2022; see Paragraph 1.2) and in the stronger responses for contralateral peripheral stimuli revealed with fMRI in humans (Sylvester et al., 2007; see Paragraph 1.2). The ethological relevance for peripheral stimuli in the general detection system of primates can be indirectly derived by the behavioral bias for stimuli located in the temporal hemifield (known as temporal–nasal asymmetry, see Paragraph 1.2) found in humans. This has been shown in studies focused on target detection, saccadic movements and attentional orienting in healthy adults (Kristjansson et al., 2004; Rafal et al., 1991; Posner and Cohen, 1980), newborns (Lewis and Maurer, 1992; Rothbart et al., 1990) and blindsight subjects (Dodds et al., 2002).

Moreover, the leftward interhemispheric asymmetry found in this study affected only the representations of parafoveal and mid-central regions of the visual fiend. Peripheral stimuli in the wVF (**Figure 10**, upper panels) and

SL2 (**Figure 12**, last panels) experiments, instead, yielded equally-balanced representations across hemispheres, highlighting the more pronounced sensitivity to the peripheral visual field.

Upper visual field bias and overrepresentation of center/periphery within the oculomotor/attentional cortical system. We found that the upper visual field was overrepresented within the SC, and also in LIP and FEF. Both are also important hubs of the oculomotor and/or attentional the system (**Figure 14**). At the same time, FEF and LIP presented different biases for the central (up to 10° eccentricity) or the peripheral (10°- 40° eccentricity) visual field: FEF appeared to be more tuned for the periphery and LIP for the central visual field. Also at the cortical level, the observed biases remained consistent when using retinotopic maps at different significance thresholds ($p < .01$, $p < .0001$).

In area FEF the upper visual field bias has never been directly tested in detail thus far, but previous electrophysiological and fMRI data suggested a predominance of upper receptive fields (see Figure 2 in Mayo et al., 2015) or overrepresentation of polar angles in the upper visual field (see Figure 3 in Saygin and Sereno, 2008). Area LIP, instead, hosts neurons with mainly parafoveal receptive fields (Hamed et al., 2001) but no strong evidence for upper/lower asymmetries have been found yet (Hamed et al., 2001; Arcaro et al., 2011).

The quantification of the receptive fields' distribution by means of electrophysiology as well as fMRI has to be interpreted carefully. Both techniques can potentially sample from neighboring areas, or they may simply under-sample the area itself. Electrophysiology samples the target area without looking at the entire population, potentially leading to biases related to sample size, neuron types, stimulus search-set induced biases, and the location of the recording electrodes. Then it can easily detect large differences in the receptive field organization across different sectors of space, but it is less suitable to detect smaller changes in the proportion of the representations of different subfields if those subfields are minimally represented. fMRI methods, on the other side, can give a measurement of the population receptive fields of single voxels of the entire region all at once. At the same time, the atlas-based definition of cortical ROIs through coregistration of each monkey brain onto a template brain often neglects inter-subject differences, registration errors and partial volume effects. This potentially leads to a misallocation or mis- or under-sampling of specific regions. For example, LIP is a small area located into a mosaic of small areas in the intraparietal sulcus (IPS). The lower field representation is situated more anteriorly and the upper visual field more posteriorly (Hamed et al., 2001; Arcaro et al., 2011). It may be that the atlas-defined LIP ROI extracted in this study extended less anteriorly in some monkeys leading to an exclusion, on average, of visual responses for the lower visual field.

Lower visual field bias and overrepresentation of the central visual field in the pulvinar complex. Finally, it's interesting to note that the pulvinar showed inverted biases compared to the SC, hence overrepresenting the central (as much as area V1) and the lower visual fields. In this case, the lower visual field bias was independent from the size of the stimulus used during the poral angle mapping phase of the experiment. The overrepresentation of the central visual field (up to 10° eccentricity) is not so surprising. The two large visually-driven nuclei of the pulvinar complex, the dorso-lateral (PL) and the inferior (PI) pulvinar, hosts two separated but complete retinotopic maps (Bender, 1981). Both nuclei receive information from cortical and retinal afferents (Kaas and Baldwin, 2019), but PL receives striatal projections limited only to the central 7° (Ungerleider et al., 1983), and PI receives retinal projections limited only to the central 10° (Grünert et al., 2021). This overrepresentation of central vision in this retino-pulvinar pathway has been suggested to be critical in establishing the normal connections of cortico-thalamic circuits driving visually-guided behaviors such as precision grasping and object manipulation (Mundinano et al. 2018), that are, behaviors that often take place in the central or lower visual field.

5.4 General conclusions

In conclusion, our study provides insights into the visuotopic organization of the primate SC.

First, it presents a detailed picture of macaque SC retinotopic maps with fMRI aligned with most recent electrophysiological models, and emphasizes the dynamic interplay between spatial representations in the brain and stimulus context. The observed variations in (peri)foveal representations (**Figure 10A**) and the presence of upper visual field biases (**Figure 14**) depending on the extent of stimulated visual field highlight the dependency of fMRI-based retinotopic maps on the spatial extent of the stimulated visual field. This highlights the need for adequate fMRI-based mapping stimuli in light of the context-sensitive nature of the SC circuitry regulating foveal and peripheral activity during sustained fixation.

Secondly, our findings support the hypothesis that the visuotopic organization of the SC is built on a pragmatic rather than metric representation of the visual field, emphasizing the most relevant sectors of space (de Malmazet and Tripodi, 2023). The SC magnifies the central visual field such that half of its surface along the rostro-caudal axis represents the central 10°. At the same time, eccentricity maps are unbalanced for peripheral the visual field. The rostral anatomical magnification for the central visual field and the co-present

overrepresentation of the periphery in the eccentricity maps suggest that both sectors of space are relevant for the SC, probably for different functions (see below). Moreover, the upper visual field bias observed in parietal and frontal areas implies that this pragmatic organization may extend across the entire oculomotor/attentional system, resulting more tuned for the peripheral visual field in its frontal component, and more tuned for the central visual field in its parietal component. The latter projects to deeper visuo-motor SC layers (Fries, 1984) together with other parietal and frontal areas of the network for fine manipulation under foveal control (Borra et al., 2014).

Third, our study revealed a surprising interhemispheric asymmetry in the representation of eccentricities and polar angles within the macaque SC and, to a lesser extent, the posterior parietal cortex. These areas are pivotal in the visuospatial processing network. The posterior parietal cortex exhibits anatomo-functional specialization in humans and some signs of anatomical lateralization in macaques. Within these regions, the left hemisphere (LH) exhibited greater sensitivity than the right hemisphere (RH) to stimuli varying in eccentricity. Such stimuli demand a detailed analysis of the visual field in relation of the gaze center, crucial for focusing on targets and guiding fine manipulation. Conversely, the RH demonstrated higher sensitivity than the LH to stimuli varying in polar angle, offering broad visuospatial information in eye-coordinates. This information is valuable for reorienting attention or behavior relative to the direction of salient stimuli.

5.4.1. Ethological relevance of different sectors of space

In primates, SC takes part into a wide network of ascending and descending fibers covering almost the entire brain, but with particularly strong connections with extrastriatal, posterior parietal, and frontal cortices (Fries, 1984; Isa et al, 2021). The SC is involved in at least two well-investigated functional circuits, the attentional/oculomotor network for orienting and exploratory behaviors (Ignashchenkova et al. 2004; Bisley and Goldberg, 2010; Matsumoto et al, 2018), and in eye-hand coordination for guiding fine hand-object interactions (Borra et al., 2014; Nagy et al., 2006; Reyes-Puerta et al., 2010). The attentional/oculomotor system involves the frontal area FEF and the parietal area LIP that, together with the SC, showed a functional bias for the upper visual field, the sector of space conveying information from potentially far stimuli. This specialization is also present in visual maps of mice (Dräger and Hubel, 1976), where the upper visual field is source of incoming predators (de Malmazet and Tripodi, 2023) and it's probably preserved also in humans, given the shorter latencies for upward saccades in primates (Zhou and King, 2002; Greene et al., 2020).

Different sectors of space represent a source of appealing or threatening stimuli, such as pray or predators. In rodents, upward and downward stimuli evoke through the SC avoidance and approaching behaviors, respectively (Cruz et al., 2023). Whether predators can appear all over the visual field, near or far in respect to the animal, preys or appealing stimuli promotes interaction when they are located anteriorly and possibly close to the animal (Mearns et al., 2020). In simple animals like the lamprey, both orienting and evasive behaviors are induced upon stimulation of the rostral tectum, and stimulation of caudal portions predominantly elicits evasive movements (Isa e al., 2021; Bulter and Hodos, 2005). In primates, we found that the upper visual field bias was present for peripheral stimuli in the frontal component of the oculomotor/attentional system, area FEF, projecting to the superficial layers of the SC. This could facilitate fast detection, rapid foveation and possibly defensive behaviors for downward coming stimuli as potential treats. The parietal component of the oculomotor/attentional system, area LIP, instead, showed the upper visual field bias specifically for central stimuli. LIP conveys this information to intermediated SC layers where it could be integrated with other information coming from projections of the hand-object interaction system (lateral grasping network; Borra et al., 2014) for the control of approach/avoidance of central stimuli.

This study can provide a first hint in this direction. Further behavioral, electrophysiological as well as inactivation studies should be performed in the same direction to provide a more complete picture of the pragmatic saliency of different sectors of space. Even if there are data supporting the hypothesis that the upper and lower visual fields are primarily linked to extrapersonal and peripersonal space, respectively (Zhou et al., 2017), the macaque SC has never been studied in 3D space, and even less in free-moving animals. Taking into account the ecologically-relevance of different sector of space also implies the consideration of natural behaviors of the animal model used. Macaques spend a great amount of their time in trees, for rest and sleep, and they usually get off the ground for foraging and long-range locomotion. The information conveyed by upper/lower visual fields varies based on status of the individual, if in rest on trees or active on the ground.

5.4.2. Anatomical magnification of the central visual field for guiding approaching/interacting behaviors

These findings as well as most recent electrophysiological investigations (Chen et al., 2019) suggest that the rostral SC anatomically magnifies the representation of the central visual field in primates, such that half of its surface along the rostro-caudal axis represents the central 10°. Across species, preys or appealing stimuli promote interaction when located anteriorly and possibly close to the animal (Mearns et al., 2020). In snakes equipped with an infrared-detecting system, for example, the tectal region corresponding to the anterior sensory field is

crucial for pre-striking prey positioning and exhibits an enlargement, which is more pronounced for thermal than for visual stimuli (Hartline et al., 1978). Similarly to snakes, in the star-nosed mole (Condylura cristata; Crish et al., 2003) a subterranean mammal relying on tactile sensation rather than vision for navigation and object manipulation, the representation of the snout's fleshy appendage with maximum tactile acuity is magnified in the rostral SC. In mice lacking a fovea, the somatosensory map shows an anterior expansion specifically for the whisker, similar to the snout representation in the star-nosed mole (Cang et al., 2018; Dräger and Hubel, 1976). In primates, the rostral SC hosts motor cells signaling target foveation (Munoz and Wurtz, 1993) and intermediate neurons involved in gaze anchoring during reaching movements (Reyes-Puerta et al., 2010). Additionally, the somato-motor representation of the hand tends to be confined to the rostro-lateral part of the colliculus. The lateral region hosts neurons modulated by the contact of the hand with the target (Nagy et al., 2006) and encodes for downward gaze shifts and low visual field (Zhang et al., 2022), usually associated to the near, peripersonal space in which interactions with the external environment take place. For its contribution in eye-hand coordination, the SC has been proposed to be part of the network for guiding fine hand-object interactions under foveal control (Borra et al., 2014). Taken together, these findings suggest a predominant role of the SC rostral region in approaching/interacting behaviors.

5.4.3. Functional and connectivity bias for the visual representation of peripheral stimuli

Beside the role of the rostral SC to motor functions such as foveation (Munoz and Wurtz, 1993), short-range saccades (Godlove and Schall, 2016) and eye-hand coordination (Reyes-Puerta et al., 2010; Borra et al., 2014), the contribution of the rostral SC to visual maps seems to be confined in signaling (para)foveal stimuli, although less effectively than the caudal SC with peripheral stimuli (temporal-nasal asymmetry; see 1.2.). Here, we found a functional bias within the SC visual maps for peripheral stimuli with eccentricities larger than 10°, which further emphasizes the relevance of representing stimuli far outside the current attentional focus. Moreover, an interesting anatomical specialization has been documented in the rostral SC of primates: only ~4% of retino-tectal projections arise from the *pars centralis* of the retina (up to 10° eccentricity; Wilson and Toyne, 1970; Hendrickson et al., 1970; Lund, 1972; Pollack & Hickey 1979, Dilbeck et al. 2022). This means that the representation of the central visual field in the rostral SC is poorly informed by retinal input and, then, it must primarily arise from other brain structures. An optimal candidate would be the primary visual cortex, which highly magnifies central eccentricities and directly projects to superficial layers of the SC, but its ablation doesn't completely abolish visual responses in foveal superficial neurons of the SC (Shiller et al. 1974). The pulvinar is a

second good candidate, highly connected with both superficial and deeper SC layers (Benevento and Fallon, 1975; Froesel et al., 2021) and hosting multiple visual maps in retinotopic coordinates (Bender, 1981). Here we found an overrepresentation of the central (up to 10°) visual field in the pulvinar, on par with the one in area V1, together with a bias for the lower visual field. The pulvinar could then complement the visual field representation of the SC providing information on the central and lower visual field, potentially being the source of parafoveal information not supplied by retinal afferents.

5.4.4. Interhemispheric asymmetry in the retinotopic maps of the rostral SC and PPC

Interestingly, the leftward interhemispheric asymmetry found in the SC eccentricity maps along the rostro-caudal axis was limited to the rostral-most portion representing the eccentricities for which retinal projections were lacking the most (i.e. up to 10° circa). None of the other key nodes of the oculomotor/attentional network showed a similar interhemispheric asymmetry in the sensitivity to central, relatively small stimuli, which appeared confined to the SC. Furthermore, the left hemisphere showed more sensitivity to eccentricity varying stimuli along the entire rostro-caudal extent of the SC and, even more surprisingly, also in the posterior parietal cortex (PPC). The right hemisphere showed the opposite trend, with more sensitivity to polar angle varying stimuli in the SC and also in the PPC. Such stimuli either demand a detailed analysis of the visual field in relation of the gaze center (eccentricity varying stimuli), crucial for focusing on targets and guiding fine manipulation, or offer broad visuospatial information in eye-coordinates with regard to vertical and horizontal meridians (polar angle varying stimuli), valuable for reorienting attention or behavior relative to the direction of salient stimuli.

This hemispheric specialization for different types of visuospatial information opens to the possibility that functional lateralization is already manifested in the macaque brain. This functional lateralization may occur in cortical regions, as the PPC, for which anatomical lateralization has been suggested in chimpanzees and macaques (Croxon et al., 2018; Wan et al., 2021; Preuss 2011; Hopkins 2022; Bogart et al., 2012; Xia et al., 2020). In humans, the PPC is specialized (Corballis, 2012; Chen et al., 2019) for functions related to fine manipulation on the left and visuospatial processing on the right. Crucially, the stronger hemispheric specialization in our experiments was found in the superior colliculus, not in the cortex, in the manner how eccentricity varying stimuli are represented. Given the absence of an effect in monkey PPC, it is possible that such hemispheric specialization originated subcortically within the SC.

6. References

Ajina, S., & Bridge, H. (2016). Blindsight and Unconscious Vision: What They Teach Us about the Human Visual System. *Neuroscientist*, 23(5), 529-541. https://doi.org/10.1177/1073858416673817

Ajina, S., & Bridge, H. (2018). Blindsight relies on a functional connection between hMT+ and the lateral geniculate nucleus, not the pulvinar. *PLoS biology*, *16*(7), e2005769. https://doi.org/10.1371/journal.pbio.2005769

Alexander, G. E., DeLong, M. R., & Strick, P. L. (1986). Parallel organization of functionally segregated circuits linking basal ganglia and cortex. *Annual Review of Neuroscience*, 9, 357–381.

Altman, J., & Carpenter, M. B. (1961). Fiber projections of the superior colliculus in the cat. *The Journal of Comparative Neurology*, 116, 157–177. https://doi.org/10.1002/cne.901160206

Appell, P. P., & Behan, M. (1990). Sources of subcortical GABAergic projections to the superior colliculus in the cat. *Journal of Comparative Neurology*, 302(1), 143–158.

Arcaro, M. J., Pinsk, M. A., Li, X., & Kastner, S. (2011). Visuotopic organization of macaque posterior parietal cortex: a functional magnetic resonance imaging study. *Journal of Neuroscience*, 31(6), 2064-2078. https://doi.org/10.1523/JNEUROSCI.3334-10.2011.

Armendariz, M., Ban, H., Welchman, A. E., & Vanduffel, W. (2019). Areal differences in depth cue integration between monkey and human. *PLoS biology*, *17*(3), e2006405. https://doi.org/10.1371/journal.pbio.2006405

Autio, J. A., Glasser, M. F., Ose, T., Donahue, C. J., Bastiani, M., Ohno, M., Kawabata, Y., Urushibata, Y., Murata, K., Nishigori, K., Yamaguchi, M., Hori, Y., Yoshida, A., Go, Y., Coalson, T. S., Jbabdi, S., Sotiropoulos, S. N., Kennedy, H., Smith, S., Van Essen, D. C., … Hayashi, T. (2020). Towards HCP-Style macaque connectomes: 24-Channel 3T multi-array coil, MRI sequences and preprocessing. *NeuroImage*, *215*, 116800. https://doi.org/10.1016/j.neuroimage.2020.116800

Bakker, R., Tiesinga, P., & Kötter, R. (2015). The Scalable Brain Atlas: instant web-based access to public brain atlases and related content. *Neuroinformatics*. http://link.springer.com/content/pdf/10.1007/s12021-014-9258-x (author copy: arXiv:1312.6310)

Balan, P. F., Gerits, A., Zhu, Q., Kolster, H., Orban, G. A., Wardak, C., & Vanduffel, W. (2019). Fast compensatory functional network changes caused by reversible inactivation of monkey parietal cortex. *Cerebral cortex* (New York, N.Y. : 1991), 29(6), 2588–2606. https://doi.org/10.1093/cercor/bhy128

Balan, P. F., Zhu, Q., Li, X., Niu, M., Rapan, L., Funck, T., Bakker, R., Palomero-Gallagher, N., & Vanduffel, W. (2023). MEBRAINS 1.0: a new population-based macaque atlas. *bioRxiv*. https://doi.org/10.1101/2023.06.21.545953.

Barbot, A., Xue, S., & Carrasco, M. (2021). Asymmetries in visual acuity around the visual field. *Journal of vision*, *21*(1), 2. https://doi.org/10.1167/jov.21.1.2

Basso, M. A., Bickford, M. E., & Cang, J. (2021). Unraveling circuits of visual perception and cognition through the superior colliculus. *Neuron*, *109*(6), 918–937. https://doi.org/10.1016/j.neuron.2021.01.013

Ben Hamed, S., Duhamel, J. R., Bremmer, F., & Graf, W. (2001). Representation of the visual field in the lateral intraparietal area of macaque monkeys: a quantitative receptive field analysis. *Experimental brain research*, *140*(2), 127–144. https://doi.org/10.1007/s002210100785

Bender D. B. (1981). Retinotopic organization of macaque pulvinar. *Journal of neurophysiology*, *46*(3), 672–693. https://doi.org/10.1152/jn.1981.46.3.672

Benevento, L. A., & Fallon, J. H. (1975). The ascending projections of the superior colliculus in the rhesus monkey (Macaca mulatta). *The Journal of comparative neurology*, *160*(3), 339–361. https://doi.org/10.1002/cne.901600306

Benson, N. C., Jamison, K. W., Arcaro, M. J., Vu, A. T., Glasser, M. F., Coalson, T. S., Van Essen, D. C., Yacoub, E., Ugurbil, K., Winawer, J., & Kay, K. (2018). The Human Connectome Project 7 Tesla retinotopy dataset: Description and population receptive field analysis. *Journal of Vision*, 18(13), 23. https://doi.org/10.1167/18.13.23

Benson, N. C., Jamison, K. W., Arcaro, M. J., Vu, A. T., Glasser, M. F., Coalson, T. S., ... Winawer, J. (2018). The Human Connectome Project 7 Tesla retinotopy dataset: Description and population receptive field analysis. *Journal of Vision*, 18(13), 23. https://doi.org/10.1167/18.13.23.

Berman, R. A., & Wurtz, R. H. (2010). Functional identification of a pulvinar path from the superior colliculus to cortical area MT. *Journal of Neuroscience*, 30(18), 6342–6354.

Berson, D. M. (2008). Retinal ganglion cell types and their central projections. In A. I. Basbaum, A. Kaneko, G. M. Shepherd, & G. Westheimer (Eds.), The Senses: A comprehensive reference. Vol. 1, Vision I (pp. 491–520). Academic Press.

Bisley, J. W., & Goldberg, M. E. (2010). Attention, intention, and priority in the parietal lobe. *Annual review of neuroscience*, *33*, 1–21. https://doi.org/10.1146/annurev-neuro-060909-152823

Bloom, J. S., & Hynd, G. W. (2005). The role of the corpus callosum in interhemispheric transfer of information: excitation or inhibition?. *Neuropsychology review*, *15*(2), 59–71. https://doi.org/10.1007/s11065-005-6252-y

Bogadhi, A. R., Katz, L. N., Bollimunta, A., Leopold, D. A., & Krauzlis, R. J. (2021). Midbrain activity shapes high-level visual properties in the primate temporal cortex. *Neuron*, 109(4), 690-699.e5. https://doi.org/10.1016/j.neuron.2020.11.023

Bogart, S. L., Mangin, J. F., Schapiro, S. J., Reamer, L., Bennett, A. J., Pierre, P. J., & Hopkins, W. D. (2012). Cortical sulci asymmetries in chimpanzees and macaques: a new look at an old idea. *NeuroImage*, *61*(3), 533–541. https://doi.org/10.1016/j.neuroimage.2012.03.082

Borra, E., Gerbella, M., Rozzi, S., Tonelli, S., & Luppino, G. (2014). Projections to the superior colliculus from inferior parietal, ventral premotor, and ventrolateral prefrontal areas involved in controlling goal-directed hand actions in the macaque. *Cerebral cortex (New York, N.Y. : 1991)*, *24*(4), 1054–1065. https://doi.org/10.1093/cercor/bhs392

Bruce, C. J., Desimone, R., & Gross, C. G. (1986). Both striate cortex and superior colliculus contribute to visual properties of neurons in superior temporal polysensory area of macaque monkey. *Journal of neurophysiology*, *55*(5), 1057–1075. https://doi.org/10.1152/jn.1986.55.5.1057

Butler, A.B., & Hodos, W. (2005). Optic tectum. In A.B. Butler & W. Hodos (Eds.), Comparative Vertebrate Neuroanatomy: Evolution and Adaptation (2nd ed., pp. 311–340). New Jersey: Wiley.

Campbell, K.J., & Takada, M. (1989). Bilateral tectal projection of single nigrostriatal dopamine cells in the rat. Neuroscience, 33(2), 311–321.

Campbell, K.J., and Takada, M. (1989). Bilateral tectal projection of single nigrostriatal dopamine cells in the rat. *Neuroscience,* 33, 311–321.

Cang, J., Savier, E., Barchini, J., & Liu, X. (2018). Visual Function, Organization, and Development of the Mouse Superior Colliculus. *Annual review of vision science*, 4, 239–262. https://doi.org/10.1146/annurev-vision-091517-034142

Cerkevich, C. M., Lyon, D. C., Balaram, P., & Kaas, J. H. (2014). Distribution of cortical neurons projecting to the superior colliculus in macaque monkeys. *Eye and brain*, 2014(6), 121–137. https://doi.org/10.2147/EB.S53613

Chaplin, T. A., Yu, H. H., Soares, J. G., Gattass, R., & Rosa, M. G. (2013). A conserved pattern of differential expansion of cortical areas in simian primates. *Journal of Neuroscience*, 33(40), 15120–15125. https://doi.org/10.1523/JNEUROSCI.2909-13.2013

Chen, C. Y., & Hafed, Z. M. (2018). Orientation and contrast tuning properties and temporal flicker fusion characteristics of primate superior colliculus neurons. *Frontiers in Neural Circuits*, 12, 58. https://doi.org/10.3389/fncir.2018.00058

Chen, C. Y., Hoffmann, K. P., Distler, C., & Hafed, Z. M. (2019). The Foveal Visual Representation of the Primate Superior Colliculus. *Current biology : CB*, *29*(13), 2109–2119.e7. https://doi.org/10.1016/j.cub.2019.05.040

Chen, C. Y., Sonnenberg, L., Weller, S., Witschel, T., & Hafed, Z. M. (2018). Spatial frequency sensitivity in macaque midbrain. *Nature Communications*, 9, 2852. https://doi.org/10.1038/s41467-018-05238-9

Chen, Q., Beaty, R. E., Cui, Z., Sun, J., He, H., Zhuang, K., Ren, Z., Liu, G., & Qiu, J. (2019b). Brain hemispheric involvement in visuospatial and verbal divergent thinking. *NeuroImage*, 202, 116065. https://doi.org/10.1016/j.neuroimage.2019.116065

Chung, M., Hartley, R., Dalton, K. M., & Davidson, R. J. (2008). Encoding cortical surface by spherical harmonics. *Statistica Sinica,* 18, 1269-1291.

Cisek P. (2022). Evolution of behavioural control from chordates to primates. *Philosophical transactions of the Royal Society of London. Series B, Biological sciences*, 377(1844), 20200522. https://doi.org/10.1098/rstb.2020.0522

Cisek, P. (2007). Cortical mechanisms of action selection: the affordance competition hypothesis. *Philosophical Transactions of the Royal Society B: Biological Sciences*, 362(1485), 1585-1599. https://doi.org/10.1098/rstb.2007.2054.

Clower, D. M., West, R. A., Lynch, J. C., & Strick, P. L. (2001). The inferior parietal lobule is the target of output from the superior colliculus, hippocampus, and cerebellum. *Journal of Neuroscience*, 21(16), 6283–6291.

Colby, C. L., Duhamel, J. R., & Goldberg, M. E. (1993). The analysis of visual space by the lateral intraparietal area of the monkey: the role of extraretinal signals. *Progress in brain research*, *95*, 307–316. https://doi.org/10.1016/s0079-6123(08)60378-7

Comoli, E., Coizet, V., Boyes, J., Bolam, J. P., Canteras, N. S., Quirk, R. H., Overton, P. G., & Redgrave, P. (2003). A direct projection from superior colliculus to substantia nigra for detecting salient visual events. *Nature Neuroscience*, 6, 974–980. https://doi.org/10.1038/nn1113

Cowey, A., & Stoerig, P. (1995). Blindsight in monkeys. *Nature*, 373(6511), 247–249. https://doi.org/10.1038/373247a0

Crapse, T. B., & Sommer, M. A. (2009). Frontal eye field neurons with spatial representations predicted by their subcortical input. *Journal of Neuroscience*, 29(16), 5308–5318. https://doi.org/10.1523/JNEUROSCI.4906-08.2009

Crish, S. D., Comer, C. M., Marasco, P. D., & Catania, K. C. (2003). Somatosensation in the superior colliculus of the star-nosed mole. *The Journal of comparative neurology*, *464*(4), 415–425. https://doi.org/10.1002/cne.10791

Crook, J. D., Peterson, B. B., Packer, O. S., Robinson, F. R., Gamlin, P. D., Troy, J. B., & Dacey, D. M. (2008). The smooth monostratified ganglion cell: evidence for spatial diversity in the Y-cell pathway to the lateral geniculate nucleus and superior colliculus in the macaque monkey. *The Journal of neuroscience : the official journal of the Society for Neuroscience*, *28*(48), 12654–12671. https://doi.org/10.1523/JNEUROSCI.2986-08.2008

Croxson, P. L., Forkel, S. J., Cerliani, L., & Thiebaut de Schotten, M. (2018). Structural Variability Across the Primate Brain: A Cross-Species Comparison. *Cerebral cortex (New York, N.Y. : 1991)*, *28*(11), 3829–3841. https://doi.org/10.1093/cercor/bhx244

Cruz, K. G., Leow, Y. N., Le, N. M., Adam, E., Huda, R., & Sur, M. (2023). Cortical-subcortical interactions in goal-directed behavior. *Physiological reviews*, *103*(1), 347–389. https://doi.org/10.1152/physrev.00048.2021

Cusick C. G. (1988). Anatomical organization of the superior colliculus in monkeys: corticotectal pathways for visual and visuomotor functions. *Progress in brain research*, 75, 1–15. https://doi.org/10.1016/s0079-6123(08)60461-6

Cynader, M., & Berman, N. (1972). Receptive-field organization of monkey superior colliculus. *Journal of neurophysiology*, *35*(2), 187–201. https://doi.org/10.1152/jn.1972.35.2.187

Daisley, J. N., Mascalzoni, E., Rosa-Salva, O., Rugani, R., & Regolin, L. (2009). Lateralization of social cognition in the domestic chicken (Gallus gallus). *Philosophical transactions of the Royal Society of London. Series B, Biological sciences*, *364*(1519), 965–981. https://doi.org/10.1098/rstb.2008.0229

Dale, A. M., Fischl, B., & Sereno, M. I. (1999). Cortical surface-based analysis. I. Segmentation and surface reconstruction. *NeuroImage*, *9*(2), 179–194. https://doi.org/10.1006/nimg.1998.0395

Daniel, P. M., & Whitteridge, D. (1961). The representation of the visual field on the cerebral cortex in monkeys. *Journal of Physiology*, 159(2), 203-221. https://doi.org/10.1113/jphysiol.1961.sp006803

de Malmazet, D., & Tripodi, M. (2023). Collicular circuits supporting the perceptual, motor and cognitive demands of ethological environments. *Current opinion in neurobiology*, *82*, 102773. https://doi.org/10.1016/j.conb.2023.102773

Dean, P., Redgrave, P., and Westby, G.W. (1989). Event or emergency? Two response systems in the mammalian superior colliculus. *Trends Neurosci*. 12, 137–147.

DeSimone, K., Viviano, J. D., & Schneider, K. A. (2015). Population Receptive Field Estimation Reveals New Retinotopic Maps in Human Subcortex. *The Journal of neuroscience : the official journal of the Society for Neuroscience*, *35*(27), 9836–9847. https://doi.org/10.1523/JNEUROSCI.3840-14.2015

DesJardin, J. T., Holmes, A. L., Forcelli, P. A., Cole, C. E., Gale, J. T., Wellman, L. L., Gale, K., & Malkova, L. (2013). Defense-like behaviors evoked by pharmacological disinhibition of the superior colliculus in the primate. *The Journal of neuroscience : the official journal of the Society for Neuroscience*, *33*(1), 150–155. https://doi.org/10.1523/JNEUROSCI.2924-12.2013

Diao, Y. C., Wang, Y. K., & Xiao, Y. M. (1983). Representation of the binocular visual field in the superior colliculus of the albino rat. *Experimental brain research*, *52*(1), 67–72. https://doi.org/10.1007/BF00237150

Dilbeck, M. D., Spahr, Z. R., Nanjappa, R., Economides, J. R., & Horton, J. C. (2022). Columnar and Laminar Segregation of Retinal Input to the Primate Superior Colliculus Revealed by Anterograde Tracer Injection Into Each Eye. *Investigative ophthalmology & visual science*, *63*(1), 9. https://doi.org/10.1167/iovs.63.1.9

Dodds, C., Machado, L., Rafal, R., & Ro, T. (2002). A temporal/nasal asymmetry for blindsight in a localisation task: evidence for extrageniculate mediation. *Neuroreport*, *13*(5), 655–658. https://doi.org/10.1097/00001756-200204160-00024

Dräger, U. C., & Hubel, D. H. (1975). Responses to visual stimulation and relationship between visual, auditory, and somatosensory inputs in mouse superior colliculus. *Journal of neurophysiology*, *38*(3), 690–713. https://doi.org/10.1152/jn.1975.38.3.690

Dräger, U. C., & Hubel, D. H. (1976). Topography of visual and somatosensory projections to mouse superior colliculus. *Journal of neurophysiology*, *39*(1), 91–101. https://doi.org/10.1152/jn.1976.39.1.91

Dubach MF, Bowden DM (2009) "BrainInfo online 3D macaque brain atlas: a database in the shape of a brain" *Society for Neuroscience Annual Meeting, Chicago, IL* Abstract No. 199.5.

DuBois, R. M., & Cohen, M. S. (2000). Spatiotopic organization in human superior colliculus observed with fMRI. *NeuroImage*, *12*(1), 63–70. https://doi.org/10.1006/nimg.2000.0590

Dumoulin, S. O., & Wandell, B. A. (2008). Population receptive field estimates in human visual cortex. *NeuroImage*, 39(2), 647-660. https://doi.org/10.1016/j.neuroimage.2007.09.034

Dwivedi, A. K., Mallawaarachchi, I., & Alvarado, L. A. (2017). Analysis of small sample size studies using nonparametric bootstrap test with pooled resampling method. *Statistics in medicine*, *36*(14), 2187–2205. https://doi.org/10.1002/sim.7263

Edwards, S. B. (1980). The deep cell layers of the superior colliculus: their reticular characteristics and structural organization. In J. A. Hobson & M. D. Brazier (Eds.), The Reticular Formation Revisited (pp. 193-209). Raven Press.

Ellis, E. M., Gauvain, G., Sivyer, B., & Murphy, G. J. (2016). Shared and distinct retinal input to the mouse superior colliculus and dorsal lateral geniculate nucleus. *Journal of neurophysiology*, *116*(2), 602–610. https://doi.org/10.1152/jn.00227.2016

Engel, S. A., Glover, G. H., & Wandell, B. A. (1997). Retinotopic organization in human visual cortex and the spatial precision of functional MRI. *Cerebral cortex (New York, N.Y. : 1991)*, *7*(2), 181–192. https://doi.org/10.1093/cercor/7.2.181

Ferri, S., Peeters, R., Nelissen, K., Vanduffel, W., Rizzolatti, G., & Orban, G. A. (2015). A human homologue of monkey F5c. *NeuroImage*, *111*, 251–266. https://doi.org/10.1016/j.neuroimage.2015.02.033

Finlay, B. L., Schneps, S. E., Wilson, K. G., & Schneider, G. E. (1978). Topography of visual and somatosensory projections to the superior colliculus of the golden hamster. *Brain research*, *142*(2), 223–235. https://doi.org/10.1016/0006-8993(78)90632-7

Fischl, B., Sereno, M. I., & Dale, A. M. (1999). Cortical surface-based analysis. II: Inflation, flattening, and a surface-based coordinate system. *NeuroImage*, *9*(2), 195–207. https://doi.org/10.1006/nimg.1998.0396

Fize, D., Vanduffel, W., Nelissen, K., Denys, K., Chef d'Hotel, C., Faugeras, O., & Orban, G. A. (2003). The retinotopic organization of primate dorsal V4 and surrounding areas: A functional magnetic resonance imaging study in awake monkeys. *Journal of Neuroscience*, 23(19), 7395-7406. https://doi.org/10.1523/JNEUROSCI.23-19-07395.2003.

Forster, D., Helmbrecht, T.O., Mearns, D.S., Jordan, L., Mokayes, N., and Baier, H. (2020). Retinotectal circuitry of larval zebrafish is adapted to detection and pursuit of prey. *eLife* 9, e58596.

Fracasso, A., Buonocore, A., Hafed, Z.M. (2023). Peri-Saccadic Orientation Identification Performance and Visual Neural Sensitivity Are Higher in the Upper Visual Field. Journal of Neuroscience, 43(41), 6884–6897. DOI: 10.1523/JNEUROSCI.1740-22.2023

Fries W. (1984). Cortical projections to the superior colliculus in the macaque monkey: a retrograde study using horseradish peroxidase. *The Journal of comparative neurology*, *230*(1), 55–76. https://doi.org/10.1002/cne.902300106

Fries W. (1985). Inputs from motor and premotor cortex to the superior colliculus of the macaque monkey. *Behavioural brain research*, *18*(2), 95–105. https://doi.org/10.1016/0166-4328(85)90066-x

Froesel, M., Cappe, C., & Ben Hamed, S. (2021). A multisensory perspective onto primate pulvinar functions. *Neuroscience and biobehavioral reviews*, *125*, 231–243. https://doi.org/10.1016/j.neubiorev.2021.02.043

Frost, B. J., Wise, L. Z., Morgan, B., & Bird, D. (1990). Retinotopic representation of the bifoveate eye of the kestrel (Falco sparverius) on the optic tectum. *Visual Neuroscience*, 5(3), 231–239. https://doi.org/10.1017/s0952523800000304

Gandhi, N. J., & Katnani, H. A. (2011). Motor functions of the superior colliculus. *Annual review of neuroscience*, *34*, 205–231. https://doi.org/10.1146/annurev-neuro-061010-113728

Gattass, R., Galkin, T. W., Desimone, R., & Ungerleider, L. G. (2014). Subcortical connections of area V4 in the macaque. *Journal of Comparative Neurology*, 522(8), 1941-1965. https://doi.org/10.1002/cne.23513

Ghitani, N., Bayguinov, P. O., Vokoun, C. R., McMahon, S., Jackson, M. B., & Basso, M. A. (2014). Excitatory synaptic feedback from the motor layer to the sensory layers of the superior colliculus. *Journal of Neuroscience*, 34(20), 6822-6833. https://doi.org/10.1523/JNEUROSCI.3137-13.2014

Gilissen, E. P., & Hopkins, W. D. (2013). Asymmetries of the parietal operculum in chimpanzees (Pan troglodytes) in relation to handedness for tool use. *Cerebral Cortex*, 23(2), 411–422.

Glasser, M. F., Sotiropoulos, S. N., Wilson, J. A., Coalson, T. S., Fischl, B., Andersson, J. L., Xu, J., Jbabdi, S., Webster, M., Polimeni, J. R., Van Essen, D. C., Jenkinson, M., & WU-Minn HCP Consortium (2013). The minimal preprocessing pipelines for the Human Connectome Project. *NeuroImage*, *80*, 105–124. https://doi.org/10.1016/j.neuroimage.2013.04.127

Godhe, A., & Rynearson, T. (2017). The role of intraspecific variation in the ecological and evolutionary success of diatoms in changing environments. *Philosophical transactions of the Royal Society of London. Series B, Biological sciences*, *372*(1728), 20160399. https://doi.org/10.1098/rstb.2016.0399

Godlove, D. C., & Schall, J. D. (2016). Microsaccade production during saccade cancellation in a stop-signal task. Vision Research, 118, 5-16. https://doi.org/10.1016/j.visres.2014.10.025

Graham, J. (1982). Some topographical connections of the striate cortex with subcortical structures in Macaca fascicularis. *Experimental Brain Research*, 47, 1–14.

Greene, H. H., Brown, J. M., & Strauss, G. P. (2020). Shorter fixation durations for up-directed saccades during saccadic exploration: A meta-analysis. *Journal of eye movement research*, *12*(8), 10.16910/jemr.12.8.5. https://doi.org/10.16910/jemr.12.8.5

Grinvald, A., Lieke, E. E., Frostig, R. D., & Hildesheim, R. (1994). Cortical point-spread function and long-range lateral interactions revealed by real-time optical imaging of macaque monkey primary visual cortex. *The Journal of neuroscience : the official journal of the Society for Neuroscience*, *14*(5 Pt 1), 2545–2568. https://doi.org/10.1523/JNEUROSCI.14-05-02545.1994

Grünert, U., Lee, S. C. S., Kwan, W. C., Mundinano, I. C., Bourne, J. A., & Martin, P. R. (2021). Retinal ganglion cells projecting to superior colliculus and pulvinar in marmoset. *Brain structure & function*, *226*(9), 2745–2762. https://doi.org/10.1007/s00429-021-02295-8

Grüsser, O. J., Pause, M., & Schreiter, U. (1990). Localization and responses of neurones in the parieto-insular vestibular cortex of awake monkeys (Macaca fascicularis). *The Journal of physiology*, *430*, 537–557. https://doi.org/10.1113/jphysiol.1990.sp018306

Gülbetekin, E., Güntürkün, O., Dural, S., & Çetinkaya, H. (2009). Visual asymmetries in Japanese quail (*Coturnix japonica*) retain a lifelong potential for plasticity. *Behavioral Neuroscience, 123*(4), 815–821. https://doi.org/10.1037/a0016406

Güntürkün, O., Ströckens, F., & Ocklenburg, S. (2020). Brain Lateralization: A Comparative Perspective. *Physiological reviews*, *100*(3), 1019–1063. https://doi.org/10.1152/physrev.00006.2019

Hafed, Z. M., & Chen, C. Y. (2016). Sharper, stronger, faster upper visual field representation in primate superior colliculus. Current Biology, 26, 1647–1658.

Hartig, R., Glen, D., Jung, B., Logothetis, N. K., Paxinos, G., Garza-Villarreal, E. A., Messinger, A., & Evrard, H. C. (2021). The Subcortical Atlas of the Rhesus Macaque (SARM) for neuroimaging. *Neuroimage*, 235, 117996. https://doi.org/10.1016/j.neuroimage.2021.117996

Harting, J. K., & Van Lieshout, D. P. (1991). Spatial relationships of axons arising from the substantia nigra, spinal trigeminal nucleus, and pedunculopontine tegmental nucleus within the intermediate gray of the cat superior colliculus. *Journal of Comparative Neurology*, 305(4), 543–558.

Harting, J. K., Huerta, M. F., Frankfurter, A. J., Strominger, N. L., & Royce, G. J. (1980). Ascending pathways from the monkey superior colliculus: an autoradiographic analysis. *The Journal of comparative neurology*, *192*(4), 853–882. https://doi.org/10.1002/cne.901920414

Hartline, P. H., Kass, L., & Loop, M. S. (1978). Merging of modalities in the optic tectum: infrared and visual integration in rattlesnakes. *Science (New York, N.Y.)*, *199*(4334), 1225–1229. https://doi.org/10.1126/science.628839

Harvey, B. M., & Dumoulin, S. O. (2011). The relationship between cortical magnification factor and population receptive field size in human visual cortex: constancies in cortical architecture. *The Journal of neuroscience : the official journal of the Society for Neuroscience*, *31*(38), 13604–13612. https://doi.org/10.1523/JNEUROSCI.2572-11.2011

Hedreen, J. C., & Yin, T. C. (1981). Homotopic and heterotopic callosal afferents of caudal inferior parietal lobule in Macaca mulatta. *The Journal of comparative neurology*, *197*(4), 605–621. https://doi.org/10.1002/cne.901970405

Helmbrecht, T.O., dal Maschio, M., Donovan, J.C., Koutsouli, S., and Baier, H. (2018). Topography of a visuomotor transformation. *Neuron* 100,1429–1445.

Hendrickson, A., Wilson, H. E., & Toyne, M. J. (1970). The distribution of optic nerve fibers in Macaca mulatta. *Brain Research*, 23, 425-427.

Hikosaka, O., & Wurtz, R. H. (1983). Visual and oculomotor functions of monkey substantia nigra pars reticulata. IV. Relation of substantia nigra to superior colliculus. *Journal of neurophysiology*, *49*(5), 1285–1301. https://doi.org/10.1152/jn.1983.49.5.1285

Hilgetag, C. C. (2000). Spatial neglect and paradoxical lesion effects in the cat — A model based on midbrain connectivity. *Neurocomputing*, 32–33, 793-799. https://doi.org/10.1016/S0925-2312(00)00246-0.

Hofbauer, A., & Dräger, U. C. (1985). Depth segregation of retinal ganglion cells projecting to mouse superior colliculus. *The Journal of comparative neurology*, *234*(4), 465–474. https://doi.org/10.1002/cne.902340405

Hofbauer, A., & Dräger, U. C. (1985). Depth segregation of retinal ganglion cells projecting to mouse superior colliculus. *Journal of Comparative Neurology*, 234, 465–474.

Hoge, W. S., & Polimeni, J. R. (2016). Dual-polarity GRAPPA for simultaneous reconstruction and ghost correction of echo planar imaging data. *Magnetic Resonance in Medicine*, 76(1), 32-44. https://doi.org/10.1002/mrm.25839

Hopkins W. D. (2022). Neuroanatomical asymmetries in nonhuman primates in the homologs to Broca's and Wernicke's areas: a mini-review. *Emerging topics in life sciences*, *6*(3), 271–284. Advance online publication. https://doi.org/10.1042/ETLS20210279

Hopkins, W. D., & Avants, B. B. (2013). Regional and hemispheric variation in cortical thickness in chimpanzees (Pan troglodytes). *Journal of Neuroscience*, 33(12), 5241–5248.

Hopkins, W. D., Misiura, M., Pope, S. M., & Latash, E. M. (2015). Behavioral and brain asymmetries in primates: a preliminary evaluation of two evolutionary hypotheses. *Annals of the New York Academy of Sciences*, *1359*(1), 65–83. https://doi.org/10.1111/nyas.12936

Hopkins, W. D., Misiura, M., Reamer, L. A., Schaeffer, J. A., Mareno, M. C., & Schapiro, S. J. (2014). Poor receptive joint attention skills are associated with atypical gray matter asymmetry in the posterior superior temporal gyrus of chimpanzees (Pan troglodytes). *Frontiers in Psychology*, 5, 7.

Hörster, W., & Ettlinger, G. (1985). An association between hand preference and tactile discrimination performance in the rhesus monkey. *Neuropsychologia*, 23, 411–413. https://doi.org/10.1016/0028-3932(85)90027-2

Horton, J. C., & Hocking, D. R. (1996). Intrinsic variability of ocular dominance column periodicity in normal macaque monkeys. *The Journal of neuroscience : the official journal of the Society for Neuroscience*, *16*(22), 7228–7239. https://doi.org/10.1523/JNEUROSCI.16-22-07228.1996

Hoy, J. L., Bishop, H. I., & Niell, C. M. (2019). Defined Cell Types in Superior Colliculus Make Distinct Contributions to Prey Capture Behavior in the Mouse. *Current biology : CB*, *29*(23), 4130–4138.e5. https://doi.org/10.1016/j.cub.2019.10.017

Huang, L., Yuan, T., Tan, M., Xi, Y., Hu, Y., Tao, Q., Zhao, Z., Zheng, J., Han, Y., Xu, F., et al. (2017). A retinoraphe projection regulates serotonergic activity and looming-evoked defensive behavior. *Nature Communications*, 8, 14908.

Hubel, D. H., LeVay, S., & Wiesel, T. N. (1975). Mode of termination of retinotectal fibers in macaque monkey: an autoradiographic study. *Brain research*, *96*(1), 25–40. https://doi.org/10.1016/0006-8993(75)90567-3

Huerta, M. F., & Kaas, J. H. (1990). Supplementary eye field as defined by intracortical microstimulation: connections in macaques. *The Journal of comparative neurology*, *293*(2), 299–330. https://doi.org/10.1002/cne.902930211

Huerta, M., & Harting, J. (1984). The mammalian superior colliculus: Studies of its morphology and connections. In H. Vanegas (Ed.), Comparative neurology of the optic tectum (pp. 687–773). New York, NY: Plenum Press.

Hyvärinen, J. (1982). Functional Role of Parietal Cortex. In: The Parietal Cortex of Monkey and Man. Studies of Brain Function, vol 8. Springer, Berlin, Heidelberg. https://doi.org/10.1007/978-3-642-81860-8_12

Ignashchenkova, A., Dicke, P. W., Haarmeier, T., & Thier, P. (2004). Neuron-specific contribution of the superior colliculus to overt and covert shifts of attention. *Nature Neuroscience*, 7(1), 56–64.

Innocenti G. M. (2009). Dynamic interactions between the cerebral hemispheres. *Experimental brain research*, *192*(3), 417–423. https://doi.org/10.1007/s00221-008-1484-8

Isa, T., & Yoshida, M. (2021). Neural Mechanism of Blindsight in a Macaque Model. *Neuroscience*, 469, 138–161. https://doi.org/10.1016/j.neuroscience.2021.06.022

Isa, T., Endo, T., & Saito, Y. (1998). The visuo-motor pathway in the local circuit of the rat superior colliculus. *The Journal of neuroscienc : the official journal of the Society for Neuroscience*, *18*(20), 8496–8504. https://doi.org/10.1523/JNEUROSCI.18-20-08496.1998

Isa, T., Marquez-Legorreta, E., Grillner, S., & Scott, E. K. (2021). The tectum/superior colliculus as the vertebrate solution for spatial sensory integration and action. *Current biology : CB*, *31*(11), R741–R762. https://doi.org/10.1016/j.cub.2021.04.001

Itani, J., Tokuda, K., Furuya, Y., et al. (1963). The social construction of natural troops of Japanese monkeys in Takasakiyama. Primates, 4, 1–42. https://doi.org/10.1007/BF01733670

Jacobson, M., & Gaze, R. M. (1964). Types of visual response from single units in the optic tectum and optic nerve of the goldfish. Quarterly Journal of Experimental Physiology and Cognate Medical Sciences, 49, 199–209. https://doi.org/10.1113/expphysiol.1964.sp001720

Janssens, T., Keil, B., Farivar, R., McNab, J. A., Polimeni, J. R., Gerits, A., Arsenault, J. T., Wald, L. L., & Vanduffel, W. (2012). An implanted 8-channel array coil for high-resolution macaque MRI at 3T. *NeuroImage*, *62*(3), 1529–1536. https://doi.org/10.1016/j.neuroimage.2012.05.028

Janssens, T., Zhu, Q., Popivanov, I. D., & Vanduffel, W. (2014). Probabilistic and single-subject retinotopic maps reveal the topographic organization of face patches in the macaque cortex. *The Journal of neuroscience : the official journal of the Society for Neuroscience*, *34*(31), 10156–10167. https://doi.org/10.1523/JNEUROSCI.2914-13.2013

Jenkinson, M., Beckmann, C. F., Behrens, T. E., Woolrich, M. W., & Smith, S. M. (2012). FSL. *NeuroImage*, *62*(2), 782–790. https://doi.org/10.1016/j.neuroimage.2011.09.015

Jezzard, P., & Balaban, R. S. (1995). Correction for geometric distortion in echo planar images from B0 field variations. *Magnetic resonance in medicine*, *34*(1), 65–73. https://doi.org/10.1002/mrm.1910340111

Jones, H. E., Grieve, K. L., Wang, W., & Sillito, A. M. (2001). Surround suppression in primate V1. *Journal of neurophysiology*, *86*(4), 2011–2028. https://doi.org/10.1152/jn.2001.86.4.2011

Juliano, S. L., Hand, P. J., & Whitsel, B. L. (1983). Patterns of metabolic activity in cytoarchitectural area SII and surrounding cortical fields of the monkey. *Journal of neurophysiology*, *50*(4), 961–980. https://doi.org/10.1152/jn.1983.50.4.961

Jun, E. J., Bautista, A. R., Nunez, M. D., Allen, D. C., Tak, J. H., Alvarez, E., & Basso, M. A. (2021). Causal role for the primate superior colliculus in the computation of evidence for perceptual decisions. *Nature neuroscience*, *24*(8), 1121–1131. https://doi.org/10.1038/s41593-021-00878-6

Jung, B., Taylor, P.A., Seidlitz, J., Sponheim, C., Perkins P., Ungerleider, L.G., Glen, D., Messinger, A. (2021) "A comprehensive macaque fMRI pipeline and hierarchical atlas." NeuroImage, submitted. https://www.biorxiv.org/content/10.1101/2020.08.05.237818v1

Kaas, J. H., & Baldwin, M. K. L. (2019). The Evolution of the Pulvinar Complex in Primates and Its Role in the Dorsal and Ventral Streams of Cortical Processing. *Vision (Basel, Switzerland)*, *4*(1), 3. https://doi.org/10.3390/vision4010003

Kardamakis, A. A., Saitoh, K., & Grillner, S. (2015). Tectal microcircuit generating visual selection commands on gaze-controlling neurons. Proceed*ings of the National Academy of Sciences of the United States of America*, 112, E1956–E1965.

Kardamakis, A.A., Perez-Ferna´ ndez, J., and Grillner, S. (2016). Spatiotemporal interplay between multisensory excitation and recruited inhibition in the lamprey optic tectum. *eLife* 5, e16472.

Karnath, H. O., Milner, A. D., & Vallar, G. (2002). The cognitive and neural bases of spatial neglect. Oxford: Oxford University Press.

Kasai, M., & Isa, T. (2016). Imaging population dynamics of surround suppression in the superior colliculus. *The European journal of neuroscience*, *44*(8), 2543–2556. https://doi.org/10.1111/ejn.13371

Katyal, S., Zughni, S., Greene, C., & Ress, D. (2010). Topography of covert visual attention in human superior colliculus. *Journal of neurophysiology*, *104*(6), 3074–3083. https://doi.org/10.1152/jn.00283.2010

Kinoshita, M., Kato, R., Isa, K., Kobayashi, K., Kobayashi, K., Onoe, H., & Isa, T. (2019). Dissecting the circuit for blindsight to reveal the critical role of pulvinar and superior colliculus. *Nature communications*, *10*(1), 135. https://doi.org/10.1038/s41467-018-08058-0

Klink, P. C., Chen, X., Vanduffel, W., & Roelfsema, P. R. (2021). Population receptive fields in nonhuman primates from whole-brain fMRI and large-scale neurophysiology in visual cortex. *eLife*, *10*, e67304. https://doi.org/10.7554/eLife.67304

Kolster, H., Janssens, T., Orban, G. A., & Vanduffel, W. (2014). The retinotopic organization of macaque occipitotemporal cortex anterior to V4 and caudoventral to the middle temporal (MT) cluster. *The Journal of neuroscience: the official journal of the Society for Neuroscience*, *34*(31), 10168–10191. https://doi.org/10.1523/JNEUROSCI.3288-13.2014

Kristjánsson, A., Vandenbroucke, M. W., & Driver, J. (2004). When pros become cons for anti- versus prosaccades: factors with opposite or common effects on different saccade types. *Experimental brain research*, *155*(2), 231–244. https://doi.org/10.1007/s00221-003-1717-9

Künzle, H., Akert, K., & Wurtz, R. H. (1976). Projection of area 8 (frontal eye field) to superior colliculus in the monkey. An autoradiographic study. *Brain research*, *117*(3), 487–492. https://doi.org/10.1016/0006-8993(76)90754-x

Lee, C., Rohrer, W. H., & Sparks, D. L. (1988). Population coding of saccadic eye movements by neurons in the superior colliculus. *Nature*, 332(6161), 357–360.

Lehman, R. A. (1978). The handedness of rhesus monkeys–I. Distribution. *Neuropsychologia*, 16, 33–42. https://doi.org/10.1016/0028-3932(78)90040-4

Leichnetz G. R. (2001). Connections of the medial posterior parietal cortex (area 7m) in the monkey. *The Anatomical record*, *263*(2), 215–236. https://doi.org/10.1002/ar.1082

Leichnetz, G. R., Spencer, R. F., Hardy, S. G. P., & Astruc, J. (1981). The prefrontal corticotectal projection in the monkey: An anterograde and retrograde horseradish peroxidase study. *Neuroscience*, 6(6), 1023-1041. https://doi.org/10.1016/0306-4522(81)90068-3.

Leichnetz, G. R., Spencer, R. F., Hardy, S. G., & Astruc, J. (1981). The prefrontal corticotectal projection in the monkey; an anterograde and retrograde horseradish peroxidase study. *Neuroscience*, *6*(6), 1023–1041. https://doi.org/10.1016/0306-4522(81)90068-3

Leite, F. P., Tsao, D., Vanduffel, W., Fize, D., Sasaki, Y., Wald, L. L., Dale, A. M., Kwong, K. K., Orban, G. A., Rosen, B. R., Tootell, R. B., & Mandeville, J. B. (2002). Repeated fMRI using iron oxide contrast agent in awake, behaving macaques at 3 Tesla. *NeuroImage*, *16*(2), 283–294. https://doi.org/10.1006/nimg.2002.1110

Levitt, J. B., & Lund, J. S. (1997). Contrast dependence of contextual effects in primate visual cortex. *Nature*, *387*(6628), 73–76. https://doi.org/10.1038/387073a0

Lewis, T. L., & Maurer, D. (1992). The development of the temporal and nasal visual fields during infancy. *Vision research*, *32*(5), 903–911. https://doi.org/10.1016/0042-6989(92)90033-f

Li, L., Feng, X., Zhou, Z., Zhang, H., Shi, Q., Lei, Z., Shen, P., Yang, Q., Zhao, B., Chen, S., et al. (2018). Stress accelerates defensive responses to looming in mice and involves a locus coeruleus-superior colliculus projection. Current Biology, 28, 859–871.

Li, X., Zhu, Q., & Vanduffel, W. (2022). Submillimeter fMRI reveals an extensive, fine-grained and functionally-relevant scene-processing network in monkeys. *Progress in neurobiology*, *211*, 102230. https://doi.org/10.1016/j.pneurobio.2022.102230

Li, X., Zhu, Q., Janssens, T., Arsenault, J. T., & Vanduffel, W. (2019). In Vivo Identification of Thick, Thin, and Pale Stripes of Macaque Area V2 Using Submillimeter Resolution (f)MRI at 3 T. *Cerebral cortex (New York, N.Y. : 1991)*, *29*(2), 544–560. https://doi.org/10.1093/cercor/bhx337

Linden, R., & Perry, V. H. (1983). Massive retinotectal projection in rats. *Brain Research*, 272, 145–149.

Logothetis, N. K., Pauls, J., Augath, M., Trinath, T., & Oeltermann, A. (2001). Neurophysiological investigation of the basis of the fMRI signal. *Nature*, *412*(6843), 150–157. https://doi.org/10.1038/35084005

Lund R. D. (1972). Synaptic patterns in the superficial layers of the superior colliculus of the monkey, Macaca mulatta. *Experimental brain research*, *15*(2), 194–211. https://doi.org/10.1007/BF00235582

Lynch, J. C., Graybiel, A. M., & Lobeck, L. J. (1985). The differential projection of two cytoarchitectonic subregions of the inferior parietal lobule of macaque upon the deep layers of the superior colliculus. *Journal of Comparative Neurology*, 235, 241–254.

Lyon, D. C., Nassi, J. J., & Callaway, E. M. (2010). A disynaptic relay from superior colliculus to dorsal stream visual cortex in macaque monkey. *Neuron*, 65(2), 270–279.

Malevich, T., Zhang, T., Baumann, M. P., Bogadhi, A. R., & Hafed, Z. M. (2022). Faster detection of "darks" than "brights" by monkey superior colliculus neurons. *Journal of Neuroscience*. https://doi.org/10.1523/JNEUROSCI.1489-22

Manns, M., & Güntürkün, O. (2009). Dual coding of visual asymmetries in the pigeon brain: the interaction of bottom-up and top-down systems. *Experimental Brain Research*, 199, 323–332. https://doi.org/10.1007/s00221-009-1702-z.

Mantini, D., Corbetta, M., Romani, G. L., Orban, G. A., & Vanduffel, W. (2013). Evolutionarily novel functional networks in the human brain?. *The Journal of neuroscience: the official journal of the Society for Neuroscience*, *33*(8), 3259–3275. https://doi.org/10.1523/JNEUROSCI.4392-12.2013

Marrocco, R. T., & Li, R. H. (1977). Monkey superior colliculus: properties of single cells and their afferent inputs. *Journal of neurophysiology*, *40*(4), 844–860. https://doi.org/10.1152/jn.1977.40.4.844

Matsumoto, M., Inoue, K. I., & Takada, M. (2018). Causal role of neural signals transmitted from the frontal eye field to the superior colliculus in saccade generation. Frontiers in Neural Circuits, 12, 69.

Maunsell, J. H., & van Essen, D. C. (1983b). The connections of the middle temporal visual area (MT) and their relationship to a cortical hierarchy in the macaque monkey. *The Journal of neuroscience : the official journal of the Society for Neuroscience*, *3*(12), 2563–2586. https://doi.org/10.1523/JNEUROSCI.03-12-02563.1983

May P. J. (2006). The mammalian superior colliculus: laminar structure and connections. *Progress in brain research*, *151*, 321–378. https://doi.org/10.1016/S0079-6123(05)51011-2

May, P. J., McHaffie, J. G., Stanford, T. R., Jiang, H., Costello, M. G., Coizet, V., ... Redgrave, P. (2009). Tectonigral projections in the primate: a pathway for pre-attentive sensory input to midbrain dopaminergic neurons. European Journal of Neuroscience, 29(3), 575–587. https://doi.org/10.1111/j.1460-9568.2008.06596.x

Mayo, J. P., DiTomasso, A. R., Sommer, M. A., & Smith, M. A. (2015). Dynamics of visual receptive fields in the macaque frontal eye field. *Journal of neurophysiology*, *114*(6), 3201–3210. https://doi.org/10.1152/jn.00746.2015

McHaffie, J. G., & Stein, B. E. (1982). Eye movements evoked by electrical stimulation in the superior colliculus of rats and hamsters. *Brain research*, *247*(2), 243–253. https://doi.org/10.1016/0006-8993(82)91249-5

McHaffie, J. G., Jiang, H., May, P. J., Coizet, V., Overton, P. G., Stein, B. E., & Redgrave, P. (2006). A direct projection from superior colliculus to substantia nigra pars compacta in the cat. *Neuroscience*, 138, 221–234. https://doi.org/10.1016/j.neuroscience.2005.11.015

McPeek, R. M., & Keller, E. L. (2004). Deficits in saccade target selection after inactivation of superior colliculus. *Nature neuroscience*, *7*(7), 757–763. https://doi.org/10.1038/nn1269

Mearns, D. S., Donovan, J. C., Fernandes, A. M., Semmelhack, J. L., & Baier, H. (2020). Deconstructing Hunting Behavior Reveals a Tightly Coupled Stimulus-Response Loop. *Current biology : CB*, *30*(1), 54–69.e9. https://doi.org/10.1016/j.cub.2019.11.022

Meredith, M. A., & Stein, B. E. (1986). Visual, auditory, and somatosensory convergence on cells in superior colliculus results in multisensory integration. *Journal of neurophysiology*, *56*(3), 640–662. https://doi.org/10.1152/jn.1986.56.3.640

Mesulam, M. M., Van Hoesen, G. W., Pandya, D. N., & Geschwind, N. (1977). Limbic and sensory connections of the inferior parietal lobule (area PG) in the rhesus monkey: a study with a new method for horseradish peroxidase histochemistry. *Brain research*, *136*(3), 393–414. https://doi.org/10.1016/0006-8993(77)90066-x

Michael C. R. (1970). Integration of retinal and cortical information in the superior colliculus of the ground squirrel. *Brain, behavior and evolution*, *3*(1), 205–209. https://doi.org/10.1159/000125472

Mohler, C. W., Goldberg, M. E., & Wurtz, R. H. (1973). Visual receptive fields of frontal eye field neurons. *Brain Research*, 61, 385-389.

Moore, B., Li, K., Kaas, J. H., Liao, C. C., Boal, A. M., Mavity-Hudson, J., & Casagrande, V. (2019). Cortical projections to the two retinotopic maps of primate pulvinar are distinct. *Journal of Comparative Neurology*, 527(3), 577-588. https://doi.org/10.1002/cne.24515

Moore, T., & Armstrong, K. M. (2003). Selective gating of visual signals by microstimulation of frontal cortex. *Nature*, 421(6921), 370–373.

Moore, T., & Fallah, M. (2001). Control of eye movements and spatial attention. *Proceedings of the National Academy of Sciences of the United States of America*, 98(3), 1273–1276.

Mountcastle, V. B., Lynch, J. C., Georgopoulos, A., Sakata, H., & Acuna, C. (1975). Posterior parietal association cortex of the monkey: command functions for operations within extrapersonal space. *Journal of neurophysiology*, *38*(4), 871–908. https://doi.org/10.1152/jn.1975.38.4.871

Mundinano, I.C., Fox, D.M., Kwan, W.C., Vidaurre, D., Teo, L., Homman-Ludiye, J., Goodale, M.A., Leopold, D.A., & Bourne, J.A. (2018). Transient visual pathway critical for normal development of primate grasping behavior. *Proceedings of the National Academy of Sciences of the United States of America*, 115, 1364–1369. https://doi.org/10.1073/pnas.1717016115

Munoz, D. P., & Istvan, P. J. (1998). Lateral inhibitory interactions in the intermediate layers of the monkey superior colliculus. *Journal of neurophysiology*, *79*(3), 1193–1209. https://doi.org/10.1152/jn.1998.79.3.1193

Munoz, D. P., & Wurtz, R. H. (1993). Fixation cells in monkey superior colliculus. I. Characteristics of cell discharge. *Journal of neurophysiology*, *70*(2), 559–575. https://doi.org/10.1152/jn.1993.70.2.559

Nagy, A., Kruse, W., Rottmann, S., Dannenberg, S., & Hoffmann, K. P. (2006). Somatosensory-motor neuronal activity in the superior colliculus of the primate. *Neuron*, *52*(3), 525–534. https://doi.org/10.1016/j.neuron.2006.08.010

Nagy, M., Akos, Z., Biro, D., & Vicsek, T. (2010). Hierarchical group dynamics in pigeon flocks. *Nature*, 464, 890–893. https://doi.org/10.1038/nature08891

Nemec, P., Altmann, J., Marhold, S., Burda, H., & Oelschlager, H. H. (2001). Neuroanatomy of magnetoreception: The superior colliculus involved in magnetic orientation in a mammal. *Science*, 294(5541), 366–368.

Nummela, S. U., & Krauzlis, R. J. (2010). Inactivation of primate superior colliculus biases target choice for smooth pursuit, saccades, and button press responses. *Journal of neurophysiology*, *104*(3), 1538–1548. https://doi.org/10.1152/jn.00406.2010

Ogawa, S., Lee, T. M., Kay, A. R., & Tank, D. W. (1990). Brain magnetic resonance imaging with contrast dependent on blood oxygenation. Proceedings of the National Academy of Sciences, 87(24), 9868–9872.

Olivier, E., Corvisier, J., Pauluis, Q., & Hardy, O. (2000). Evidence for glutamatergic tectotectal neurons in the cat superior colliculus: a comparison with GABAergic tectotectal neurons. European Journal of Neuroscience, 12, 2354–2366.

Olivier, E., Porter, J. D., & May, P. J. (1998). Comparison of the distribution and somatodendritic morphology of tectotectal neurons in the cat and monkey. Visual Neuroscience, 15, 903–922.

Orban, G. A., Claeys, K., Nelissen, K., Smans, R., Sunaert, S., Todd, J. T., Wardak, C., Durand, J. B., & Vanduffel, W. (2006). Mapping the parietal cortex of human and non-human primates. *Neuropsychologia*, *44*(13), 2647–2667. https://doi.org/10.1016/j.neuropsychologia.2005.11.001

Orban, G. A., Sepe, A., & Bonini, L. (2021). Parietal maps of visual signals for bodily action planning. *Brain structure & function*, 226(9), 2967–2988. https://doi.org/10.1007/s00429-021-02378-6

Ottes, F. P., Van Gisbergen, J. A., & Eggermont, J. J. (1986). Visuomotor fields of the superior colliculus: a quantitative model. *Vision research*, *26*(6), 857–873. https://doi.org/10.1016/0042-6989(86)90144-6

Panormita, M., Li, X., Sepe, A., Zhu, Q., Bonini, L.., Leopold, D.A., Tamietto, M., Vanduffel, W. (2023) Position invariant processing of different visual categories in the macaque. Abstract presented at the Annual Meeting of the Society for Neuroscience (SfN). Washington, D.C., USA.

Paxinos, G., Huang, X. F., & Toga, A. W. (2000). The Rhesus Monkey Brain in Stereotaxic Coordinates. Academic Press.

Perez-Fernandez, J., Kardamakis, A.A., Suzuki, D.G., Robertson, B., & Grillner, S. (2017). Direct dopaminergic projections from the SNc modulate visuomotor transformation in the lamprey tectum. Neuron, 96(7), 910–924.

Perry, V.H., & Cowey, A. (1984). Retinal ganglion cells that project to the superior colliculus and pretectum in macaque monkey. Neuroscience, 12, 1125–1137.

Pessoa, L., & Adolphs, R. (2010). Emotion processing and the amygdala: From a 'low road' to 'many roads' of evaluating biological significance. Nature Reviews Neuroscience, 11(11), 773–783. DOI: 10.1038/nrn2920

Phillips, K.A., Schaeffer, J.A., & Hopkins, W.D. (2013). Corpus callosal microstructure influences intermanual transfer in chimpanzees. Frontiers in Systems Neuroscience, 7, 125.

Phongphanphanee, P., Marino, R. A., Kaneda, K., Yanagawa, Y., Munoz, D. P., & Isa, T. (2014). Distinct local circuit properties of the superficial and intermediate layers of the rodent superior colliculus. *The European journal of neuroscience*, *40*(2), 2329–2343. https://doi.org/10.1111/ejn.12579

Polat, U. (1999). Functional architecture of long-range perceptual interactions. *Spatial Vision*, 12(2), 143–162. https://doi.org/10.1163/156856899X00094

Pollack, J. G., & Hickey, T. L. (1979). The distribution of retino-collicular axon terminals in rhesus monkey. *The Journal of Comparative Neurology*, 185(4), 587–602. https://doi.org/10.1002/cne.901850402

Popivanov, I. D., Jastorff, J., Vanduffel, W., & Vogels, R. (2012). Stimulus representations in body-selective regions of the macaque cortex assessed with event-related fMRI. *NeuroImage*, 63(2), 723–741. https://doi.org/10.1016/j.neuroimage.2012.07.013

Posner, M. I., & Cohen, Y. (1980). Attention and control of movements. In: Tutorials in Motor Behavior, edited by Stelmach GE, Region J. Amsterdam: North Holland Publ, 1980, p. 243–258.

Prabhakaran, G. T., Carvalho, J., Invernizzi, A., Kanowski, M., Renken, R. J., Cornelissen, F. W., & Hoffmann, M. B. (2020). Foveal pRF properties in the visual cortex depend on the extent of stimulated visual field. *NeuroImage*, *222*, 117250. https://doi.org/10.1016/j.neuroimage.2020.117250

Preuss, T. M. (2011). The human brain: rewired and running hot. Annals of the New York Academy of Sciences, 1225(Suppl 1), E182-91. https://doi.org/10.1111/j.1749-6632.2011.06001.x. PMID: 21599696; PMCID: PMC3103088.

Prior, H., Wiltschko, R., Stapput, K., Güntürkün, O., & Wiltschko, W. (2004). Visual lateralization and homing in pigeons. *Behavioral Brain Research*, 154, 301–310. https://doi.org/10.1016/j.bbr.2004.02.018.

Rafal, R., Henik, A., & Smith, J. (1991). Extrageniculate contributions to reflex visual orienting in normal humans: a temporal hemifield advantage. *Journal of cognitive neuroscience*, *3*(4), 322–328. https://doi.org/10.1162/jocn.1991.3.4.322

Redgrave, P., Coizet, V., Comoli, E., McHaffie, J. G., Leriche, M., Vautrelle, N., ... Overton, P. (2010). Interactions between the Midbrain Superior Colliculus and the Basal Ganglia. *Front Neuroanat*, 4, 132. https://doi.org/10.3389/fnana.2010.00132

Reveley, C., Gruslys, A., Ye, F. Q., Glen, D., Samaha, J., Russ, E., ... Saleem, K. S. (2017). Three-Dimensional Digital Template Atlas of the Macaque Brain. *Cereb Cortex*, 27(9), 4463-4477. https://doi.org/10.1093/cercor/bhw248

Reyes-Puerta, V., Philipp, R., Lindner, W., & Hoffmann, K. P. (2010). Role of the rostral superior colliculus in gaze anchoring during reach movements. *Journal of neurophysiology*, 103(6), 3153–3166. https://doi.org/10.1152/jn.00989.2009

Rizzolatti, G., Camarda, R., Grupp, L. A., & Pisa, M. (1974). Inhibitory effect of remote visual stimuli on visual responses of cat superior colliculus: spatial and temporal factors. *Journal of neurophysiology*, 37, 1262–1275.

Robinson D. A. (1972). Eye movements evoked by collicular stimulation in the alert monkey. *Vision research*, *12*(11), 1795–1808. https://doi.org/10.1016/0042-6989(72)90070-3

Robinson, D. L., Goldberg, M. E., & Stanton, G. B. (1978). Parietal association cortex in the primate: sensory mechanisms and behavioral modulations. *Journal of neurophysiology*, *41*(4), 910–932. https://doi.org/10.1152/jn.1978.41.4.910

Rodman, H. R., Gross, C. G., & Albright, T. D. (1990). Afferent basis of visual response properties in area MT of the macaque. II. Effects of superior colliculus removal. *The Journal of neuroscience : the official journal of the Society for Neuroscience*, *10*(4), 1154–1164. https://doi.org/10.1523/JNEUROSCI.10-04-01154.1990

Rogers L. J. (1990). Light input and the reversal of functional lateralization in the chicken brain. *Behavioural brain research*, *38*(3), 211–221. https://doi.org/10.1016/0166-4328(90)90176-f

Rohlfing, T., Kroenke, C. D., Sullivan, E. V., Dubach, M. F., Bowden, D. M., Grant, K. A., & Pfefferbaum, A. (2012). The INIA19 Template and NeuroMaps Atlas for Primate Brain Image Parcellation and Spatial Normalization. Frontiers in Neuroinformatics, 6, 27.

Rolls, E. T. (1994). Brain mechanisms for invariant visual recognition and learning. *Behavioural Processes*, 33(1–2), 113-138. https://doi.org/10.1016/0376-6357(94)90062-0.

Romanski, L. M., Giguere, M., Bates, J. F., & Goldman-Rakic, P. S. (1997). Topographic organization of medial pulvinar connections with the prefrontal cortex in the rhesus monkey. *The Journal of Comparative Neurology*, 379(3), 313–332.

Rothbart, M. K., Posner, M. I., & Boylan, A. (1990). Regulatory mechanisms in infant development. In J. T. Enns (Ed.), The Development of Attention: Research and Theory (pp. 139–160). Amsterdam: Elsevier.

Rounis, E., Halai, A., Pizzamiglio, G., & Lambon Ralph, M. A. (2021). Characterising factors underlying praxis deficits in chronic left hemisphere stroke patients. *Cortex*, 142, 154-168. https://doi.org/10.1016/j.cortex.2021.04.019

Sadikot, A. F., & Rymar, V. V. (2009). The primate centromedian-parafascicular complex: anatomical organization with a note on neuromodulation. *Brain Research Bulletin*, 78(2–3), 122–130.

Sahibzada, N., Dean, P., & Redgrave, P. (1986). Movements resembling orientation or avoidance elicited by electrical stimulation of the superior colliculus in rats. *Journal of Neuroscience*, 6, 723–733.

Saito, Y., & Isa, T. (2004). Laminar specific distribution of lateral excitatory connections in the rat superior colliculus. *Journal of neurophysiology*, *92*(6), 3500–3510. https://doi.org/10.1152/jn.00033.2004

Saitoh, K., Ménard, A., & Grillner, S. (2007). Tectal control of locomotion, steering, and eye movements in lamprey. *Journal of neurophysiology*, *97*(4), 3093–3108. https://doi.org/10.1152/jn.00639.2006

Sakata, H., Shibutani, H., & Kawano, K. (1980). Spatial properties of visual fixation neurons in posterior parietal association cortex of the monkey. *Journal of neurophysiology*, *43*(6), 1654–1672. https://doi.org/10.1152/jn.1980.43.6.1654

Sakata, H., Shibutani, H., & Kawano, K. (1983). Functional properties of visual tracking neurons in posterior parietal association cortex of the monkey. *Journal of neurophysiology*, *49*(6), 1364–1380. https://doi.org/10.1152/jn.1983.49.6.1364

Sawada, K. (2020). Cerebral Sulcal Asymmetry in Macaque Monkeys. Symmetry, 12, 1509. https://doi.org/10.3390/sym12091509

Saygin, A. P., & Sereno, M. I. (2008). Retinotopy and Attention in Human Occipital, Temporal, Parietal, and Frontal Cortex. *Cerebral Cortex*, 18(9), 2158–2168. https://doi.org/10.1093/cercor/bhm242

Schall, J. D., Morel, A., King, D. J., & Bullier, J. (1995). Topography of visual cortex connections with frontal eye field in macaque: convergence and segregation of processing streams. *The Journal of neuroscience : the official*

journal of the Society for Neuroscience, *15*(6), 4464–4487. https://doi.org/10.1523/JNEUROSCI.15-06-04464.1995

Schiller, P. H., & Koerner, F. (1971). Discharge characteristics of single units in superior colliculus of the alert rhesus monkey. *Journal of neurophysiology*, *34*(5), 920–936. https://doi.org/10.1152/jn.1971.34.5.920

Schiller, P. H., & Tehovnik, E. J. (2005). Neural mechanisms underlying target selection with saccadic eye movements. *Progress in brain research*, *149*, 157–171. https://doi.org/10.1016/S0079-6123(05)49012-3

Schiller, P. H., Stryker, M., Cynader, M., & Berman, N. (1974). Response characteristics of single cells in the monkey superior colliculus following ablation or cooling of visual cortex. *Journal of neurophysiology*, *37*(1), 181–194. https://doi.org/10.1152/jn.1974.37.1.181

Schneider, K. A., & Kastner, S. (2005). Visual responses of the human superior colliculus: A high-resolution functional magnetic resonance imaging study. *Journal of Neurophysiology*, 94 (4), 2491–2503,

Schneider, K.A., Richter, M.C., & Kastner, S. (2004). Retinotopic organization and functional subdivisions of the human lateral geniculate nucleus: a high-resolution functional magnetic resonance imaging study. *Journal of Neuroscience*, 24(40), 8975–8985.

Seghier M. L. (2008). Laterality index in functional MRI: methodological issues. *Magnetic resonance imaging*, *26*(5), 594–601. https://doi.org/10.1016/j.mri.2007.10.010

Seltzer, B., & Pandya, D. N. (1980). Converging visual and somatic sensory cortical input to the intraparietal sulcus of the rhesus monkey. *Brain research*, *192*(2), 339–351. https://doi.org/10.1016/0006-8993(80)90888-4

Sereno, M. I., & Huang, R. S. (2014). Multisensory maps in parietal cortex. *Current opinion in neurobiology*, *24*(1), 39–46. https://doi.org/10.1016/j.conb.2013.08.014

Sereno, M. I., Dale, A. M., Reppas, J. B., Kwong, K. K., Belliveau, J. W., Brady, T. J., ... Tootell, R. B. (1995). Borders of multiple visual areas in humans revealed by functional magnetic resonance imaging. *Science*, 268(5212), 889–893. https://pubmed.ncbi.nlm.nih.gov/7754376/

Shapley, R. M., & Victor, J. D. (1979). Nonlinear spatial summation and the contrast gain control of cat retinal ganglion cells. *The Journal of physiology*, *290*(2), 141–161. https://doi.org/10.1113/jphysiol.1979.sp012765

Smith, Y., Raju, D. V., Pare, J. F., & Sidibe, M. (2004). The thalamostriatal system: a highly specific network of the basal ganglia circuitry. Trends in Neurosciences, 27(9), 520–527.

Sommer, M. A., & Wurtz, R. H. (2002). A pathway in primate brain for internal monitoring of movements. Science, 296, 1480–1482. https://doi.org/10.1126/science.1069590

Sommer, M. A., & Wurtz, R. H. (2004). What the brain stem tells the frontal cortex: Oculomotor signals sent from superior colliculus to frontal eye field via mediodorsal thalamus. *Journal of Neurophysiology*, 91(3), 1381–1402.

Sommer, M. A., & Wurtz, R. H. (2008). Brain circuits for the internal monitoring of movements. Annual *Review of Neuroscience*, 31, 317–338.

Sparks, D.L. (1986). Translation of sensory signals into commands for control of saccadic eye movements: role of primate superior colliculus. Physiol. Rev. 66, 118–171.

Sprague J. M. (1966). Interaction of cortex and superior colliculus in mediation of visually guided behavior in the cat. *Science (New York, N.Y.)*, *153*(3743), 1544–1547. https://doi.org/10.1126/science.153.3743.1544

Stoerig, P., & Cowey, A. (1997). Blindsight in man and monkey. Brain : a journal of neurology, 120 (Pt 3), 535–559. https://doi.org/10.1093/brain/120.3.535

Ströckens, F., Güntürkün, O., & Ocklenburg, S. (2013). Limb preferences in non-human vertebrates. *Laterality*, *18*(5), 536–575. https://doi.org/10.1080/1357650X.2012.723008

Suzuki, D.G., Perez-Fernandez, J., Wibble, T., Kardamakis, A.A., and Grillner, S. (2019). The role of the optic tectum for visually evoked orienting and evasive movements. *Proc. Natl. Acad. Sci. USA* 116, 15272–15281.

Sylvester, R., Josephs, O., Driver, J., & Rees, G. (2007). Visual FMRI responses in human superior colliculus show a temporal-nasal asymmetry that is absent in lateral geniculate and visual cortex. *Journal of neurophysiology*, *97*(2), 1495–1502. https://doi.org/10.1152/jn.00835.2006

Takahashi, M., Sugiuchi, Y., & Shinoda, Y. (2007). Commissural mirror-symmetric excitation and reciprocal inhibition between the two superior colliculi and their roles in vertical and horizontal eye movements. *Journal of Neurophysiology*, 98, 2664–2682.

Takahashi, M., Sugiuchi, Y., & Shinoda, Y. (2010). Topographic organization of excitatory and inhibitory commissural connections in the superior colliculi and their functional roles in saccade generation. *Journal of neurophysiology*, *104*(6), 3146–3167. https://doi.org/10.1152/jn.00554.2010

Takahashi, M., Sugiuchi, Y., Izawa, Y., & Shinoda, Y. (2005). Commissural excitation and inhibition by the superior colliculus in tectoreticular neurons projecting to omnipause neuron and inhibitory burst neuron regions. *Journal of Neurophysiology*, 94, 1707–1726.

Takakuwa, N., Isa, K., Onoe, H., Takahashi, J., and Isa, T. (2021). Contribution of the pulvinar and lateral geniculate nucleus to the control of visually guided saccades in blindsight monkeys. J. Neurosci. 41, 1755–1768.

Talgar, C. P., & Carrasco, M. (2002). Vertical meridian asymmetry in spatial resolution: visual and attentional factors. *Psychonomic bulletin & review*, *9*(4), 714–722. https://doi.org/10.3758/bf03196326

Tardif, E., & Clarke, S. (2002). Commissural connections of human superior colliculus. *Neuroscience*, *111*(2), 363–372. https://doi.org/10.1016/s0306-4522(01)00600-5

Taylor, A. M., Jeffery, G., & Lieberman, A. R. (1986). Subcortical afferent and efferent connections of the superior colliculus in the rat and comparisons between albino and pigmented strains. *Experimental brain research*, *62*(1), 131–142. https://doi.org/10.1007/BF00237409

Tommasi, L., & Vallortigara, G. (2001). Encoding of geometric and landmark information in the left and right hemispheres of the avian brain. *Behavioral Neuroscience, 115*(3), 602–613. https://doi.org/10.1037/0735-7044.115.3.602

Tommasi, L., Chiandetti, C., Pecchia, T., Sovrano, V. A., & Vallortigara, G. (2012). From natural geometry to spatial cognition. *Neuroscience and biobehavioral reviews*, *36*(2), 799–824. https://doi.org/10.1016/j.neubiorev.2011.12.007

Tootell, R. B., Tsao, D., & Vanduffel, W. (2003). Neuroimaging weighs in: humans meet macaques in "primate" visual cortex. Journal of Neuroscience, 23(10), 3981-3989. https://doi.org/10.1523/JNEUROSCI.23-10-03981.2003.

Ungerleider, L. G., Galkin, T. W., & Mishkin, M. (1983, June 20). Visuotopic organization of projections from striate cortex to inferior and lateral pulvinar in rhesus monkey. Journal of Comparative Neurology, 217(2), 137-157. https://doi.org/10.1002/cne.902170203

Valero-Cabré, A., Toba, M. N., Hilgetag, C. C., & Rushmore, R. J. (2020). Perturbation-driven paradoxical facilitation of visuo-spatial function: Revisiting the 'Sprague effect'. *Cortex; a journal devoted to the study of the nervous system and behavior*, *122*, 10–39. https://doi.org/10.1016/j.cortex.2019.01.031

Vallortigara, G., & Andrew, R. J. (1994). Differential involvement of right and left hemisphere in individual recognition in the domestic chick. *Behavioural processes*, *33*(1-2), 41–57. https://doi.org/10.1016/0376-6357(94)90059-0

Van der Werf, Y. D., Witter, M. P., & Groenewegen, H. J. (2002). The intralaminar and midline nuclei of the thalamus: Anatomical and functional evidence for participation in processes of arousal and awareness. Brain Research Brain Research Reviews, 39(2–3), 107–140.

Van Essen, D. C. (2004). Organization of visual areas in macaque and human cerebral cortex. In L. M. Chalupa & J. S. Werner (Eds.), The visual neurosciences (Vol. 1, pp. 507–521). Cambridge, MA: MIT Press

Vanduffel, W., Fize, D., Mandeville, J. B., Nelissen, K., Van Hecke, P., Rosen, B. R., Tootell, R. B., & Orban, G. A. (2001). Visual motion processing investigated using contrast agent-enhanced fMRI in awake behaving monkeys. *Neuron*, *32*(4), 565–577. https://doi.org/10.1016/s0896-6273(01)00502-5

Vanduffel, W., Fize, D., Peuskens, H., Denys, K., Sunaert, S., Todd, J. T., & Orban, G. A. (2002). Extracting 3D from motion: differences in human and monkey intraparietal cortex. *Science (New York, N.Y.)*, *298*(5592), 413–415. https://doi.org/10.1126/science.1073574

Vanduffel, W., Zhu, Q., & Orban, G. A. (2014). Monkey cortex through fMRI glasses. *Neuron*, *83*(3), 533–550. https://doi.org/10.1016/j.neuron.2014.07.015

Vaney, D. I., Peichl, L., Wässle, H., & Illing, R. B. (1981). Almost all ganglion cells in the rabbit retina project to the superior colliculus. Brain Research, 212, 447–453.

Vickery, S., Eickhoff, S. B., & Friedrich, P. (2022). Hemispheric Specialization of the Primate Inferior Parietal Lobule. *Neuroscience bulletin*, *38*(3), 334–336. https://doi.org/10.1007/s12264-021-00807-4

Waguespack, H. F., Aguilar, B. L., Malkova, L., & Forcelli, P. A. (2020). Inhibition of the deep and intermediate layers of the superior colliculus disrupts sensorimotor gating in monkeys. Frontiers in Behavioral Neuroscience, 14, 610702. https://doi.org/10.3389/fnbeh.2020.610702

Wan, B., Bayrak, Ş., Xu, T., Schaare, H. L., Bethlehem, R. A. I., Bernhardt, B. C., & Valk, S. L. (2022). Heritability and cross-species comparisons of human cortical functional organization asymmetry. *eLife*, *11*, e77215. https://doi.org/10.7554/eLife.77215

Wang, D., Buckner, R. L., & Liu, H. (2014). Functional specialization in the human brain estimated by intrinsic hemispheric interaction. Journal of Neuroscience, 34(37), 12341–12352.

Wang, Y., Chen, Z., Ma, G., Wang, L., Liu, Y., Qin, M., Fei, X., Wu, Y., Xu, M., & Zhang, S. (2023). A frontal transcallosal inhibition loop mediates interhemispheric balance in visuospatial processing. *Nature communications*, *14*(1), 5213. https://doi.org/10.1038/s41467-023-40985-5

Warren, J. M. (1953). Handedness in the Rhesus monkey. Science, 118(3073), 622–623. https://doi.org/10.1126/science.118.3073.622

Wässle, H., & Illing, R. B. (1980). The retinal projection to the superior colliculus in the cat: a quantitative study with HRP. *The Journal of comparative neurology*, *190*(2), 333–356. https://doi.org/10.1002/cne.901900208

Weddell R. A. (2004). Subcortical modulation of spatial attention including evidence that the Sprague effect extends to man. *Brain and cognition*, *55*(3), 497–506. https://doi.org/10.1016/j.bandc.2004.02.075

Weiskrantz, L., Warrington, E. K., Sanders, M. D., & Marshall, J. (1974). Visual capacity in the hemianopic field following a restricted occipital ablation. *Brain : a journal of neurology*, *97*(4), 709–728. https://doi.org/10.1093/brain/97.1.709

Wild, B., & Treue, S. (2021). Primate extrastriate cortical area MST: a gateway between sensation and cognition. *Journal of neurophysiology*, *125*(5), 1851–1882. https://doi.org/10.1152/jn.00384.2020

Wilke, M., Kagan, I., & Andersen, R. A. (2012). Functional imaging reveals rapid reorganization of cortical activity after parietal inactivation in monkeys. *Proceedings of the National Academy of Sciences of the United States of America*, *109*(21), 8274–8279. https://doi.org/10.1073/pnas.1204789109

Willett S. M. (2019). Vision: Magnified Foveal Representation in Monkey Midbrain. *Current biology: CB*, *29*(13), R625–R627. https://doi.org/10.1016/j.cub.2019.05.052

Williams, A. L., Singh, K. D., & Smith, A. T. (2003). Surround modulation measured with functional MRI in the human visual cortex. *Journal of neurophysiology*, *89*(1), 525–533. https://doi.org/10.1152/jn.00048.2002

Wilson, M. E., & Toyne, M. J. (1970). Retino-tectal and cortico-tectal projections in Macaca mulatta. *Brain research*, *24*(3), 395–406. https://doi.org/10.1016/0006-8993(70)90181-2

Wiltschko, R., & Wiltschko, W. (2019). Magnetoreception in birds. *Journal of the Royal Society, Interface*, *16*(158), 20190295. https://doi.org/10.1098/rsif.2019.0295

Wurtz, R. H., & Albano, J. E. (1980). Visual-motor function of the primate superior colliculus. *Annual Review of Neuroscience*, 3, 189-226

Wurtz, R. H., & Mohler, C. W. (1976). Organization of monkey superior colliculus: Enhanced visual response of superficial layer cells. Journal of Neurophysiology, 39, 745-765.

Wurtz, R., & Albano, J.E. (1980). Visual-motor function of the primate superior colliculus. Annual review of neuroscience, 3, 189-226.

Xia, J., Wang, F., Wu, Z., Wang, L., Zhang, C., Shen, D., & Li, G. (2020). Mapping hemispheric asymmetries of the macaque cerebral cortex during early brain development. Human Brain Mapping, 41(1), 95-106. https://doi.org/10.1002/hbm.24789

Yamazaki, Y., Aust, U., Huber, L., Hausmann, M., & Güntürkün, O. (2007). Lateralized cognition: Asymmetrical and complementary strategies of pigeons during discrimination of the "human concept". Cognition, 104, 315–344. https://doi.org/10.1016/j.cognition.2006.07.004Yu, H. H., Rowley, D. P., Price, N. S. C., Rosa, M. G. P., & Zavitz, E. (2020). A twisted visual field map in the primate dorsomedial cortex predicted by topographic continuity. *Science advances*, *6*(44), eaaz8673. https://doi.org/10.1126/sciadv.aaz8673

Zeki S. M. (1971). Cortical projections from two prestriate areas in the monkey. Brain research, 34(1), 19–35. https://doi.org/10.1016/0006-8993(71)90348-9

Zeymer, M., von der Emde, G., & Wullimann, M. F. (2018). The mormyrid optic tectum is a topographic interface for active electrolocation and visual sensing. Frontiers in Neuroanatomy, 12, 79.

Zhang, T., Malevich, T., Baumann, M.P. *et al.* Superior colliculus saccade motor bursts do not dictate movement kinematics. *Commun Biol* 5, 1222 (2022). https://doi.org/10.1038/s42003-022-04203-0

Zhou, W., & King, W. M. (2002). Attentional sensitivity and asymmetries of vertical saccade generation in monkey. *Vision research*, *42*(6), 771–779. https://doi.org/10.1016/s0042-6989(01)00319-4

Zhou, Y., Yu, G., Yu, X., Wu, S., & Zhang, M. (2017). Asymmetric representations of upper and lower visual fields in egocentric and allocentric references. *Journal of vision*, *17*(1), 9. https://doi.org/10.1167/17.1.9

Zhu, Q., & Vanduffel, W. (2019). Submillimeter fMRI reveals a layout of dorsal visual cortex in macaques, remarkably similar to New World monkeys. *Proceedings of the National Academy of Sciences of the United States of America*, *116*(6), 2306–2311. https://doi.org/10.1073/pnas.1805561116

Zhu, Q., Nelissen, K., Van den Stock, J., De Winter, F. L., Pauwels, K., de Gelder, B., Vanduffel, W., & Vandenbulcke, M. (2013). Dissimilar processing of emotional facial expressions in human and monkey temporal cortex. *NeuroImage*, *66*, 402–411. https://doi.org/10.1016/j.neuroimage.2012.10.083